To Be or Not to Be: Does Bacterial Peptidoglycan Remain in the Chloroplast Envelope of Vascular Plants?

Dissertation

der Mathematisch-Naturwissenschaftlichen Fakultät

der Eberhard Karls Universität Tübingen

zur Erlangung des Grades eines

Doktors der Naturwissenschaften

(Dr. rer. nat.)

vorgelegt von

Xuan Tran

aus Berlin

Tübingen

2024

Gedruckt mit Genehmigung der Mathematisch-Naturwissenschaftlichen Fakultät der Eberhard Karls Universität Tübingen.

Tag der mündlichen Qualifikation:	17.10.2024
Dekan:	Prof. Dr. Thilo Stehle
1. Berichterstatter/-in:	Prof. Dr. Klaus Harter
2. Berichterstatter/-in:	Prof. Dr. Karl Forchhammer

Zusammenfassung

Pflanzliche Plastiden weisen einige Merkmale von Bakterien auf, weshalb davon ausgegangen wird, dass diese von Cyanobakterien abstammen, weche endosymbiotisch in eukaryotische Zellen aufgenommen wurden. Es wird allgemein davon ausgegangen, dass Peptidoglycan, ein wesentlicher Bestandteil der bakteriellen Zellwand, in Plastiden nicht mehr vorhanden ist. Jüngste Entdeckungen haben jedoch nachweisen können, dass Peptidoglycan weiterhin in der Chloroplastenhülle von Moosen zu finden ist. Dies, und phylogenomische Vergleiche zwischen bakteriellen und pflanzlichen Genomen führten zu der Frage, ob ähnliche Strukturen in Chloroplasten von Angiospermen existieren.

Mittels Click-Chemie und Fluoreszenzmikroskopie wurden kanonische Peptidoglycan-Aminosäuren, welche die Chloroplasten von *A. thaliana* und *N. benthamiana* umgeben, sichtbar gemacht. Transiente Expressionsstudien und die fluoreszenzmikroskopische Visualisierung mehrerer Peptidoglycan-bindender Proteine aus Bakterien und Tieren, die als Intrabodies fungieren, unterstützten diese Ergebnisse. Die Auswirkungen von Peptidoglycan-verdauenden Enzymen und D-cycloserine (DCS) auf *A. thaliana* wurden in dieser Studie ebenfalls untersucht. Die Ergebnisse zeigten, dass die Morphologie der Plastiden durch Substanzen, welche in die Struktur von Peptidoglycan eingreifen, verändert wird. Weitere Untersuchungen an *ddl*- und *murE*-Knockout-Linien von *A. thaliana*, welche beide an der Peptidoglycan-Biosynthese beteiligt sind, unterstrichen die Bedeutung dieses Stoffwechsels für die Struktur und Teilung von Plastiden.

Insgesamt belegt diese Studie, dass Peptidoglycan in der Chloroplastenhülle von Angiospermen vorhanden ist und eine wichtige Rolle in der Chloroplastengenese spielt, was auf eine Erhaltung und Anpassung dieses Strukturelements in der Evolution der Angiospermen hindeutet.

Summary

Given that plant plastids retain many bacterial characteristics, it is believed that they originated from cyanobacteria through endosymbiosis. Peptidoglycan, an essential bacterial cell wall component, was once thought to be absent in plastids. However, recent findings have demonstrated its presence in the chloroplast envelope of mosses. Phylogenomic comparisons between bacterial and plant genomes led to the question of whether similar structures exist in angiosperm chloroplasts.

With click chemistry and fluorescence microscopy, canonical peptidoglycan amino acids surrounding the chloroplasts of *A. thaliana* and *N. benthamiana* were visualized. Transient expression studies and fluorescence microscopy visualization of several peptidoglycan-binding proteins from bacteria and animals acting as intrabodies supported this finding. The effects of peptidoglycan-digesting enzymes and D-cycloserine (DCS) on *A. thaliana* were also examined in this study. The results demonstrated that plastid morphology is altered by substances that interfere with the peptidoglycan structure. Additional research on *A. thaliana ddl* and *murE* knockout lines, which are both involved in peptidoglycan biosynthesis, highlighted the importance of this pathway in plastid genesis and division.

Overall, this study provides evidence that peptidoglycan is present in the chloroplast envelope of angiosperms and plays a significant role in chloroplast genesis, indicating conservation and adaptation of this structural element in the evolution of angiosperms.

Table of Contents

List of Abbreviations

ADA	azido-D-alanine
ADL	azido-D-lysine
ALA	azido-L-alanine
ALL	azido-L-lysine
AMIN	amidase N-terminal domain
***At*DAT1**	D-amino transaminase 1 from *A. thaliana*
***At*DDL**	D-alanyl-D-alanine ligase from *A. thaliana*
Atddl	*A. thaliana* D-alanyl-D-alanine ligase mutant
A. thaliana	*Arabidopsis thaliana*
A. thumefaciens	*Agrobacterium thumefaciens*
***At*MurE**	MurE from *A. thaliana*
AtmurE	*A. thaliana* MurE mutant
B. subtilis	*Bacillus subtilis*
cDNA	copy DNA
C. trachomatis	*Chlamydia trachomatis*
CuAAC	copper(I)-catalyzed azide-alkine cycloaddition
DA-DA	D-alanyl-D-alanine
D-Ala	D-alanine
DAT1	D-amino-transaminase 1
DCS	D-cycloserine
DDL	D-alanyl-D-alanine ligase
D-Glu	D-glutamic acid
D-Lys	D-lysine
D. melanogaster	*Drosophila melanogaster*
D-Met	D-methionine
***Dm*PGRP**	*D. melanogaster* peptidoglycan recognizing protein
DNA	desoxyribonucleic acid
***Ec*AMIN**	*E. coli* amidase N-terminal domain
E. coli	*Escherichia coli*
EDA	ethynyl-D-alanine
EDA-DA	ethynyl-D-alanyl-D-alanine
EDTA	ethylenediaminetetraacetic acid
EGTA	ethylene glycol-bis(β-aminoethyl ether)-*N,N,N',N'*-tetraacetic acid

FACS	fluorescence-activated cell sorting
gDNA	genomic DNA
GFP	green fluorescent protein
Glc*N*Ac	*N*-acetylglucosamine
Gly	Glycine
HEPES	4-(2-hydroxyethyl)-1-piperazineethanesulfonic acid
HRP	horseradish peroxidase
H. sapiens	*Homo sapiens*
***Hs*PGRP**	*H. sapiens* peptidoglycan recognizing protein
IPTG	Isopropyl β-D-1-thiogalactopyranoside
KO	knockout
L-Ala	L-alanine
L. esculentum	*Lycopersicon esculentum*
L-Lys	L-lysine
LPS	lipopolysaccharide
***m*-DAP**	*meso*-diaminopimelic acid
M. polymorpha	*Marchantia polymorpha*
MurE	UDP-*N*-acetylmuramoyl-L-alanyl-D-glutamate–2,6-diaminopimelate ligase
Mur*N*Ac	*N*-acetylmuramic acid
NAP	*N*-acetylputrescine
N. benthamiana	*Nicotiana benthamiana*
***Np*AmiC2cat**	catalytical active domain of AmiC2 from *N. punctiforme*
N. punctiforme	*Nostoc punctiforme*
PAMP	pathogen-associated molecular pattern
PBP	penicillin-binding protein
PCR	polymerase chain reaction
PGN	peptidoglycan
PGRP	peptidoglycan-recognizing protein
P. patens	*Physcomitrium patens*
***Pp*DDL**	DDL from *P. patens*
Ppddl	*P. patens* DDL mutant
***Pp*MurE**	MurE from *P. patens*
PpmurE	*P. patens* MurE mutant
PRR	pattern-recognition receptor
RFP	red fluorescent protein

RNA	ribonucleic acid
RT-PCR	reverse transcription polymerase chain reaction
S. aureus	*Staphylococcus aureus*
SDS-PAGE	sodium dodecylsulfate polyacrylamide gel electrophoresis
S. elongatus	*Synechococcus elongatus*
SSC	side scatter
SSC-A	side scatter area
SSC-H	side scatter height
SSC-W	side scatter width
T-DNA	transfer DNA
UPLC/MS	ultra-performance liquid chromatography mass spectrometry
UDP	uridine diphosphate

1 Introduction

A cell is the smallest unit of life, which is self-sufficient and can exist on its own. Therefore, molecular machines inside the cell undergo complex interactions in order to carry out various reactions. Different organic macromolecules are needed to form these unique tiny apparatuses. The first unicellular organisms able to support themselves were prokaryotes, including bacteria (Cantine and Fournier, 2015; Maréchal, 2018).

Around 15 % of our global biomass is made up of bacteria, which is the second major contributor after plants with ~ 80 % (Bar-On et al., 2018). Bacteria are the most diverse and abundant group of organisms and inhabit nearly every environment on earth (Horner-Devine et al., 2004; Errington, 2013). They can be found in soil, water (including salt water, ice, and even hot springs), but also living in and on other organisms like plants and animals (Horner-Devine et al., 2004). They are presumably the very first life form on earth, which emerged over 3 billion years ago (Errington, 2013). Microorganisms and bacteria in particular play a vital role in our ecosystem, shaping the biosphere by providing organic and inorganic material through active decomposition and recycling of organic matter (Madsen, 2011; Sokol et al., 2022).

Cyanobacteria were the first oxygenic photoautotrophic prokaryotes on earth (Campbell and Reece, 2006, pp. 610, 636). They are capable of binding free carbon dioxide and creating oxygen through photocatalytical decomposition of water. Due to their ability to produce free oxygen, the development of oxygen-consuming life was possible. This diverse group of photosynthetic prokaryotes is found in a variety of morphologies, which include unicellular and filamentous species as well as nitrogen-fixing cells, which are the main organisms to supply nitrogen to the biosphere (Potapova and Koksharova, 2020).

The most important step for the evolution of eukaryotes was the acquisition of energy-generating organelles, namely mitochondria and plastids (Machida et al., 2006; Ku et al., 2015). The endosymbiotic theory suggests that an ancient eukaryotic cell engulfed an α-proteobacterium to form mitochondria capable of aerobic respiration, whereas plastids derived from symbiotically engulfed oxygenic photoautotrophic cyanobacteria (Kutschera and Niklas, 2005; Zimorski et al., 2014; Martin et al., 2015). This work will focus on plastids, which differentiate into various forms. Chloroplasts are chlorophyll-containing plastids that can carry out photosynthesis to produce energy in plants (Maréchal, 2018). Both plant cells and cyanobacteria are able to turn sunlight into chemical energy by combining carbon dioxide, water, and other elements to synthesize organic molecules like carbohydrates and amino acids. So one can say that "it is more than a figure of speech [...] that plants create life out of thin air" (Pollan, 2006). Organotrophic organisms can use these reduced organic compounds to grow, develop, and sustain themselves (Pace, 1997).

There are some characteristics that support the endosymbiotic theory. Mitochondria and plastids are limited by a double membrane envelope. They both contain small circular DNA, bacterial 70S ribosomes for protein synthesis, and they duplicate through binary fission. They cannot be produced *de novo* and are not connected to the endomembrane system,

which makes them semi-autonomous organelles. It was also shown that specific bacterial transporter proteins are also present in the outer membrane of mitochondria and plastids. It is also important to point out that the lipid composition of the inner and outer organelle membrane is more similar to the ones of their respective bacterial origins (Maréchal, 2018).

Living organisms on earth are made up of biomolecules, which are essential for biological processes such as growth, development, morphogenesis, and cell division. All important biological molecules have one trait in common: they are chiral molecules. In a *chiral* system, an object and its mirror image are distinguishable and cannot be superimposed onto each other (Petitjean, 2020). Chiral homogeneity plays a fundamental role in the existence of life. Homochiral molecules are the building blocks of essential biomolecules, like desoxyribonucleic acid (DNA), ribonucleic acid (RNA), and proteins (Bonner, 1995). "[Louis Pasteur] speculated that the origin of the asymmetry of chiral biomolecules might hold the key to the nature of life" (Pikuta et al., 2006). Enantiomers, or optical isomers, have the same chemical composition but are chiral molecules (Lorenz et al., 2006).

Although organotrophic organisms use exclusively amino acids in their enantiomeric L-form for ribosomal protein synthesis (Julg, 1989; Genchi, 2017), D-amino acids exist in nature and play a significant role, either directly or indirectly, in animal pathogen defense (Dziarski and Gupta, 2006), neurotransmission and neurogenesis in mammals (Sasabe and Suzuki, 2018), and bacterial cell wall synthesis (Vollmer et al., 2008). The bacterial production of extracellular effectors, for example, is used to control and shape the biodiversity of a complex microbial community. The production and release of non-proteiogenic D-amino acids by bacteria is important since they serve different functions. They can act as a carbon and nitrogen source, are important for physiological pathways in eukaryotic organisms, and are involved in biofilm and spore formation, as well as cell wall biosynthesis (Aliashkevich et al., 2018).

1.1 Composition and Biosynthesis of the Bacterial Peptidoglycan Layer

Peptidoglycan (PGN) is one of the few cases where D-amino acids are used to synthesize a large biological molecule. It is an integral component of the bacterial cell wall, needed to maintain thw cells' shape and to provide stability against its inner osmotic pressure (Typas et al.; Egan and Vollmer, 2013). It is used as an anchor by other cell wall components like proteins and plays an essential role during cell growth and division (Vollmer et al., 2008).

Prokaryotes propagate through binary fission. During this process, mother cells grow in size, duplicate their genetic material, and split into two identical daughter cells. This process seems quite simple at first sight, but it requires a complex assembly of molecules and a coordinated interaction of different proteins to divide cells into two (Margolin, 2000; Donachie, 2001; Angert, 2005). The molecular assembly needed for this procedure is called the bacterial divisome (Egan and Vollmer, 2013; Rowlett and Margolin, 2015; Söderström and Daley, 2017). Binary fission, carried out by the divisome, is a tightly regulated mech-

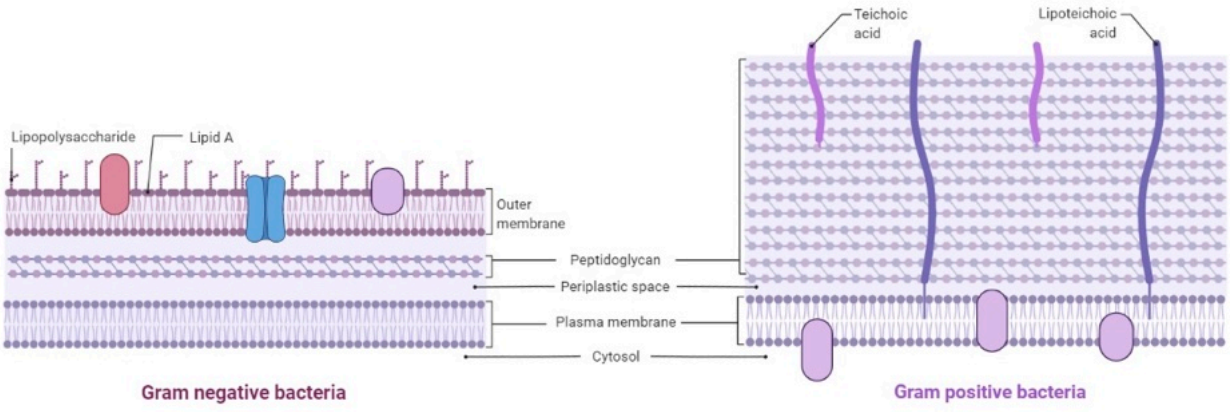

Figure 1.1: Cell wall structure of Gram-negative and Gram-positive bacteria. Adapted from "Gram-Negative Bacteria Cell Wall" and "Gram-Positive Bacteria Cell Wall", by BioRender.com (2024).

anism where a complicated interplay of protein localization, peptidoglycan synthesis, and degradation is required to ensure that mother and daughter cells are perfect copies of each other (den Blaauwen and Luirink, 2019).

In general, bacteria can be categorized into two classes due to their cell wall morphology (Smith and Hussey, 2016). In 1884, the Danish bacteriologist Hans Christian Gram developed a technique to differentiate between two types of bacteria in a quick and easy way. This method was named after its inventor and is commonly known as Gram-staining. Since it is cheap, easy, and fast to do, it is still widely used to identify bacteria today. Gram-negative bacteria like *Escherichia coli* (*E. coli*) have a thinner peptidoglycan layer ($\sim 3-6\,\mathrm{nm}$) embedded in between the plasma membrane and a lipopolysaccharide (LPS) layer, while Gram-positive bacteria like *Bacillus subtilis* (*B. subtilis*) have a thicker peptidoglycan layer ($\sim 15-80\,\mathrm{nm}$) and no LPS layer (Fig. 1.1). It is also important to point out that many cyanobacterial strains like *Synechococcus elongatus* (*S. elongatus*) are classified as Gram-negative but have a much thicker peptidoglycan layer that is around $10-35\,\mathrm{nm}$ (Hoiczyk and Hansel, 2000).

The PGN macromolecule, also known as murein, has a backbone composed of two alternating sugar derivatives, *N*-acetylglucosamine (Glc*N*Ac) and *N*-acetylmuramic acid (Mur*N*Ac), connected through a β-(1-4)-glycosidic bond. A short peptide chain is attached to Mur*N*Ac, which usually consists of L-alanine, D-glutamic acid, *meso*-diaminopimelic acid, and two D-alanine molecules (L-Ala–D-Glu–*m*-DAP–D-Ala–D-Ala) in Gram-negative bacteria. The removal of a terminal D-Ala generates energy, which is used to cross-link two adjacent PGN chains via peptide bonds between the third amino acid (*m*-DAP) of one chain and the fourth amino acid (D-Ala) of another. Gram-positive bacteria usually incorporate L-lysine (L-Lys) as the third amino acid, and neighboring strands are cross-linked through a five-Glycine (Gly) bridge (Vollmer et al., 2008). It is important to point out that there are a lot of variations in the composition of bacterial peptidoglycan (Schleifer and Kandler, 1972).

As shown in Fig. 1.2, this process involves a series of enzymes. Mur genes catalyze peptidoglycan monomer synthesis in the bacterial cytosol. MurA and B are modifying Glc*N*Ac to Mur*N*Ac. MurC – MurF are creating an oligopeptide chain by adding amino acids one by one.

A D-alanyl-D-alanine (DA-DA) dipeptide is produced by D-alanyl-D-alanine ligase (DDL) before it is attached to the peptide stem. In subsequent steps, the PGN monomer is transported into the periplasm and added to the growing peptidoglycan chain. Transpeptidases, including penicillin-binding proteins (PBPs), catalyze the formation of peptide bonds to cross-link PGN chains and strengthen the cell wall (Vollmer et al., 2008).

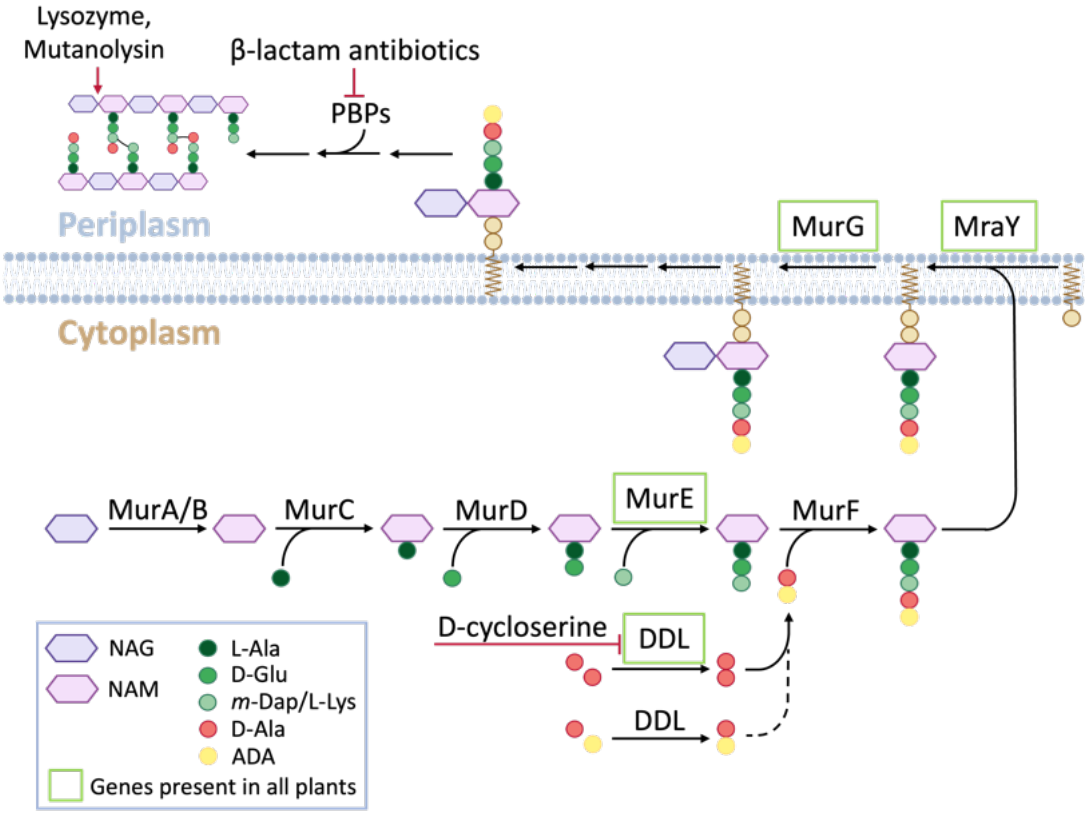

Figure 1.2: Peptidoglycan biosynthesis scheme of Gram-negative bacteria. Different proteins (MurA–G, MraY) are necessary to synthesis the cell wall component peptidoglycan (PGN). Different antibiotics (depicted in red) target specific enzymes of this pathway and disturb PGN biosynthesis. *N*-acetylglucosamine (Glc*N*Ac), *N*-acetylmuramic acid (Mur*N*Ac), L-alanine (L-Ala), D-glutamic acid (D-Glu), *meso*-diaminopimelic acid (*m*-DAP), L-lysine (L-Lys), D-alanine (D-Ala), azido-D-alanine (ADA), penicillin-binding protein (PBP), azido-D-alanine (ADA). Enzymes of "four PGN" plants are boxed in green. Adapted from Tran et al. (2023)

Peptidoglycan biosynthesis is tightly regulated since bacteria must maintain a balance between growth and cell wall stability during cell elongation and division. Many antibiotics inhibit this crucial peptidoglycan biosynthesis process, causing bacterial cell death. Penicillin is a popular example of an antibiotic that inhibits peptidoglycan formation. It belongs to the β-lactam antibiotics that target and inhibit the so-called penicillin-binding protein (PBP), necessary for PGN cross-linking in bacteria. It mimics the terminal DA-DA dipeptide of the peptidoglycan oligopeptide stem. The active binding site of PBPs attacks and opens up the β-lactam ring and forms a covalent acyl-enzyme complex, preventing further reactions with other molecules (Tipper, 1985; Zapun et al., 2008).

It was shown that a temperature-sensitive *E. coli* mutant with an impaired DDL protein had a weaker cell wall (Lugtenberg and Schijndel-van Dam, 1973). This strain was only able to grow at elevated temperatures in high osmotic media or with the addition of D-Ala in high

concentrations. DCS is another antibiotic that blocks PGN biosynthesis. Its structure mimics D-Ala and binds D-alanyl-D-alanine ligase, preventing the formation of DA-DA dipeptide, which is an important building block for peptidoglycan synthesis in bacteria (Bruning et al., 2011). The inhibition of DDL by DCS leads to cell lysis, similar to the *E. coli* mutant strain with an impaired DDL.

Cyanobacteria are the largest and probably most diverse group among bacteria, and their cell wall structure is very interesting (Hoiczyk and Hansel, 2000). They are classified as Gram-negative, although their peptidoglycan layer is generally much thicker compared to most Gram-negative bacteria. The degree of cross-linking between adjacent PGN strands is also higher. In most species that have been studied, an oligopeptide chain containing *m*-DAP was found, whereas L-DAP or L-Lys are commonly found in Gram-positive bacteria. *Anabaena cylindrica*, on the other hand, was found to incorporate L-Lys into the PGN oligopeptide chain. It is important to notice that peptidoglycan synthesis in filamentous cyanobacteria is not researched as thoroughly as i.e., *E. coli* or *B. subtilis*; thus, little is known about the variations and modifications of the sugar backbone and peptide chain (Bok, 2022).

Therefore, peptidoglycan is a very interesting macromolecule and subject of many studies since it is vital for bacterial stability and propagation, but the focus of this thesis will be the existence and functions of peptidoglycan in plants.

1.2 Peptidoglycan in Plants

As described in Section 1, mitochondria as well as plastids are former free-living bacteria that underwent symbiosis with an eukaryotic cell to form today's semi-autonomous energy-generating organelles. It is also common knowledge that both organelles are surrounded by a double membrane. Furthermore, it is believed that they lost the peptidoglycan layer, which is an integral cell wall layer in bacteria. It was speculated that there was no need for protection and stability against outer stressors anymore. The question is: How did it become common knowledge that we think plastids lost such an integral cell wall component over the course of evolution? The answer might be found in the discovery and investigation of plastids throughout history.

1.2.1 Early Microscopic Discovery and Endosymbiosis Theory of Plastids

The first electron microscopy technique was invented around 1930 (Gelderblom and Krüger, 2014). The first electron micrographs of mitochondria and plastids were published around 1950 – 1960 (Leyon and von Wettstein, 1954; Mühlethaler and Frey-Wyssling, 1959; Heslop-Harrison, 1963). These authors investigated the morphology and formation or differentiation of plastids in general. They all observed that these organelles have two envelope layers, an outer and an inner layer. Although Schötz and Diers (1966) could also see the formation of "stromal substances and thylakoids" in the intermembrane space between chloroplast

envelope membranes in some samples. All of these early publications about microscopic observations focused on energy-generating compartments, limited by two envelope layers.

Around that time, the origin of energy-generating organelles was still indefinite. Constantin Mereschkowsky (1905) was one of the first authors to discuss the theory of endosymbiosis based on observations by Andreas Schimper (1883) about chloroplast division. This theory gained more popularity with the publication of Lynn Sagan (1967) with the revolutionary idea about the "origin of mitosing cells". Up to that point, it was common sense that energy-generating organelles developed throughout evolution as part of eukaryotic cells. Since Sagan's publication, it is widely accepted that mitochondria and plastids originated from bacteria. It is thought that the outer membrane of those organelles originated from the hosts' plasma membrane after phagocytosis. In contrast to that, later investigations could show that the protein and lipid composition of those organelles are more similar to their respective ancestors (see Maréchal (2018) for more details).

This means that the structure of mitochondria and plastids was observed before the broad acceptance of the endosymbiotic theory. It is possible that those early structural investigations were not reevaluated in the light of endosymbiosis. This may have led to the conclusion that these organelles no longer possess a peptidoglycan layer. In recent years, more evidences have been found, suggesting that some members of the plant phylogenetic tree have in fact retained a peptidoglycan layer (Björn, 2020; Radin and Haswell, 2022).

1.2.2 Bacterial Peptidoglycan Biosynthesis Genes in the Plant Kingdom

As described previously, cyanobacteria have undergone endosymbiosis with ancient eukaryotic cells to form today's plastids in the plant kingdom. While peptidoglycan is an essential component of the cell wall in bacteria, it was long thought to be lost over the course of evolution in plants, with the exception of Glaucophyte plastids (Pfanzagl et al., 1996). However, recent phylogenetic studies from Karol et al. (2012) and van Baren et al. (2016) have shown that land plants still have most genes required for PGN biosynthesis. This leads to the question of why plants have preserved these genes. Although various results could show that different peptidoglycan synthesis genes still play an important role in chloroplast division in non-vascular plants, it was suggested that these genes must have taken on another function in vascular plants (see Garcia et al. (2008) and Hirano et al. (2016) for more information).

Peptidoglycan biosynthesis involves ten key enzymes (see Section 1.1), which can also be found to some extent in the genome of green algae and plants (van Baren et al., 2016). Fig. 1.3 shows that at least four genes (MurE, DDL, MraY, and MurG) are found the the Viridiplantae. Plant species that retain homologs of MurE, DDL, MraY, and MurG will be referred to as "four PGN" plants, whereas plants containing all ten genes are referred to as "full PGN" plants. Some major plant lineages contain all genes required for peptidoglycan synthesis with the exception of PBP. *A. thaliana* is a "4-PGN" plant; *N. benthamiana* has all genes, with the exception of PBP ("full PGN - PBP"), and *P. patens* contains all ten genes ("full PGN" plant).

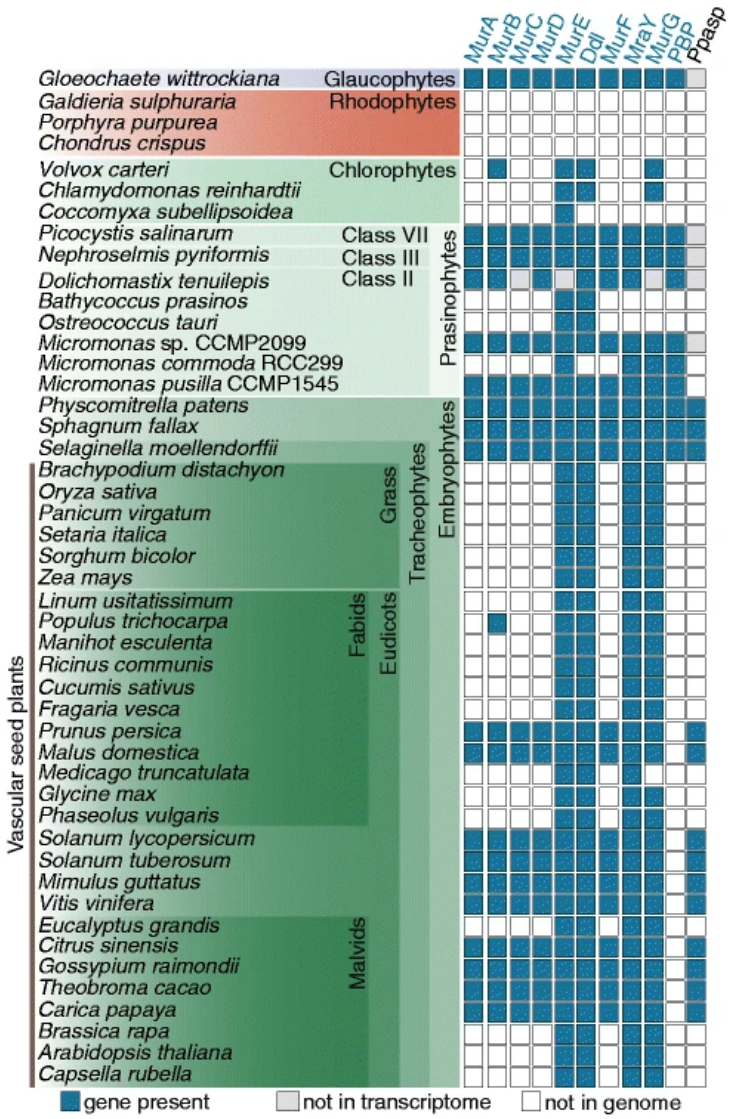

Figure 1.3: Peptidoglycan pathway proteins in the Archaeplastida. Four genes - UDP-*N*-acetylmuramoyl-L-alanyl-D-glutamate–2,6-diaminopimelate ligase (MurE), MurG, DDL and MraY - are present throughout green plants ("four PGN" plants), whereas some major plant lineages contain all genes necessary for peptidoglycan synthesis with the exception of PBP ("full PGN - PBP" plants). Plant species, that retain homologs of al ten peptidoglycan biosynthesis genes are referred to as "full PGN" plants. Adapted from van Baren et al. (2016).

After endosymbiosis, several genes necessary for peptidoglycan synthesis remained in all analyzed plant genomes, including DDL (van Baren et al., 2016). A closer examination of the DDL gene sequence of different plant species, including DDL from *P. patens* (*Pp*DDL) and D-alanyl-D-alanine ligase from *A. thaliana* (*At*DDL), revealed a gene sequence that encodes for a fusion protein consisting of two bacterial DDL proteins (Thimmapuram et al., 2005; Machida et al., 2006). Hirano et al. (2016) studied the DDL gene in *P. patens*. A knockout (KO) of DDL leads to a giant chloroplast phenotype, which could already be observed in mosses treated with β-lactam antibiotics and in MurE KO mutants. This phenomenon could be reversed when the missing DDL product DA-DA was introduced into the system. They were also able to visualize PGN in *P. patens* using a newly developed labeling technique described in Section 1.3.1. They could show that moss chloroplasts incorporate D-amino

acids into their envelope, which is an integral component of bacterial peptidoglycan. In conclusion, DDL appears to play an important role in plastid division of mosses as well. In comparison to that, *At*DDL KO mutants (*Atddl*-1 and *Atddl*-2) did not exhibit a giant chloroplast phenotype like *P. patens* DDL mutants. Due to these results, Hirano et al. (2016) concluded that *A. thaliana* does not have a peptidoglycan layer since *Atddl* mutant chloroplast division was not dependent on PGN synthesis and the typical giant chloroplast phenotype was not observable. It was also suggested that the DDL enzyme in *A. thaliana* has taken on another function instead of DA-DA dipeptide synthesis.

Machida et al. (2006) and Garcia et al. (2008) investigated the inhibition of another peptidoglycan synthesis gene, namely MurE, in *P. patens*. They could show that MurE KO mutants had the same giant chloroplast phenotype as described by Kasten and Reski (1997). Complementation assays showed that the MurE homolog from the cyanobacterium *Anabaena* sp. PCC7120 was able to rescue the giant chloroplast phenotype in transformed *P. patens* MurE KO mutants, but a MurE homolog from *A. thaliana* was not able to. They suggested that MurE, a UDP-*N*-acetylmuramoyl-L-alanyl-D-glutamate–2,6-diaminopimelate ligase that attaches the third amino acid to the oligopeptide chain in peptidoglycan monomers, was essential for chloroplast division in *P. patens* and that the protein structure is similar to the cyanobacterial homolog since it was able to rescue the giant chloroplast phenotype. It was suggested that *A. thaliana* MurE, on the other hand, has taken on another function since its homolog was not able to reverse the phenotype. They concluded that peptidoglycan was still present in non-vascular plants but not in evolutionary younger vascular plants.

Overall, there are numerous compelling evidences that plants, at least in earlier diverging land plants like *Marchantia polymorpha* (*M. polymorpha*) and *P. patens*, still have a peptidoglycan layer similar to bacterial PGN with similar function in binary fission.

1.2.3 Effects of Antibiotics on Plant and Plastid Morphology

Green algae and plants do not only retain some (if not all) genes of the PGN pathway, but experiments using antibiotics specifically affecting bacterial peptidoglycan synthesis had an effect on chloroplast division and morphology.

Kasten and Reski (1997), for example, tested the effect of different β-lactam antibiotics on plastid division in *P. patens* and tomato (*Lycopersicon esculentum*). They noticed that chloroplast division in the tips of dividing *P. patens* protonema cells was inhibited, resulting in a reduced number of chloroplasts per cell. Affected moss cells had giant chloroplasts or macrochloroplasts, which were structurally unaffected with a well-developed inner membrane. This phenomenon was reversible when antibiotics were removed, but they could not observe an inhibition of chloroplast division in tomato. Tounou et al. (2002) observed similar results in the liverwort *M. polymorpha*. Cell cultures treated with ampicillin had a decreased number of chloroplasts, which were very large.

Katayama et al. (2003) tested the effect of various antibiotics on *P. patens* chloroplasts and found out that D-cycloserine (DCS) had a similar effect on plastid division as β-lactam antibiotics, resulting in a macrochloroplast phenotype. Matsumoto et al. (2012) studied

the microscopic effect of antibiotics on chloroplast division in chloroplasts of the green algal *Closterium peracerosum–strigosum–littorale* complex, a unicellular charophyte closely related to land plants. They observed that chloroplast division was also affected by ampicillin and D-cycloserine, similar to *P. patens*. These results implied that a peptidoglycan-related system might have been conserved in non-vascular plants, which is also sensitive to PGN biosynthesis inhibiting antibiotics.

Not only green algae and non-vascular plants are affected by antibiotics, but many studies show that vascular plants like *A. thaliana* and crops are also affected. Hillis et al. (2011) tested the effect of ten antibiotics in three different vascular plant species (alfalfa, carrot, and lettuce) and could show that almost all of them had a dramatic effect on root elongation, but no significant effects on seed germination were observed. Opriş et al. (2013) could show that antibiotics can influence secondary metabolites and physiological characteristics in wheat. Minden et al. (2017) tested the effect of small concentrations of antibiotics typically found in soil on the time of germination and trait development. They showed that the germination time was delayed for some species and biomass was reduced for others. *A. thaliana* root architecture was modified by β-lactam antibiotics (Gudiño et al., 2018). Wang et al. (2015) point out that "researchers have to be well aware of the potential effects of antibiotics on mitochondrial and chloroplast function, gene expression, and cell proliferation.".

1.3 Tools for the Detection and Characterization of Peptidoglycan

1.3.1 Click Chemistry: A 2-step *in situ* Labeling Technique

Kolb et al. (2001) used a known chemical mechanism to synthesize complex organic molecules in an easier and more inexpensive way with high yields. Byproducts of the so-called *click chemistry reaction* are easy to remove, so chromatography or recrystallization is not needed. It has a broad range of usage and is easy and quick to perform under mild reaction conditions. It can be performed in an aqueous solution with a wide range of pH values, which makes it suitable for *in vivo* applications in biological systems.

One of the most widely used click reactions is a Huigens 1,3-dipolar cycloaddition, more precisely a copper(I)-catalyzed azide-alkine cycloaddition (CuAAC). This reaction allows for the efficient and specific conjugation of azide and alkyne functional groups and has a wide range of applications, including the synthesis of biomaterials, the development of pharmaceuticals, and the study of biological systems (Devaraj and Finn, 2021).

Fig. 1.4 shows the general reaction mechanism and reaction scheme of a CuAAC (Worrell et al., 2013). For this, an azide-modified molecule acts as a dipole and an alkyne-modified molecule acts as dipolarophile, which both undergo a reaction to form triazoles. To enhance the reactivity of terminal alkynes towards azides and to increase the yield of 1,4-disubstituted 1,2,3-triazoles, a metal catalyst is used to elevate its dipolarophile. In this case, copper sulfate is used as a simple Cu(II) source, and sodium azide is used to reduce Cu(II) to Cu(I) ions,

which is used in this reaction as a catalyst. To protect biological molecules from the reactive Cu(I) species, a ligand like BTTAA or THPTA is used to chelate the Cu-ion.

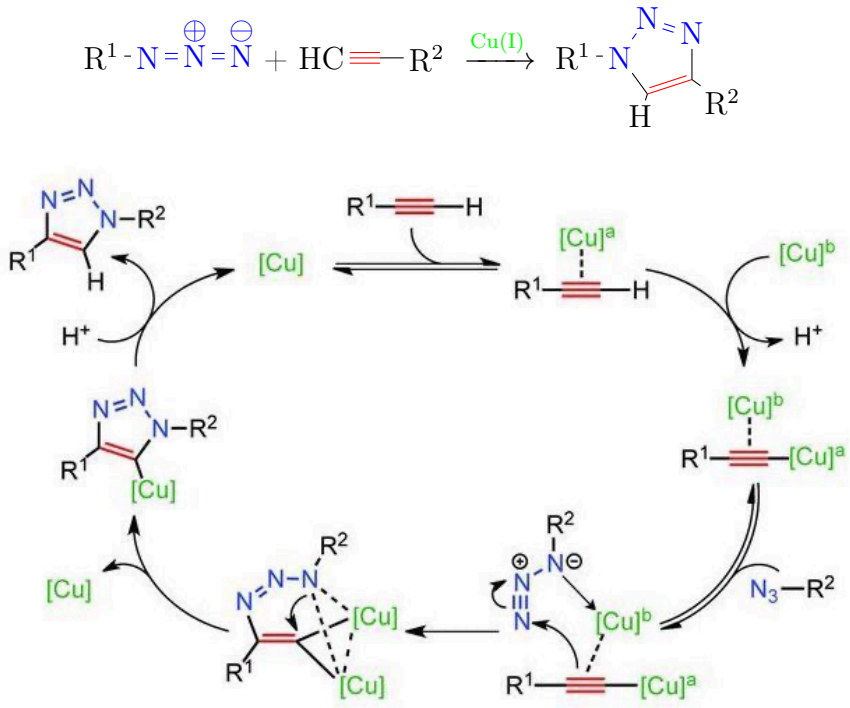

Figure 1.4: CuAAC reaction equation (top) and reaction mechanism (bottom) adapted from Worrell et al. (2013).

Click chemistry has been used to study different interactions like carbohydrate-protein interaction (Zhang et al., 2006), to synthesize a broad variety of organic molecules and polymers for material and pharmaceutical science (Hein et al., 2008), as well as for bioorthogonal bioconjucations to study physiological processes in living organisms (McKay and Finn, 2014; Kenry and Liu, 2019; Hatzenpichler et al., 2020). In 2022, Carolyn R. Bertozzi, Morten Meldal, and K. Barry Sharpless received the Nobel Prize in Chemistry "for the development of click chemistry and bioorthogonal chemistry" since it is such a versatile tool. "Click chemistry and bioorthogonal reactions have taken chemistry into the era of functionalism, bringing the greatest benefit to humankind." (Ramström, 2022).

An example where click chemistry was used to solve a year-long riddle was the "clamydial anomaly". *Chlamydia trachomatis* (*C. trachomatis*) is a Gram-negative bacteria that can only replicate itself inside a host cell. It has all required genes to synthesize peptidoglycan, yet the presence of PGN in *C. trachomatis* could not be shown by conventional methods until recently. Liechti et al. (2013) used click chemistry in living systems to unravel the clamydial anomaly. They were one of the first groups to use this technique in living systems to label and image biological molecules *in vivo*.

1.3.2 Peptidoglycan-Recognizing Proteins (PGRPs)

To fight off invading pathogens, animals developed an immune system over the course of evolution. It is a complex organization of specialized cells and consists of two major parts:

the adaptive and the innate immune systems (Delves and Roitt, 2000). The adaptive immune system responds to repeated infection with a pathogen by activation and expression of antigen-specific receptors during invasion (Schenten and Medzhitov, 2011). The innate immune system consists of a variety of cells and mediates the first interaction with pathogens. It includes highly conserved pattern recognition receptors (PRRs), which recognize unique pathogen associated molecular patterns (PAMPs) (Shaw et al., 2010; Kumar et al., 2011).

Peptidoglycan-recognizing proteins (PGRPs) are the best-known peptidoglycan binding proteins. They are PRRs and therefore part of the innate immune system. They are found in insects and mammals and recognize peptidoglycan (PGN), a very unique bacterial cell wall component, which is described in Section 1.1. There are up to 19 different PGRPs in insects, whereas mammals just have four. The expression of these proteins is upregulated upon bacterial exposure to eliminate invading pathogens in different ways, e.g., recruiting other immune cells to the infection site by activating the Toll pathway to generate antimicrobial substances, binding PGN to inhibit cell division, or hydrolyzing PGN to destroy the cells (Pankey and Sabath, 2004; Dziarski, 2004; Dziarski and Gupta, 2006).

Many PGRPs have a C-terminal domain similar to bacteriophage amidase 2 and an N-terminal PGRP-specific segment for subsequent signaling (Kim et al., 2005; Guan et al., 2005). The structure of PGRPs shows a PGN-binding groove, which is amidase-active if it contains an active Zn^{2+}-binding site like bacteriophage amidase 2 (Wang et al., 2003). An amino acid of the Zn^{2+}-binding site is substituted for non-amidase-active PGRPs (Mellroth et al., 2003). Most PGRPs recognize at least the Mur*N*Ac-tripeptide motif (Kim et al., 2005; Wang et al., 2003; Guan et al., 2004; Chang et al., 2005; Lim et al., 2006). Due to the variable third amino acid of the PGN-oligopeptide chain, different PGRPs have a higher binding affinity either to DAP-type or Lys-type PGN, depending on the amino acid configuration in its PGN-binding groove (Kumar et al., 2005; Swaminathan et al., 2006).

All in all, peptidoglycan-recognizing proteins are an essential part of the innate immune system in animals to fight off bacterial pathogens. They have a specific binding affinity to the unique bacterial cell wall component peptidoglycan and are able to break it down either directly or upon subsequent signaling pathways.

1.3.3 Structural Characterization of Peptidoglycan

To isolate and analyze bacterial peptidoglycan, the protocols of Kühner et al. (2014) and Bertsche and Gust (2017) were used in this study. Bacterial cultures are harvested and lysed by boiling in a high-concentration sodium chloride solution. The resulting cell walls are broken down into smaller fragments by sonication. In further steps, DNA, RNA, and cell wall-bound proteins are removed with DNAse, RNAse, and trypsin, which in turn are inactivated by boiling. HCl treatment releases bound wall teichoic acids and other glycophosphates. Afterwards, several washing steps are needed to neutralize the pH value. Further enzymatic digestion of the isolated peptidoglycan molecule with lysozyme and mutanolysin is carried out for ultra-performance liquid chromatography mass spectrometry (UPLC/MS) analysis. Usually, Mur*N*Ac residues are reduced with sodium borohydrate to avoid double

peaks of the non-reduced glycan ends, which was skipped in this study. Liquid chromatography was performed using a trifluoracetic acid and a methanol gradient. Trifluoracetic acid is an ion pairing agent that forms ion bonds with muropeptides, resulting in better separation of mixed analytes. It is also volatile, so it can be used for both liquid chromatography and mass spectrometry analysis.

2 Research Objective

New research suggests that peptidoglycan, a macromolecule commonly part of bacterial cell walls, is found in the chloroplasts of non-vascular plants and algae. The purpose of this study was to answer the question if chloroplasts of vascular plants also contain a peptidoglycan layer and which putative functions it may fulfill.

Multiple approaches were used to investigate the presence, structure, and function of peptidoglycan (PGN) in plastids of vascular plants. Therefore, peptidoglycan-specific components should be visualized *in planta* via click chemistry. Analytical characterization via mass spectrometry should be applied to resolve the molecular composition of plant peptidoglycan. Biochemical studies, including localization and binding experiments with peptidoglycan-binding proteins, were planned to get further information about the structural similarities of bacterial and plant peptidoglycan. The effect of antibiotics on plant growth and plastid morphology should provide more information on the biological function of peptidoglycan and its respective genes in plants. Some of the conclusions drawn from the experiments described before should be verified in genetic approaches with KO mutant plants of PGN biosynthesis genes.

3 Results

3.1 Molecular Characterization of *Arabidopsis thaliana* D-alanyl-D-alanine ligase

The chloroplast morphology in *P. patens* was dependent on the presence of DA-DA dipeptide, either through internal biosynthesis by D-alanyl-D-alanine ligase or external supplementation in growth media (Hirano et al., 2016). An important question still remained unanswered: Why could this particular giant chloroplast phenotype not be observed in DDL mutants of vascular plants like *A. thaliana*?

The DDL genes in *P. patens* as well as *A. thaliana* are predicted to encode for a fusion protein consisting of two bacterial DDL proteins. Hirano et al. (2016) examined the fusion protein in *A. thaliana* using reverse transcription polymerase chain reaction (RT-PCR) experiments. Both available DDL mutants in *A. thaliana*, *Atddl*-1 (SALK 092419C) and *Atddl*-2 (SAIL 906_E06), have a T-DNA insertion in the first half of the gene (Fig. 3.1a). A closer look into the experimental design revealed that they were using primers for RT-PCR analyses framing the N-terminal part of the DDL gene, where both T-DNA insertions are located.

A more detailed examination of the second half of the *At*DDL gene revealed a translatable coding sequence including a start and stop codon (Fig. 3.1a, green box). RT-PCR experiments with *Atddl* mutants and appropriate primers binding the second half of the DDL gene, indicated by arrows in Fig. 3.1a, produced a transcript (Fig. 3.1b). This suggests translation of a functional C-terminal *At*DDL protein $At\text{DDL}_{\Delta\text{N}}$ (Tran et al., 2023). Interestingly, a recent study investigated a third *At*DDL mutant (*Atddl*-3) with a T-DNA insertion in the C-terminal part of the DDL gene (Temnyk, 2024). There were also no morphological defects observed in growth experiments with this mutant allele.

To investigate the translation and localization of $At\text{DDL}_{\Delta\text{N}}$ *in planta*, it was fused to the genetically encoded green fluorescent protein (GFP) marker (Fig. 3.1a, green box). Fig. 3.1c shows a cytosolic protein expression of pH7FWG2-$At\text{DDL}_{\Delta\text{N}}$-GFP in transiently transformed *N. benthamiana* leaves. Both experiments indicate that the available *At*DDL mutants *Atddl*-1 and *Atddl*-2 may still produce a truncated $At\text{DDL}_{\Delta\text{N}}$ protein.

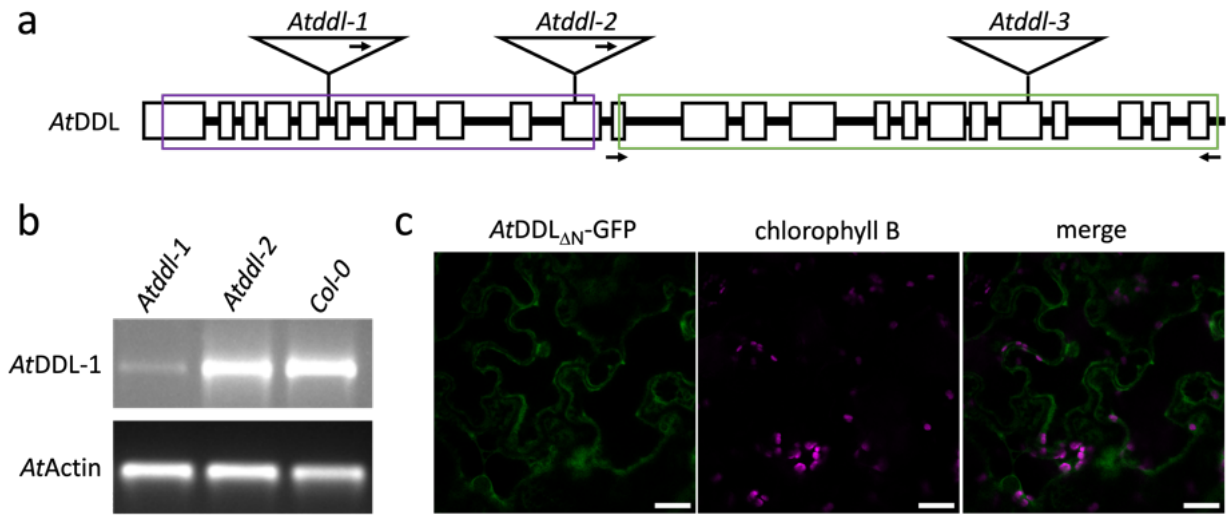

Figure 3.1: Transcription of *At*DDL in *Atddl*-1 and *Atddl*-2. **(a)** Structure of the *At*DDL gene. Exons are represented by black boxes and introns by black lines. Positions of T-DNA insertion sites of *Atddl*-1, *Atddl*-2 and *Atddl*-3 are marked by triangles. Arrows in the triangles indicate position of left border in the insertions. Genomic regions encoding putative complete DDL enzymes are framed in purple and green boxes. Arrows under the scheme mark the positions of primers used for RT-PCR analysis. **(b)** RT-PCR analysis of *At*DDL-1 in *Atddl*-1, *Atddl*-2 and corresponding wild type seedlings (*Col-0*). Expression of *At*DDL-1 is shown in the upper row, whereas expression of constitutive control (*At*Actin2) is shown below. **(c)** Fluorescence microscopic image of *N. benthamiana* cells expressing *At*DDL$_{\Delta N}$-GFP (green, left), image of chlorophyll B autofluorescence (magenta, middle) and merge of both images (right). Adapted from Tran et al. (2023).

3.2 Physiological Effect of D-cycloserine on Plant Growth

Many different antibiotics target enzymes important for peptidoglycan synthesis in bacteria (Höltje, 1976; Waxman and Strominger, 1983; Schneider and Sahl, 2010). It was also shown that antibiotics affect chloroplast morphology and number in mosses (Kasten and Reski, 1997; Tounou et al., 2002; Katayama et al., 2003), indicating that genes involved in bacterial peptidoglycan biosynthesis are needed for proper plastid division in non-vascular plants. D-cycloserine (DCS) is an antibiotic that acts as a D-Ala analogue and inhibits the DDL enzyme by blocking the active binding site (Bruning et al., 2011).

As discussed in Section 3.1, *A. thaliana* DDL KO mutants were able to produce a truncated *At*DDL$_{\Delta N}$ protein, which might still have remaining enzymatic activity. The following experiment makes use of DCS as a DDL inhibitor. Therefore, *A. thaliana* plants were grown on DCS in order to investigate the physiological effect of DDL inhibition on seed germination, plant growth, and plastid morphology. *A. thaliana* wild type, as well as DDL KO mutants *Atddl*-1 and *Atddl*-2, were tested to see if a comparable phenotypical effect observed in DCS-treated moss cells (Katayama et al., 2003) is detectable in *A. thaliana* wild type and DDL mutants. The root length of 12-day-old *A. thaliana* seedlings grown on medium with DCS in different concentrations was much shorter compared to control plants grown without DCS (Fig. 3.2). Moreover, the root length decreases with increasing DCS concentration. After a certain DCS concentration, seeds were not germinating (Fig. A.1).

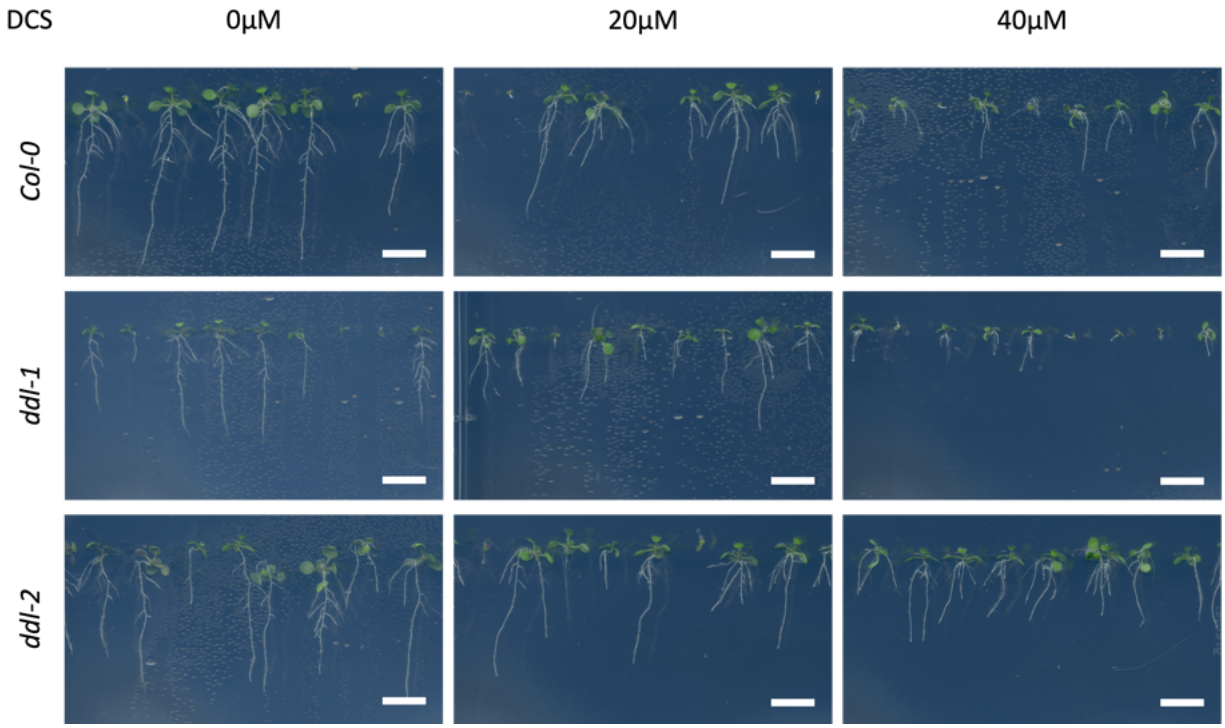

Figure 3.2: *A. thaliana* seedling germination and root growth is inhibited by D-cycloserine. *A. thaliana* wild-type *Col-0* and *At*DDL mutants *Atddl*-1 and *Atddl*-2 were germinated for 12 days under long day conditions on growth media, containing 0, 20, and 40 µM D-cycloserine. Scale bar: 10 mm.

Fig. 3.3 shows the root length of 8-day-old *Col-0*, *Atddl*-1, and *Atddl*-2 seedlings grown on medium with 0, 20, or 40 µM D-cycloserine. A general decrease in root length is observable, although roots of *Atddl*-2 mutants seem to be slightly longer at 40 µM DCS compared to the others.

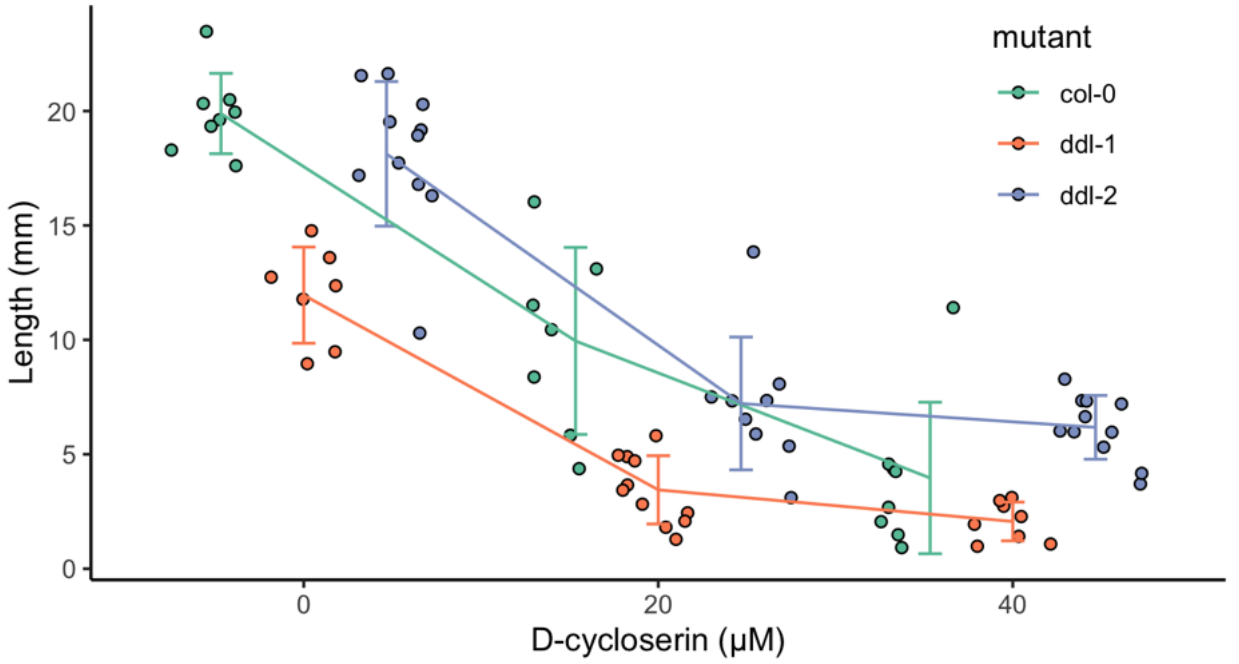

Figure 3.3: *A. thaliana* seedling root growth is inhibited by D-cycloserine. Measured root length of 8 day old *A. thaliana* seedlings (wild-type *Col-0*, *Atddl*-1 and *Atddl*-2) grown on media containing 0, 20, and 40 µM D-cycloserine. Root length generally decreases with increasing DCS concentration.

To examine the chloroplast structure in those seedlings, mesophyll cells were fixed as described in Section 6.1.3. Fig. 3.4 shows microscopic images of *A. thaliana* wild type *Col-0* grown on medium with 0, 20, or 40 µM DCS for 12 days.

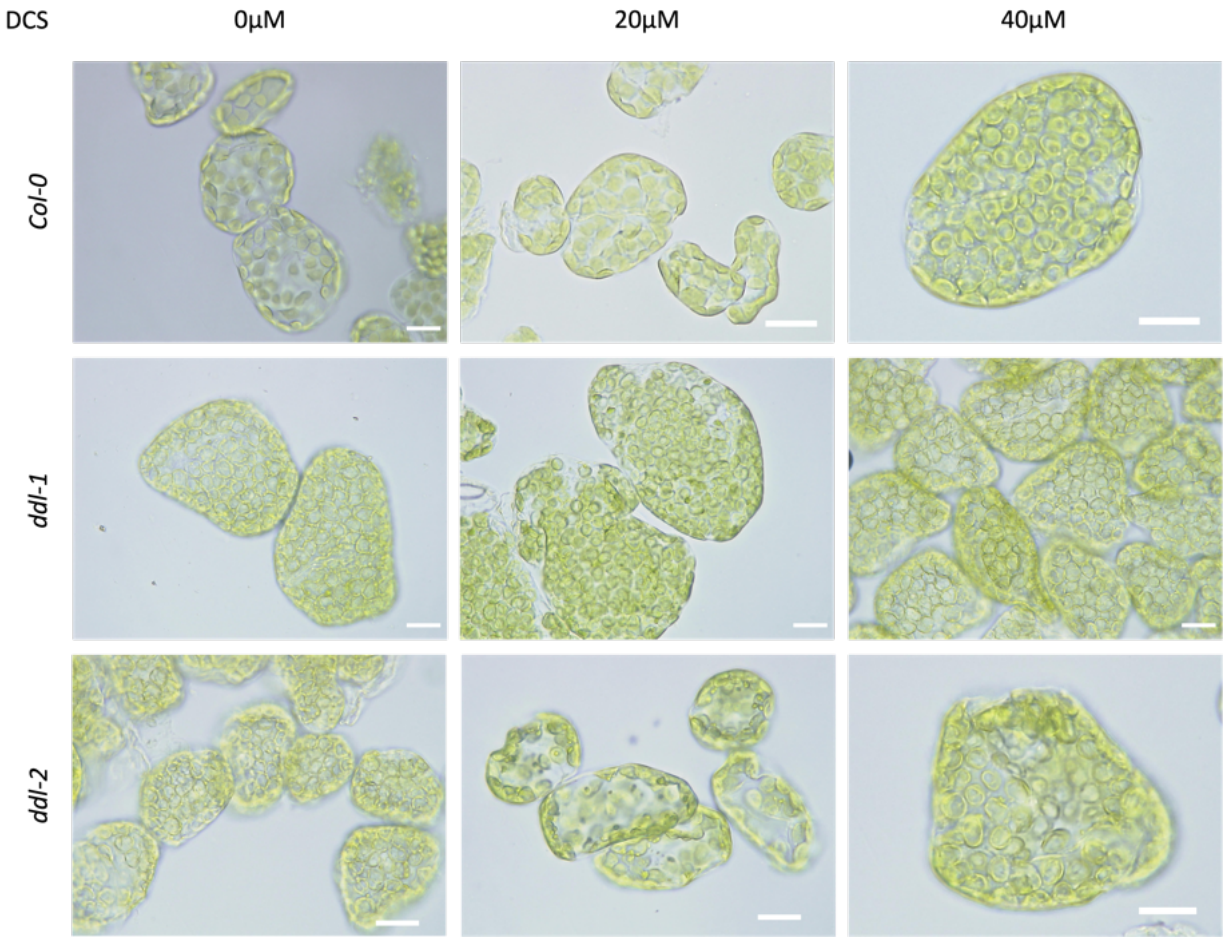

Figure 3.4: Microscopic images of fixed mesophyll cells of *A. thaliana* seedlings *Col-0*, *Atddl*-1, and *Atddl*-2 grown on media containing 0, 20, and 40 µM D-cycloserine for 12 days. Scale bar: 20 µm.

Some plastids from seedlings treated with 20 µM DCS appear slightly bigger and less round in shape compared to untreated cells. The green chlorophyll in mesophyll cells treated with 40 µM DCS seem to accumulate closer to the membrane of chloroplasts, leaving a translucent hole in the middle.

Some samples of untreated *Atddl*-1 seedlings looked similar to *Col-0* treated with 40 µM DCS, although it seems like the chloroplasts are damaged, so the chlorophyll is accumulating in the cytoplasm. *Atddl*-1 seedlings treated with 20 µM DCS appear to have a plastidic phenotype similar to untreated *Atddl*-1 and *Col-0* treated with 40 µM DCS with some "hollow" and some "leaky" chloroplasts where chlorophyll seams to leak into the cytoplasm. Chloroplasts of *Atddl*-1 seedlings treated with 40 µM DCS looked like *Col-0* treated with 40 µM DCS but with a much bigger colorless empty space.

Chloroplasts of untreated *Atddl*-2 seedlings looked similar to untreated *Atddl*-1 samples. *Atddl*-2 mutants treated with *Atddl*-2 20 µM DCS looked like they had trouble separating during division. Plastids in mesophyll cells of *Atddl*-2 seedlings seem to have the same

phenotype as *Atddl*-1 (20 µM DCS). These results indicate that DCS as a DDL inhibitor had an effect on chloroplast structure.

3.3 Visualization of Peptidoglycan Components in Plants with Click Chemistry

The so-called *click chemistry* is a CuAAC reaction that can be used to label various structures *in vivo*. This technique was used by Liechti et al. (2013) and Hirano et al. (2016) to label specific cell wall structures, namely PGN of different bacterial strains such as *Staphylococcus aureus* (*S. aureus*) and *E. coli*, but also the envelope of *P. patens* moss chloroplasts. Ethynyl-D-alanyl-D-alanine (EDA-DA) was used as an DA-DA analogue in both cases, which is incorporated into the PGN macromolecule by MurF (see Fig. 1.2). Hirano et al. (2016) were able to show that *Pp*DDL mutants displayed a giant chloroplast phenotype, which was reversible when DA-DA was exogenously applied. This experiment was repeated using ethynylated D-alanyl-D-alanine (EDA-DA), which was also able to rescue the giant chloroplast phenotype by incorporation of the modified DA-DA molecule. Since the ethynylated molecule could be labeled using an azide-modified fluorophore, the exact location of the incorporated molecule could be detected with a fluorescent microscope. It turned out that EDA-DA was incorporated into the chloroplast envelope of *P. patens* DDL mutant (*Ppddl*) protonema cells. These results proved that moss chloroplasts have retained a peptidoglycan layer in their envelope, containing D-amino acids.

As DCS affected chloroplast biogenesis in *A. thaliana* (Sec. 3.2), the next question was if peptidoglycan is also part of plastid envelopes of vascular plants. To address this question, the "click chemistry" method was used in this work to investigate the chloroplast envelope of vascular plants in a similar manner. Therefore, this technique was introduced and optimized, using azide-modified amino acids instead of ethenyl-modified amino acids, as well as ethenyl-modified fluorescence markers for vascular plants. This modified experimental setup was used to visualize and localize the peptidoglycan macromolecule around chloroplasts of different angiosperm species using modified canonical peptidoglycan amino acids.

3.3.1 Visualization of Canonical PGN Amino Acid in *Physcomitrium patens*

Commercially available azide-modified amino acids, such as ADA, were used to simplify the click chemistry process *in planta* instead of ethynyl-D-alanine (EDA) or EDA-DA to circumvent the synthesis and purification of ethenyl derivatives. An experimental setup comparable to Hirano et al. (2016) was used to test whether similar results were obtained using modified educts. In such a proof-of-principle experiment, ADA was fed to *P. patens* protonema cells and subsequently labeled with ethenyl derivatives of fluorescent dyes such as Atto-514-alkyne.

Hirano et al. (2016) could show that chloroplasts of protonema cells from *P. patens* were surrounded by a fluorescent ring-like structure (Fig. 3.5a), indicating the incorporation of EDA-DA into the envelope of moss chloroplasts. Fig. 3.5b shows a comparable result using ADA as an D-Ala analogue instead of EDA-DA.

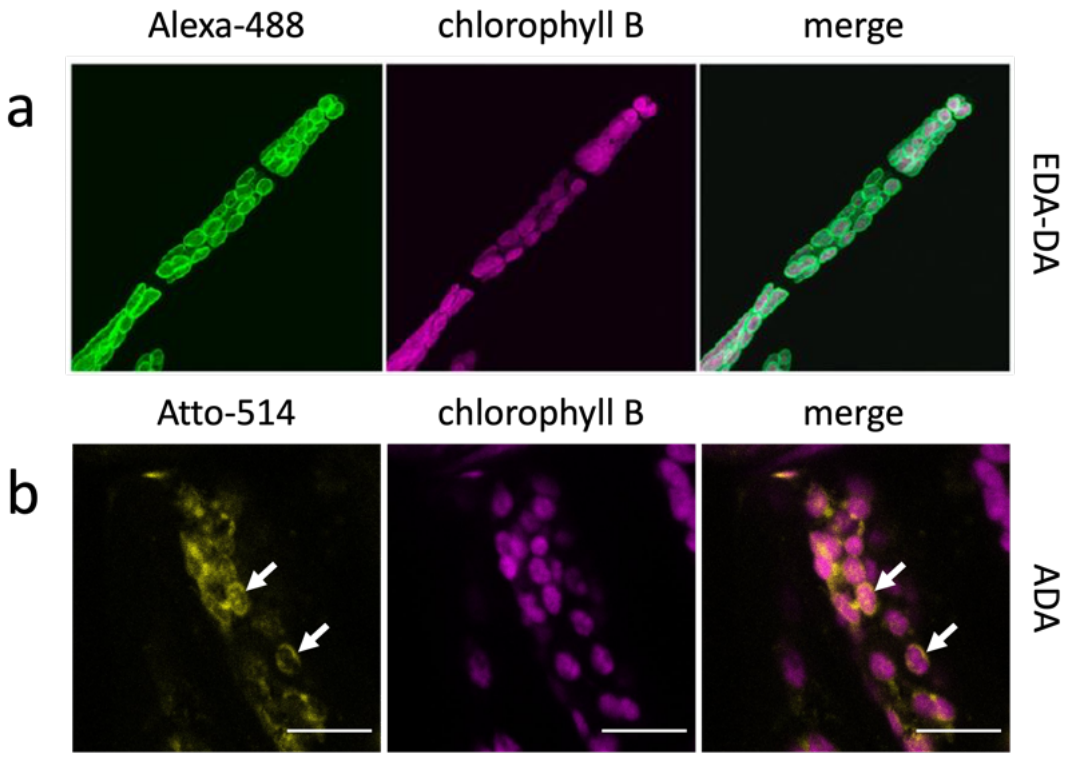

Figure 3.5: Fluorescent microscopic detection of peptidoglycan around plastids in *P. patens* protonema cells. **(a)** *Ppddl* mutants grown in liquid medium with EDA-DA. Cells were fixed and permeabilized, EDA-DA was bound to Alexa-Fluor-488-azide with click chemistry and visualized with confocal microscopy. Adapted from Hirano et al. (2016). **(b)** *P. patens* chloroplasts of wild-type protonema cells treated with ADA and Atto-514-alkyne and visualized with fluorescent confocal microscopy (scale bar 10 µm). Adapted from Tran et al. (2023).

ADA accumulates around *P. patens* chloroplasts, indicated by white arrows, which proves that azide-modified canonical amino acids were metabolized and integrated into the envelope in a similar manner as ethynylated amino acids. This experiment could prove that not just DA-DA dipeptides but also a single D-Ala amino acid derivative is incorporated by moss chloroplasts. It also demonstrates that azide-amino acids can be used in further click chemistry experiments instead of ethenyl derivatives to visualize putative PGN structures in other plant species.

3.3.2 Visualization of Canonical PGN Amino Acids in *Arabidopsis thaliana*

The labeling system with amino acid derivatives produced comparable results to published ones in non-vascular plants using azido-D-alanine instead of ethynyl-D-alanyl-D-alanine dipeptide, as this technique has not been applied in vascular plants, specifically angiosperms like *A. thaliana*. A specific protocol was developed and implemented, which is described in

Section 6.14. The D-Ala derivative ADA accumulated around chloroplasts in very specific patterns, as shown in Fig. 3.6a. White arrows point out ring-like accumulations of fluorescent dye. Another structure could also be observed, where the fluorescent signal accumulated in between two separating plastids. Blue arrows indicate these septa, which look like division planes between two dividing plastids. It was also observed that not all mesophyll cells were labeled, suggesting an incorporation of ADA only in newly formed cells (Fig. A.2).

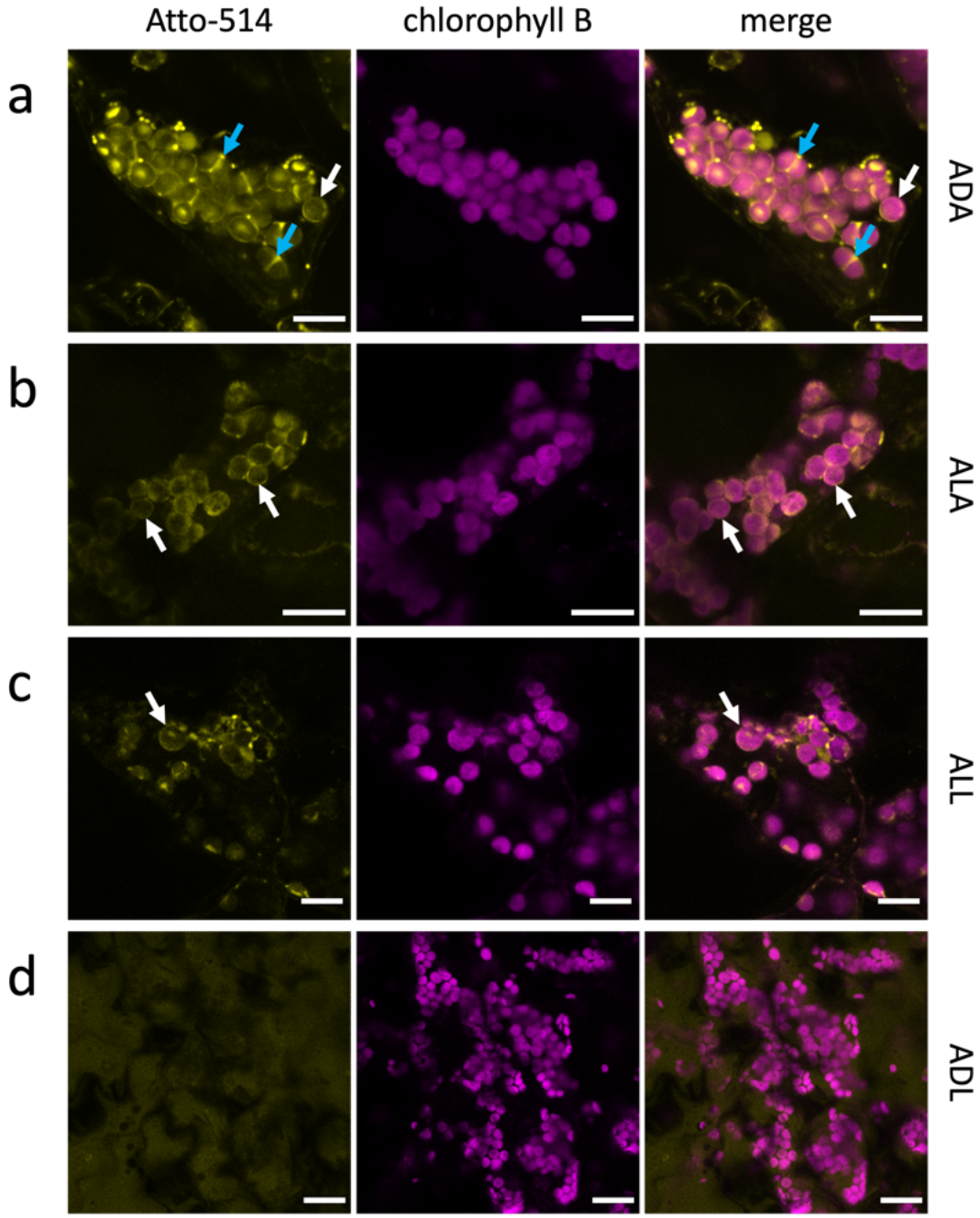

Figure 3.6: Fluorescent microscopic detection of canonical PGN amino acids around plastids in *A. thaliana* cells. *A. thaliana* chloroplasts of wild-type *Col-0* cells treated with **(a)** ADA (scale bar 10 µm), **(b)** ALA (scale bar 15 µm), **(c)** ALL (scale bar 10 µm), **(d)** azido-D-lysine (ADL) (scale bar 20 µm) and Atto-514-alkyne. White arrows indicate ring-like accumulations of azide amino acids around chloroplasts, while blue arrows show division planes of dividing plastids. Adapted from Tran et al. (2023).

This experiment was repeated with L-Ala and L-Lys, two canonical amino acids often found in bacterial PGN. The corresponding amino acid derivatives azido-L-alanine (ALA) and azido-L-lysine (ALL) appear to be incorporated in a similar manner as ADA, as shown in Fig. 3.6b and 3.6c, where fluorescent signals accumulated specifically around chloroplasts. To rule out the possibility that azide-modified amino acids are generally accumulating in this specific pattern, control experiments were carried out using an amino acid derivative, namely azido-D-lysine (ADL), which is commonly not found in any known peptidoglycan structure (Schleifer and Kandler, 1972). As seen in Fig. 3.6d, ADL showed a cytosolic localization with random distribution rather than a distinct pattern, suggesting that it is not incorporated into the same structure as ADA, ALA, and ALL.

To exclude the possibility of unspecific accumulation due to the derivatization of used amino acids and fluorescent dyes, control experiments have been carried out. Therefore, plants have been solely treated with amino acid derivatives, which are shown in Fig. A.3. It was expected that no fluorescence signal would be detected, which was true for all tested azide-modified amino acids. On the other hand, plants that have been treated solely with modified fluorescent dyes, display a rather homogeneous distribution with no distinct pattern or accumulation of fluorescent signal. Dyes were found to localize either vacuolar (Fig. A.4a) or cytosolic (Fig. A.4b, c). As previously described in Fig. 3.6d, ADL was used as a non-canonical D-amino acid derivative that localizes mainly in the cytosol with no specific pattern. These results were comparable to observations obtained for plants that had just been treated with modified fluorescent dyes (Fig. A.4c), indicating that only very specific amino acids are metabolized in a way, that they are detectable in a specific pattern.

Next, the following experiment uses the implemented click chemistry method in *A. thaliana*, to study the localization of azido-D-alanine in *Atddl* mutants. Figure 3.7 shows that fluorescent signals of ADA accumulate around *Atddl* chloroplasts, indicated by white arrows.

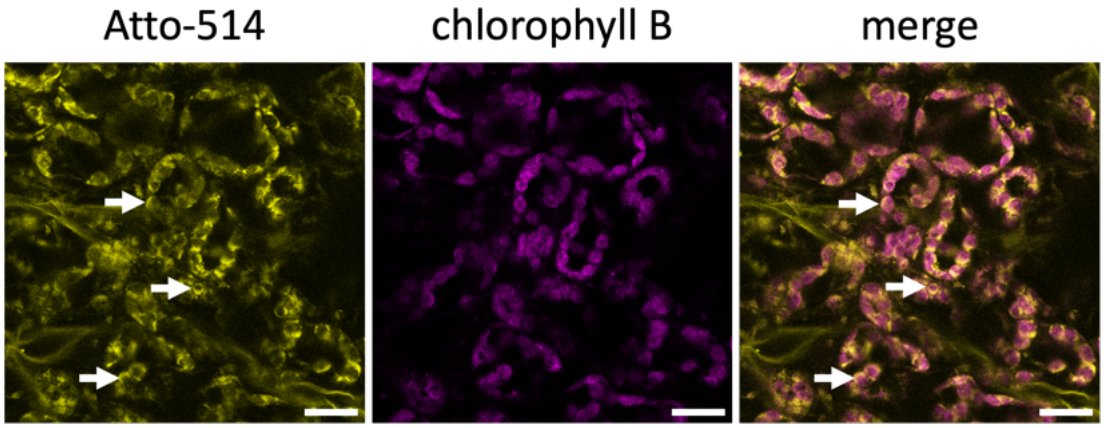

Figure 3.7: Fluorescent microscopic detection of ADA around plastids in *Atddl*-1 cells. *A. thaliana* chloroplasts of *Atddl*-1 cells treated with ADA and Atto-514-alkyne (scale bar 20 µm). White arrows indicate ring-like accumulations of ADA around *Atddl*-1 chloroplasts. Adapted from Tran et al. (2023).

These results are similar to observations seen in *A. thaliana* wild-type plants treated with ADA (Fig. 3.6a), which suggests that ADA is transported and incorporated by the used *Atddl* mutants in a similar manner as in *A. thaliana* wild-type plants. This may be ex-

plained by the enzymatic activity of the truncated AtDDL$_{\Delta N}$ protein, which is sufficient to incorporate D-Ala into the plastidic envelope.

Alternatively, click chemistry experiments for PGN labeling in *A. thaliana* were carried out to test and visualize the effect of the DDL inhibitor DCS on amino acid accumulation around plastids. Therefore, *A. thaliana* seedlings were treated with DCS and ADA simultaneously. As it can be seen in Fig. 3.8, the chlorophyll B autofluorescence of some mesophyll cells is no longer found in confined structures but rather spread all over the mesophyll cell, suggesting a disruption of their respective chloroplast. Additionally, a typical ring-like structure observed so far for ADA-treated *A. thaliana* plants, was not observable for plants treated with ADA and DCS at the same time, underpinning the observations discussed in Section 3.2. Nevertheless, some cells still show intact plastid structures, indicating that DCS impact is limited only to newly dividing cells.

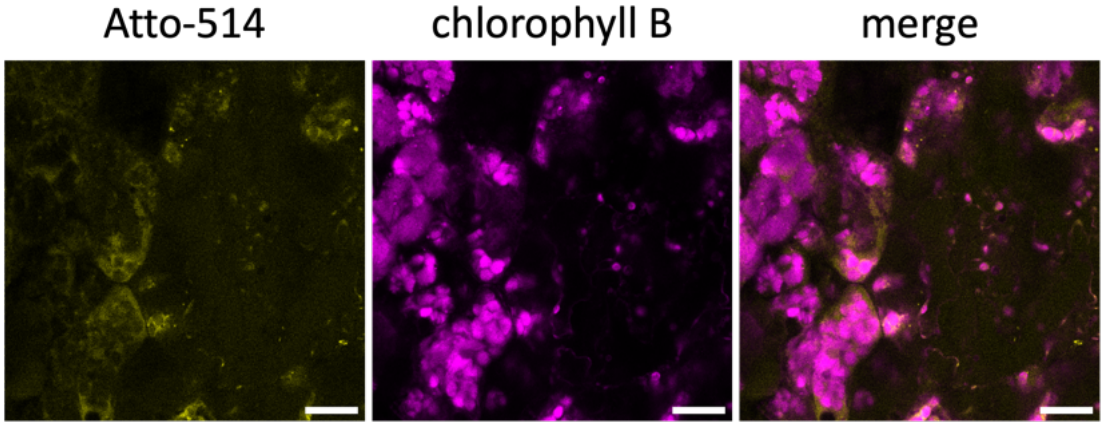

Figure 3.8: Fluorescent microscopic detection of ADA in *A. thaliana* cells with DCS treatment. *A. thaliana* chloroplasts of *Atddl*-1 cells treated with ADA, 200 µM DCS and Atto-514-alkyne show a loss of chloroplast structure and specific accumulation of fluorescent dyes inside mesophyll cells. Scale bar: 20 µm. Adapted from Tran et al. (2023).

It was shown that DCS has an impact on chloroplast genesis (Sec. 3.2), but in addition to that, it could be shown that DCS inhibits proper chloroplast division and inhibits the incorporation of PGN amino acids into the chloroplast envelope.

These experiments could show that amino acids like D-Ala, L-Ala, and L-Lys usually found in peptidoglycan were incorporated into the envelope of newly divided *A. thaliana* chloroplasts. Instead, a non-canonical amino acid – D-lysine – was not accumulating specifically around plastids, suggesting the presence of peptidoglycan in *A. thaliana* chloroplasts with a canonical amino acid of bacterial origin. These results could also prove that *Atddl* mutants did not display a changed chloroplast morphology compared to wild-type plants and were still able to incorporate ADA into their envelope, which indicates a residual activity of DDL protein in *Atddl* mutants. Since *Atddl* mutants do not display a change in chloroplast morphology, experiments were carried out to study the effect of D-cycloserine as a D-alanyl-D-alanine ligase inhibitor. DCS treatment in *A. thaliana* seedlings not only led to a disrupted chloroplast phenotype (Sec. 3.2), but was also inhibiting the incorporation of ADA into the chloroplast envelope in newly dividing mesophyll cells, suggesting a disturbed

DDL function for DA-DA synthesis. These are some indications that *A. thaliana*, a "four PGN" plant, also possesses a peptidoglycan layer in their chloroplast envelope.

3.3.3 Visualization of Canonical PGN Amino Acids in *Nicotiana benthamiana*

The click chemistry labeling technique was also used to study chloroplasts of another plant species. This time *N. benthamiana* was examined, which has a complete set of PGN-biosynthesis genes ("full PGN - PBP"), similar to mosses. *N. benthamiana* plants were treated as described in Section 6.14, and the localization of metabolized amino acid derivatives was investigated in the same way as previously described click chemistry experiments in *P. patens* and *A. thaliana*.

The localization of ADA (Fig. 3.9a), ALA (Fig. 3.9b), and ALL (Fig. 3.9c) in *N. benthamiana* leaves was detected in the typical fluorescent ring-like accumulation (white arrows). Furthermore, some putative division planes (blue arrows) in tobacco chloroplasts of newly formed mesophyll cells were observed once again, indicating a comparable uptake and incorporation of amino acid derivatives as observed in *P. patens* and *A. thaliana*.

To rule out unspecific binding of amino acid derivatives in *N. benthamiana* leaves, the same control experiments were conducted as described in Section 3.3.2. Fig. A.5a – d show leaves treated solely with azide-modified amino acids, and no fluorescent signal was observable. In plants treated with dyes only (Fig. A.5e), no distinct pattern or localization was seen, which was also true for ADL (Fig. 3.9d).

This indicates that *N. benthamiana* as well as *A. thaliana* both incorporate canonical amino acids into the chloroplast envelope in a similar manner to *P. patens*, which suggests that the peptidoglycan structure has been preserved after endosymbiosis throughout the whole plant kingdom.

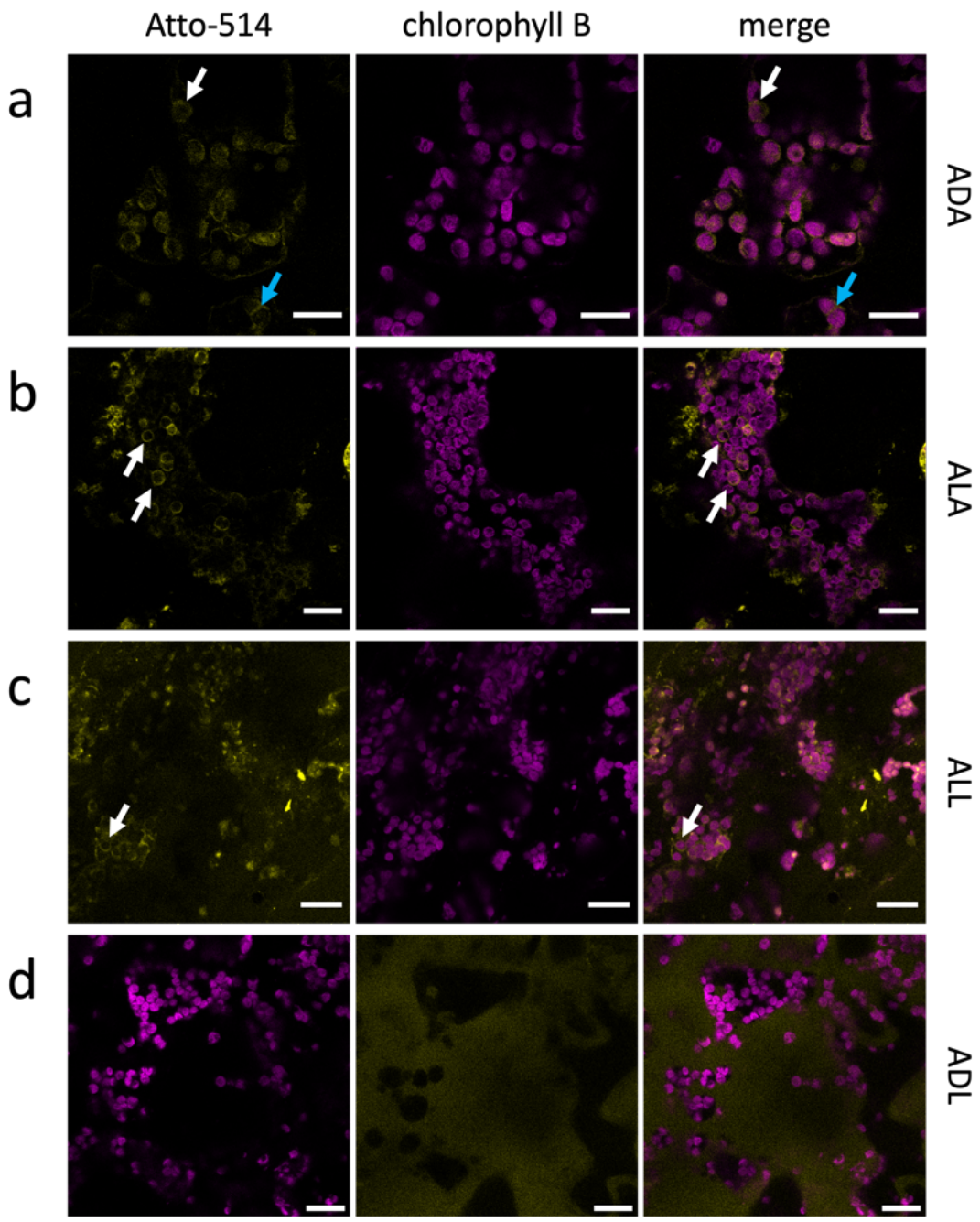

Figure 3.9: Fluorescent microscopic detection of canonical PGN amino acids around plastids in *N. benthamiana* cells. *N. benthamiana* chloroplasts of wild type cells treated with **(a)** ADA (scale bar 15 µm), **(b)** ALA (scale bar 20 µm), **(c)** ALL (scale bar 20 µm), **(d)** ADL (scale bar 20 µm) and Atto-514-alkyne. White arrows indicate ring-like accumulations of azide amino acids around chloroplasts, while blue arrows show division planes of dividing plastids. Adapted from Tran et al. (2023).

3.3.4 Visualization of Azide Modified *N*-acetylmuramic acid

In line with this topic, Haag (2023) tested the incorporation of a commercially available azide modified Mur*N*Ac molecule in click chemistry experiments. These experiments were carried out to test and verify the presence of peptidoglycan in vascular plant chloroplasts and its similarity to bacterial peptidoglycan. Therefore, the same procedure was conducted as described in Section 6.14. Mur*N*Ac-azide also accumulates in the characteristic ring-like structure around chloroplasts of *N. benthamiana* (Fig. 3.10, white arrows), as well as *A. thaliana* chloroplasts (Fig. A.7). Control experiments (Fig. A.6) show that Atto-514 signals are specific. These results support the findings about the presence of a peptidoglycan layer around chloroplasts of vascular plants with a similar molecular composition to bacterial peptidoglycan.

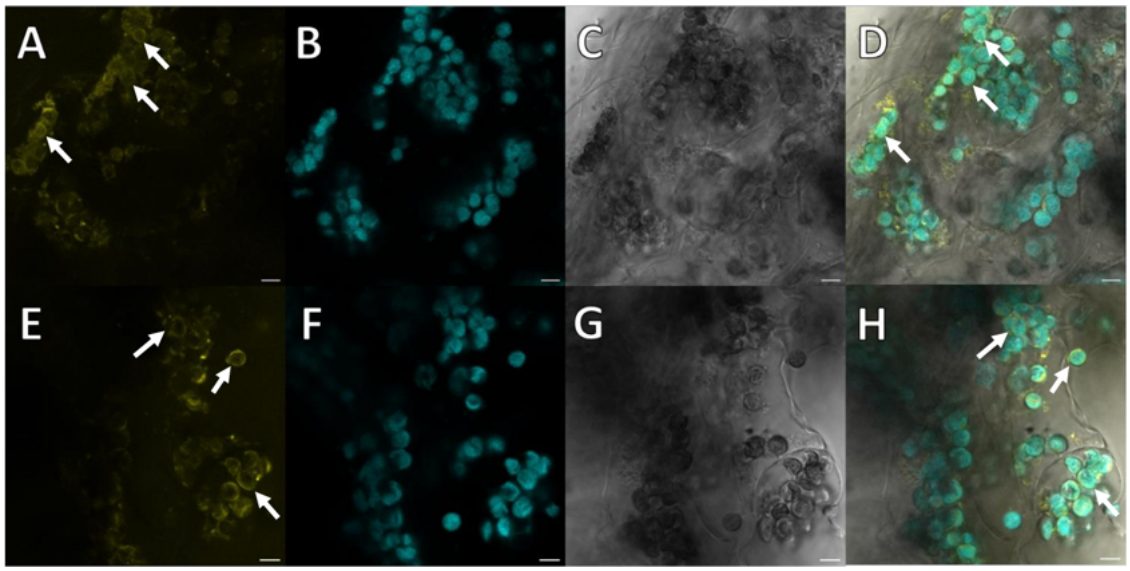

Figure 3.10: Haag (2023): Click chemistry with NAM-azide for visualization of PGN in adult *N. benthamiana* plants. Fluorescent emission was detected exciting at 514 nm. **A-H**: Nicotiana leaves infiltrated with 0.125 mM NAM-azide and cut-outs incubated in Click-iT cell reaction cocktail containing Atto-514-alkyne. **A, E** Atto-514 emission. **B, F** autofluorescence of chlorophyll. **C, G** brightfield channel. **D, H** merged image of A/E, B/F and C/G. White arrows indicate chloroplasts surrounded by fluorescent ring-like structures. The scale bar is 5 µm.

3.4 Structural Analysis of Plant Peptidoglycan

In previous sections, physiological and microscopic methods were described to analyze the composition and localization of peptidoglycan in vascular plants. The following experiments make use of naturally evolved proteins capable to recognize and binding bacterial peptidoglycan in a very specific manner (Section 1.3.2), to test if plant peptidoglycan has a similar molecular structure.

3.4.1 Microscopic and Biochemical Studies with PGN-Binding Proteins

Different proteins, able to detect a specific peptidoglycan motif, were used as intrabodies by transiently expressing them in *N. benthamiana* leaves and *A. thaliana* seedlings according to Section 6.7. Their *in vitro* localization was analyzed using confocal microscopy.

3.4.1.1 PGRPs in Transient Protein Expression Experiments

PGRPs, which are part of the innate immune system of mammals and insects, can recognize and bind peptidoglycan and kill off bacteria either directly or by activating other downstream pathways (Sec. 1.3.2). To investigate the similarity of bacterial and plant peptidoglycan, localization studies were done using peptidoglycan-recognizing proteins. Therefore, *Dm*PGRP-SA from *Drosophila melanogaster* (NM_132499.3) and *Homo sapiens* PGLYRP-1 (NM_005091.3) were selected. Both protein sequences were codon optimized for *in planta* expression. *Dm*PGRP and *Hs*PGRP without the N-terminal secretory signal peptide (first 26 and 21 encoding amino acids, respectively) were cloned into the expression vector pH7FWG2 (Gateway destination vector) with a C-terminal GFP tag. Fig. A.8 shows the coding and amino acid sequence of *Dm*PGRP$_{\Delta SP}$ and *Hs*PGRP$_{\Delta SP}$. Subsequent localization studies of transient protein expression in *N. benthamiana* leaves were carried out using confocal fluorescent microscopy (Tran et al., 2023).

Transformed *N. benthamiana* mesophyll cells with *Hs*PGRP$_{\Delta SP}$-GFP (Fig. 3.11a) and *Dm*PGRP$_{\Delta SP}$-GFP (Fig. 3.11b) show that expressed proteins appear to accumulate in and around tobacco chloroplasts. Transient PGRP expression and localization studies were repeated in *A. thaliana* seedlings. The localization of translated PGRP$_{\Delta SP}$-GFP proteins was very similar to results observed in tobacco leaves, indicating the presence of a peptidoglycan similar structure in the chloroplast envelope of both angiosperm plant species. Transient protein expression of a vector containing only GFP revealed cytosolic localization in *N. benthamiana* (Fig. A.9).

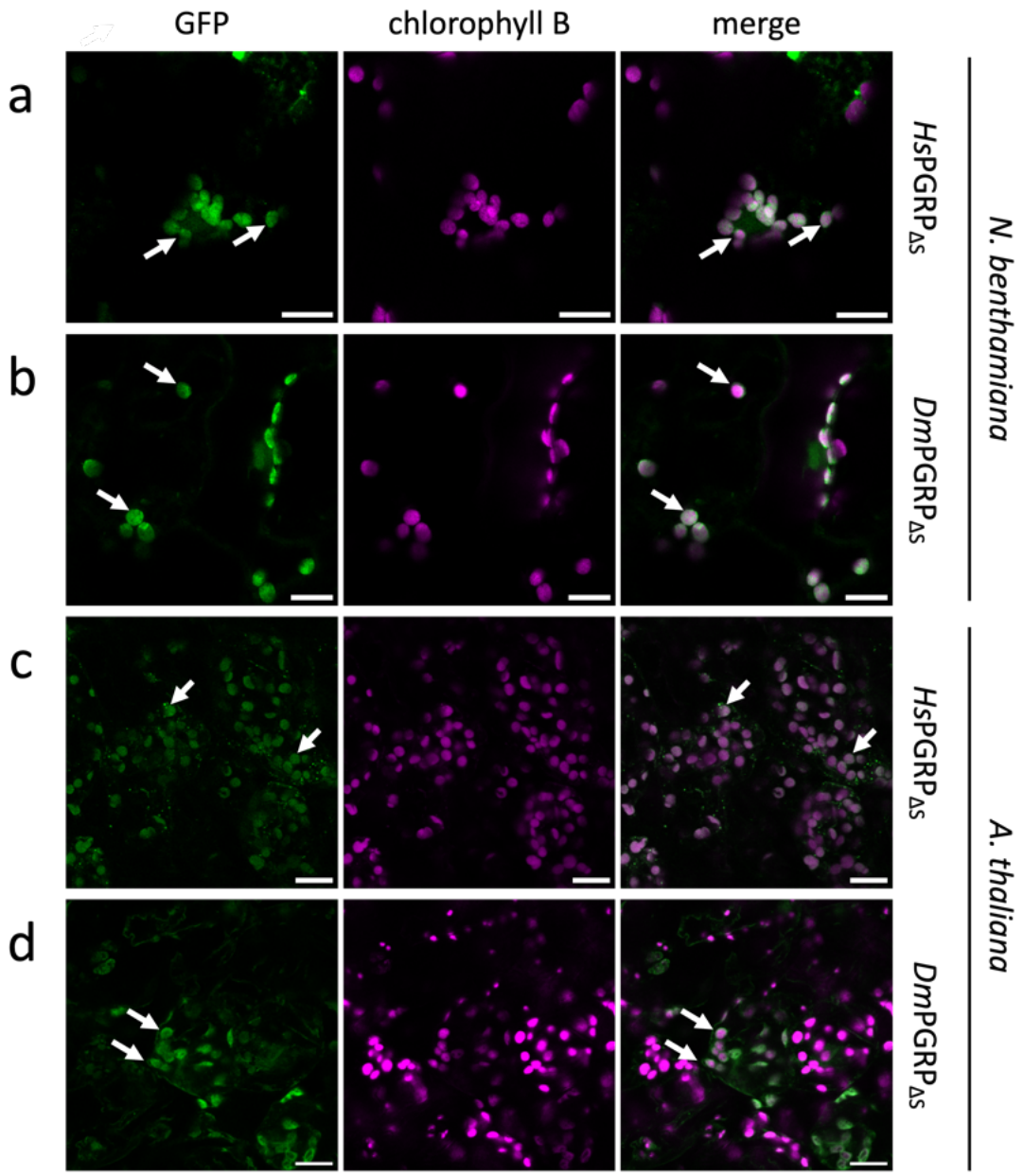

Figure 3.11: Fluorescent detection of transient protein expression of PGRPs in vascular plant cells. PGRPs localize in and around chloroplasts of *N. benthamiana* and *A. thaliana* cells. **(a)** *Hs*PGRP$_{\Delta SP}$-GFP and **(b)** *Dm*PGRP$_{\Delta SP}$-GFP are expressed and accumulate around chloroplasts in *N. benthamiana* cells (scale bars 15 µm). **(c)** *Hs*PGRP$_{\Delta SP}$-GFP and **(d)** *Dm*PGRP$_{\Delta SP}$-GFP are expressed and accumulate around chloroplasts in *A. thaliana Col-0* cells (scale bars 20 µm). Adapted from Tran et al. (2023).

3.4.1.2 *N*-acetylmuramoyl-L-alanine amidase AmiC in Transient Protein Expression Experiments

Another peptidoglycan binding protein, but of bacterial origin, was analyzed, using a similar approach of transient protein expression studies in *N. benthamiana* and *A. thaliana* plants, like in Section 3.4.1.1. PGN amidases are responsible for degradation and recycling of PGN during cell propagation. Periplasmic PGN amidases AmiA, B, and C are *N*-acetylmuramoyl-L-alanine and cleave the Mur*N*Ac-L-Ala bond of septal PGN during cytokinesis, so cell separation can occur (Heidrich et al., 2001). The *N*-acetylmuramoyl-L-alanine amidase AmiC

is required for binary fission in bacteria and usually consists of two parts: a peptidoglycan binding amidase N-terminal domain (AMIN) domain and a catalytical active domain. The localization of the AMIN domain of AmiC from *E. coli* (*Ec*AMIN) fused to GFP in tobacco mesophyll cells shown in Fig. 3.12a was similar to previously shown results for PGRPs (Fig. 3.11). Expressed proteins tend to accumulate around chloroplasts (white arrows), which was also observed in transiently transformed *A. thaliana* mesophyll cells (Fig. 3.12c). Similar experiments with a catalytical active AmiC2cat domain from *Nostoc punctiforme* (*Np*AmiC2cat) led either to a hardly detectable GFP signal or resulted in damaged chloroplasts when proteins were expressed in tobacco cells (Fig. 3.12b).

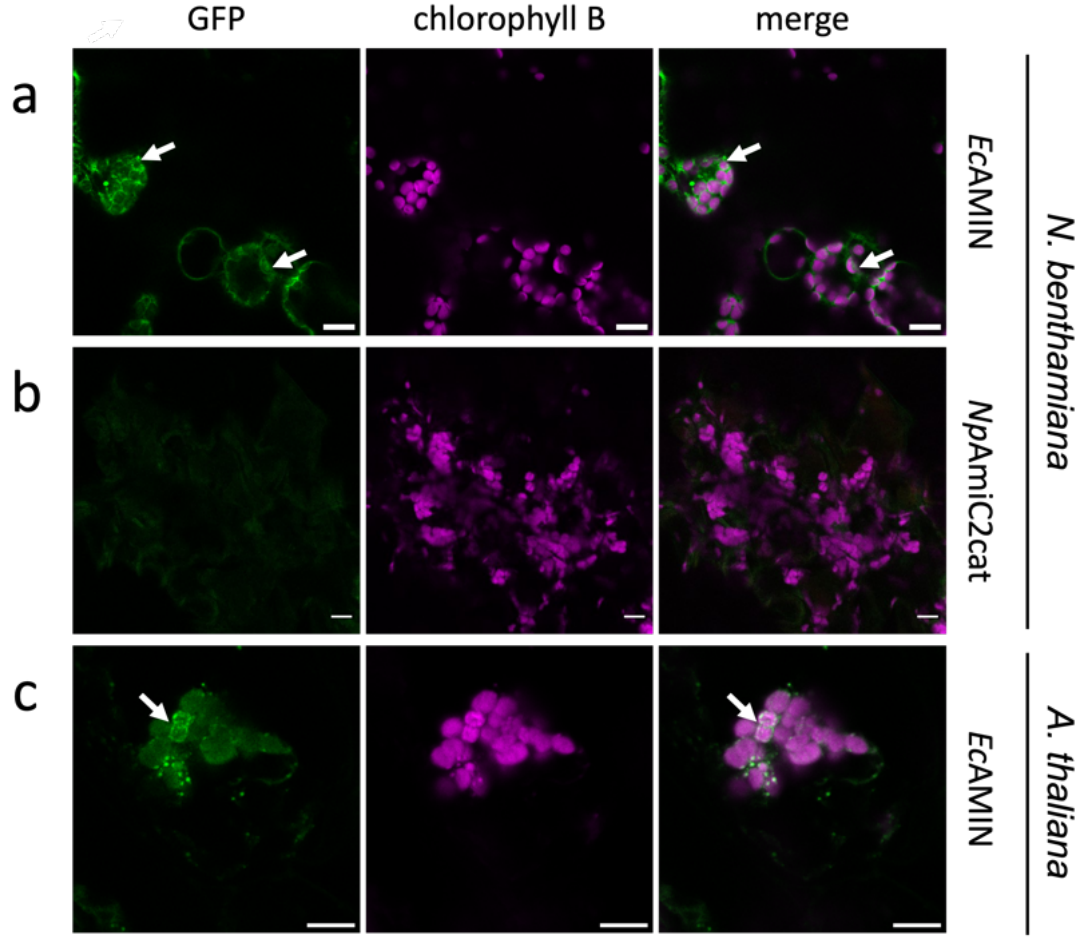

Figure 3.12: Fluorescent detection of transiently expressed *Ec*AMIN and *Np*AmiC2cat in vascular plant cells. **(a)** *Ec*AMIN is expressed and accumulates around chloroplasts of *N. benthamiana* cells (scale bar 15 µm). **(b)** *Np*AmiC2cat in *N. benthamiana* cells (scale bar 10 µm). **(a)** *Ec*AMIN is expressed and accumulates around chloroplasts of *A. thaliana* cells (scale bar 10 µm). Adapted from Tran et al. (2023).

These transient protein expression experiments revealed that a certain structure may be present in vascular plant chloroplasts, which is recognized by peptidoglycan binding proteins of various origins. Considering the specificity of these proteins to recognize and bind bacterial peptidoglycan, it is reasonable to consider that this structure may be preserved and present in *A. thaliana* and *N. benthamiana*.

3.4.1.3 Peptidoglycan Binding Assay

To verify the interaction of peptidoglycan-binding proteins with a putative plant peptidoglycan, an *in vitro* binding assay was carried out as described by Rocaboy et al. (2013) with minor modifications (see Sec. 6.11). Therefore, proteins were expressed as described in Section 6.8.1. Both proteins used in this experiment were cloned into expression vectors containing a His-tag. *Np*AmiC2cat was kindly provided by RG Forchhammer (IMIT, University of Tübingen). Bacterial and plant peptidoglycan were isolated according to Section 6.10. This method is comparable to protein immunoprecipitation, but instead of isolating a specific protein from a crude protein extract of either plants or animals using an antibody, isolated peptidoglycan is used as "bait" to verify an interaction with peptidoglycan-binding proteins.

This experiment was carried out to investigate the interaction of PGN recognizing proteins and peptidoglycan from plants. D-amino transaminase 1 from *A. thaliana* (*At*DAT1, Suarez et al. (2019)) was used as a negative control, since it does not bind bacterial peptidoglycan. Isolated peptidoglycan from *E. coli* was used as a positive control. After incubating the two PGN samples with *At*DAT1 and *Np*AmiC2cat protein crude extracts, His-tagged proteins were labeled with an α-His-tag antibody and an anti-species specific antibody fused to the reporter enzyme horseradish peroxidase (HRP) for chemiluminescence detection. Fig. 3.13 shows that no *At*DAT1 was pulled down in the pellet fraction. *Np*AmiC2cat was found in both fractions containing either *E. coli* or *A. thaliana* PGN, but not in the sample containing no peptidoglycan. These results suggest an interaction of *Np*AmiC2cat with isolated peptidoglycan from both *E. coli* as well as *A. thaliana*; hence, a structure was isolated from *A. thaliana* similar in structure to bacterial peptidoglycan.

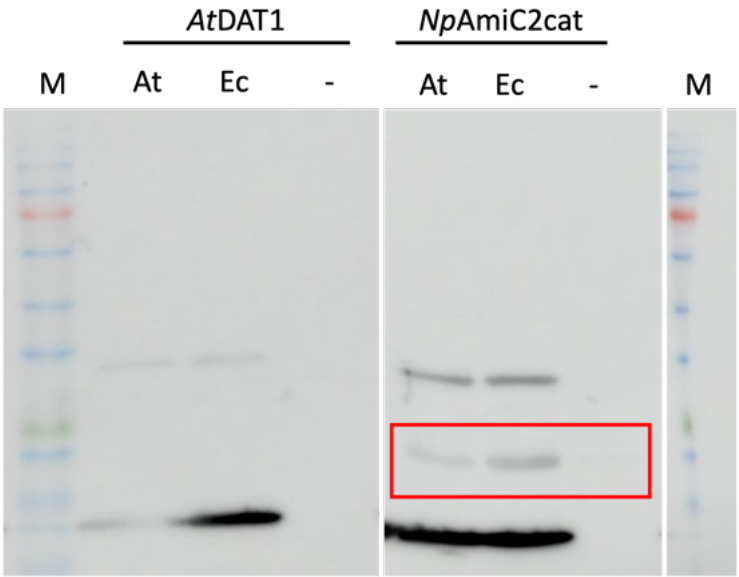

Figure 3.13: Peptidoglycan from *E. coli* and *A. thaliana* chloroplasts lead to precipitation of *Np*AmiC2cat in PGN binding assays. Pellets of *At*DAT1 (left) and *Np*AmiC2cat (right) of PGN binding assays with PGN preparations from *A. thaliana* (At), *E. coli* (Ec), and with no added PGN (–) are shown. Precipitated *Np*AmiC2cat by peptidoglycan is marked by a red box. Adapted from Tran et al. (2023).

3.4.2 Analytical Characterization of Plant Peptidoglycan

In this experiment, *E. coli* and isolated chloroplasts from *A. thaliana* were used as starting material to extract peptidoglycan according to a protocol published by Bertsche and Gust (2017) with minor modifications (see Sec. 6.10) to characterize the molecular composition of plant peptidoglycan in comparison to bacterial peptidoglycan. The supernatant of mutanolysin- and lysozyme-digested peptidoglycan was analyzed according to Kühner et al. (2014). The samples were analyzed using ultra-performance liquid chromatography mass spectrometry with electrospray ionization (UPLC/MS ES+). Fig. A.10 shows the base peak ion chromatogram of isolated peptidoglycan from *E. coli* (top) and *A. thaliana* (bottom). There are over 500 fragments found only in *E. coli*, 8 *A. thaliana* specific masses, and around 500 measured compounds that are detectable in both samples. It seems, that the extraction method used for bacterial peptidoglycan was partially successful in *A. thaliana*.

Mutanolysin and lysozyme were used to digest isolated peptidoglycan. Soluble fragments were analyzed and based on the assumption that chloroplasts came from cyanobacteria, different fragment sizes of peptidoglycan from Gram-negative bacteria were calculated. Only basic monomers and dimers with varying peptide stem lengths of Gram-negative were calculated for this analysis (see Table A.1). It does not include any peptidoglycan variation or modifications found in different bacterial species. Table 3.1 shows some m/z that were found in this data set.

Table 3.1: Peptidoglycan fragments isolated from *E. coli* and *A. thaliana* chloroplasts and detected by mass spectrometry with expected mass:charge (m/z) ratios and detected values as listed. Peptidoglycan fragments are made up of glycans Glc*N*Ac (G) and Mur*N*Ac (M), as well as canonical amino acids L-Ala, D-Glu, *m*-DAP and D-Ala.

PGN fragment	**Detected species**	**Expected m/z**	**Detected m/z**	**Found in**
G-M-L-Ala-D-Glu-*m*-DAP	(M+H)+	869.3491	869.3657	*E. coli*
G-M-L-Ala-D-Glu-*m*-DAP-D-Ala	(M+H)+	940.3952	940.4016	*E. coli*
2x(L-Ala-D-Glu-*m*-DAP-D-Ala)	(M+2H)2+	453.2163	453.2409	*E. coli*
2x(G-M-L-Ala-D-Glu-*m*-DAP)-D-Ala	(M+2H)2+	895.86195	895.8783	*E. coli*
2x(G-M-L-Ala-D-Glu-*m*-DAP-D-Ala)	(M+2H)2+	931.3879	931.3971	*E. coli*

Two peptidoglycan monomers and three dimers could be detected in the *E. coli* sample. As expected for *E. coli* as a Gram-negative bacterium, those fragments contained *m*-DAP and not L-Lys. This data set needs a more in-depth comparative analysis with either published data on other peptidoglycan fragments isolated from plants or cyanobacteria as its closest ancestor.

3.5 Biological Functions of Peptidoglycan in Plants

3.5.1 Effects of Peptidoglycan-Digesting Enzymes on Chloroplast Structure

Peptidoglycan digesting enzymes like mutanolysin and lysozyme can catalyze a hydrolysis of the β-1-4-glycosidic bond between Mur*N*Ac and Glc*N*Ac, which causes cell lysis in bacteria due to a cell wall weakening (Ragland and Criss, 2017). The following experiment was carried out as described in Section 6.13 to analyze the effect of mutanolysin and lysozyme on chloroplast structure. Hereby, the deformation of chloroplasts with and without enzymatic treatment was observed microscopically. Untreated or "intact" chloroplasts (dark gray) were defined as single, circular shaped organelles with an even envelope structure as shown in Fig. A.11. Chloroplasts with enzyme treatment that are labeled as "defect" (light gray) looked deformed, had burst, or were found in agglomerations. The following experiments were conducted to analyze these structures either by manual counting or using fluorescence-activated cell sorting (FACS).

Figure 3.14 shows a quantitative analysis by manual counting of isolated chloroplasts treated with active enzymes lysozyme (L), mutanolysin (M), or both (LM). In control samples (Fig. A.11a) without enzyme treatment, only about 20 % of chloroplasts were intact, but they were rarely found in agglomerates. Samples treated with lysozyme and lysozyme/mutanolysin (Fig. A.11b, c) formed agglomerates and had significantly fewer intact chloroplasts ($< 10\,\%$) compared to the control. Mutanolysin-only treated samples did not form agglomerates (Fig. A.11d), and quantitative analysis of the ratio of intact and defective chloroplasts had almost the same distribution as untreated samples (Keskin, 2020).

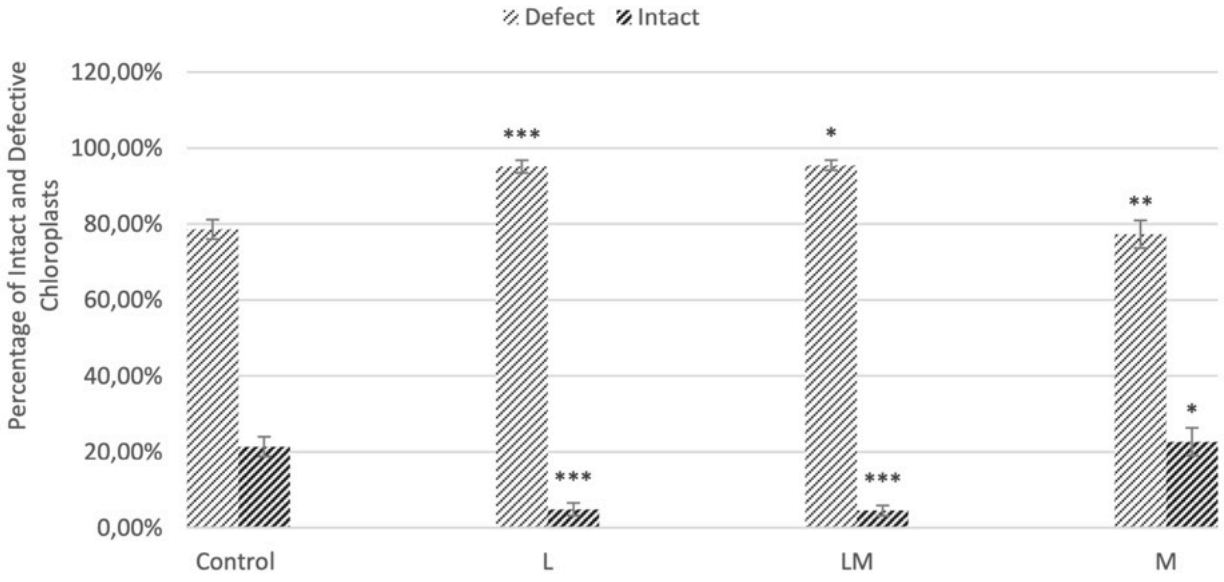

Figure 3.14: Keskin (2020): "Quantitative analysis of isolated chloroplasts after enzymatic digestion with active lysozyme (L), lysozyme and mutanolysin (LM) and mutanolysin (M). The chloroplasts were counted manually with ImageJ and classified according to their appearance over several microscopic images."

The same experiment was repeated with heat-inactivated enzymes (Fig. A.11e - g) to verify the effect of enzyme treatment. Samples treated with inactivated lysozyme (Fig. A.11e) and inactivated lysozyme/mutanolysin (Fig. A.11f) did not form agglomerates as samples treated with active enzymes did. Statistical analysis (Fig. 3.15) shows that around 19 % of chloroplasts treated with inactive lysozyme were intact. About 22 % of samples treated with inactivated lysozyme/mutanolysin were intact. The statistical significance of samples with inactivated enzyme treatment was calculated in relation to the active enzymes and indicates that the deformation was likely caused by the enzymes.

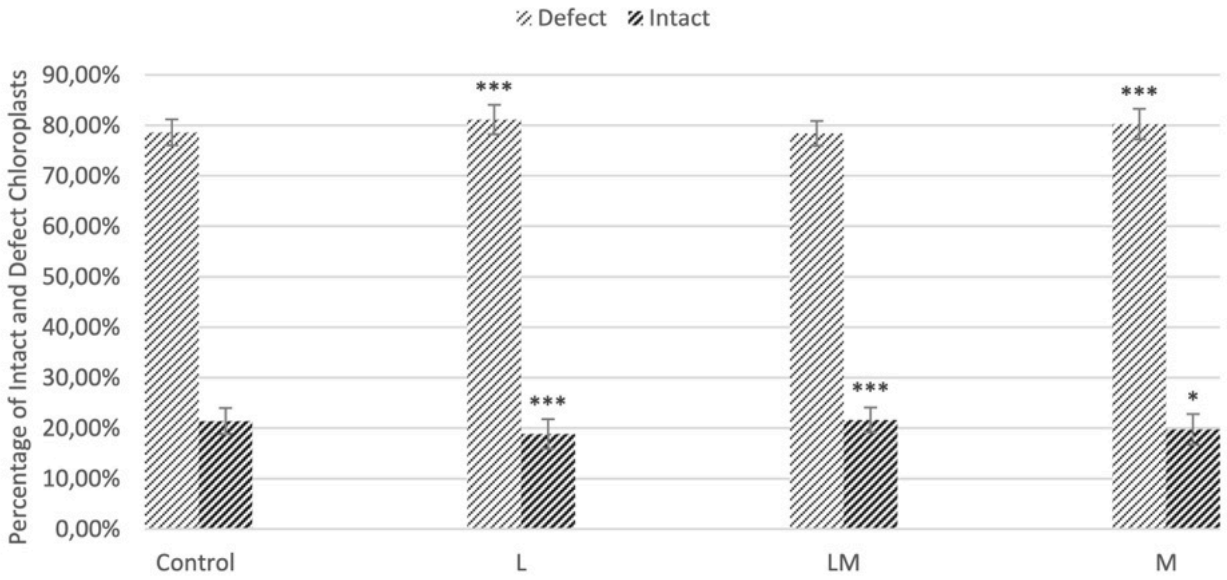

Figure 3.15: Keskin (2020): "Quantitative analysis of isolated chloroplasts after enzymatic digestion with inactive lysozyme (L), lysozyme and mutanolysin (LM) and mutanolysin (M). The chloroplasts were counted manually with ImageJ and classified according to their appearance over several microscopic images."

In another experiment FACS, was used to measure and quantify chloroplast deformation after enzyme treatment (Winkler, 2022). Therefore, chloroplasts were isolated (Sec. 6.9), treated with different concentrations of lysozyme, and analyzed with FACS (Sec. 6.13). To analyze the effect of lysozyme on chloroplast structure, the FACS parameter side scatter (SSC) was analyzed. The side scatter area (SSC-A) was plotted against the side scatter height (SSC-H) in Fig. 3.16 and shows that both the area and the height increase with increasing lysozyme concentration. An increase in SSC-A and SSC-H indicates that the samples granularity increased gradually. These results support the observation of the preceding experiments that the treatment of chloroplasts with peptidoglycan-degrading enzymes leads to their deformation.

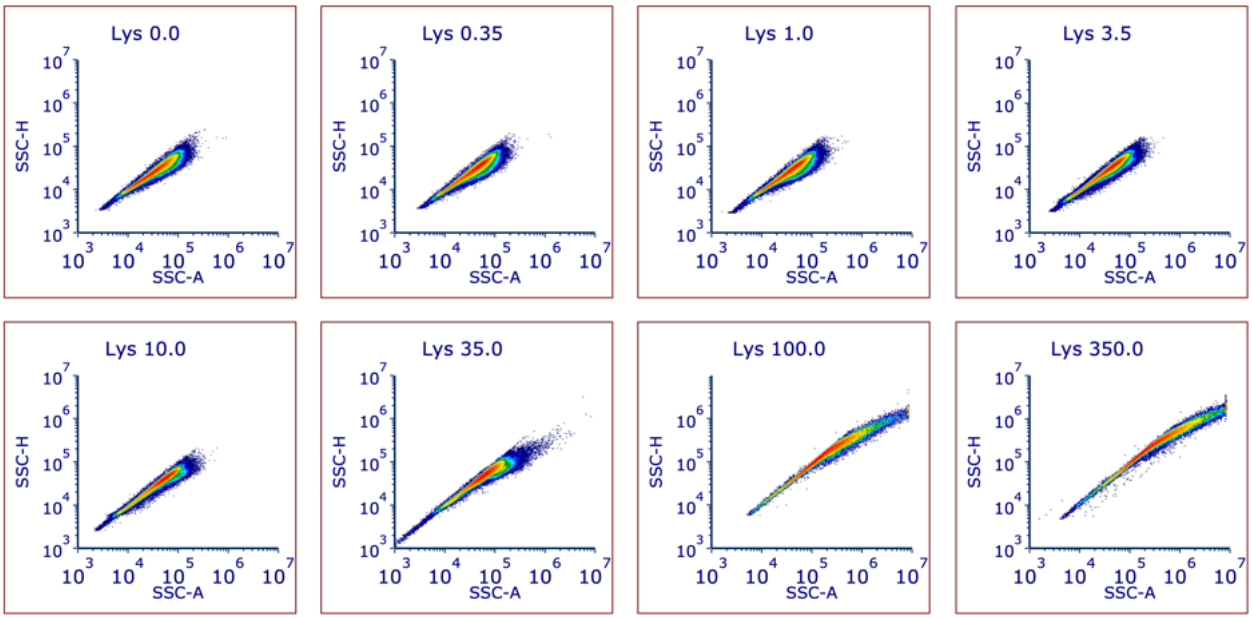

Figure 3.16: FACS analysis of isolated *A. thaliana* chloroplasts after lysozyme treatment. Side scatter of *A. thaliana* chloroplasts increases with increasing lysozyme concentration. The side scatter height (SSC-H) increases in relation to the side scatter area (SSC-A) in FACS experiments of isolated *A. thaliana* chloroplasts treated with different lysozyme concentrations (0, 0.35, 1, 3.5, 10, 35, 100, 350 µg/mL). Dr. Kenneth Berendzen (ZMBP, University of Tübingen) reanalyzed the data by Winkler (2022) used in this section and provided the graphs for this figure.

3.5.2 Analysis of *A. thaliana murE* KO Mutants

Several enzymes are involved in the synthesis of bacterial peptidoglycan. Most of the genes coding for these enzymes are still present in the genomes of various plant species (van Baren et al., 2016). A disruption of just one of these enzymes either by inhibition with antibiotics or mutations should lead to severe consequences not only in bacteria but also in mosses, as described earlier (Sec. 1.1, 3.1). To test the hypothesis for peptidoglycan in vascular plants, *A. thaliana* mutants with defective genes involved in PGN synthesis were analyzed. One of those candidates would be DDL, but it was shown earlier (Sec. 3.1) that *Atddl* mutants are phenotypically not apparently affected due to potentially remaining DDL activity in the mutant. Another PGN biosynthesis gene that was analyzed and shown to have a plastidic phenotype is MurE. Machida et al. (2006) could show that MurE was involved in plastid

division in *P. patens* (see Sec. 1.2). Therefore, the following *A. thaliana* MurE mutants (*AtmurE*) were analyzed: *AtmurE*-3 and -4 were previously characterized by Garcia et al. (2008). *AtmurE*-5 (pde316, CS16226) was an uncharacterized mutant allele with an albino or pale green phenotype described by Meinke (2020) analyzed in this work.

Mutants *AtmurE*-3 and *AtmurE*-4 contain a disruptive T-DNA insertion in the first exon. For *AtmurE*-5, it was found that part of the first exon and the whole second exon were deleted (Fig. 3.17a). To confirm the loss of transcription of the MurE gene in this mutant, an RT-PCR was carried out. No transcript was detectable (Fig. 3.17b). Homozygous seedlings had a pale green phenotype (Fig. 3.17c), similar to previously described *AtmurE* mutants (Garcia et al., 2008).

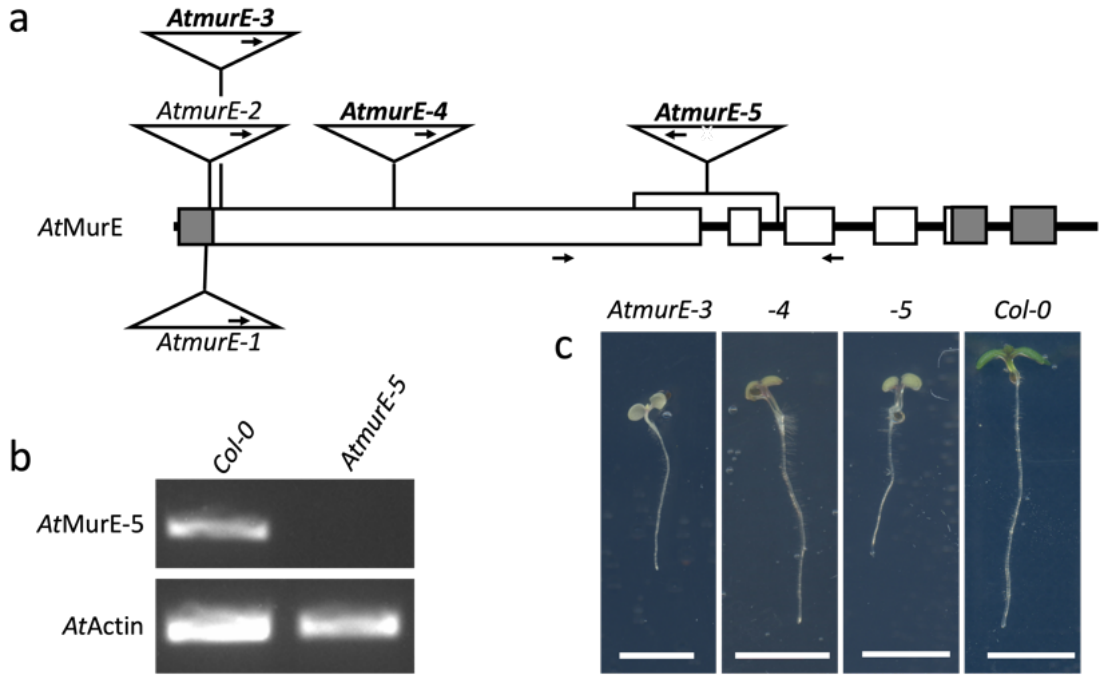

Figure 3.17: Peptidoglycan synthesis gene MurE in *A. thaliana* (*AtmurE*). **(a)** Structure of the MurE from *A. thaliana* (*At*MurE) gene. Exons are represented by black boxes and introns by black lines. Positions of T-DNA insertion sites of *AtmurE*-1 to -5 are marked by triangles. Arrows in the triangles indicate position of left border in the insertions. **(b)** RT-PCR analysis of *At*MurE-5 in *AtmurE*-5 and corresponding wild type seedlings (*Col-0*). Expression of *At*MurE-5 is shown in the upper row, whereas expression of constitutive control (*At*Actin2) is shown below. **(c)** Phenotype o *AtmurE*-3, *AtmurE*-4, *AtmurE*-5 and corresponding wild-type seedlings. Scale bar 5 mm. Adapted from Tran et al. (2023).

Fig. 3.18a and 3.18b show microscopic images of *P. patens* protonema cells (Garcia et al., 2008). Plastids of *P. patens* MurE mutants were disrupted in their division and had a giant chloroplast phenotype similar to *Ppddl* analyzed by Hirano et al. (2016) (see Sec. 3.1). In comparison to that, *AtmurE*-3, -4, and -5 homozygous seedlings had defective plastids (Fig. 3.18c - e). In comparison to the wild type (Fig. 3.18f), a distinct chloroplast structure was not observable. There is a structure similar to plastids, but they contain little to no chlorophyll, resulting in a pale green phenotype. The shape and number are also very different from the wild type. In contrast to *P. patens* MurE mutants, a giant chloroplast phenotype is not observable in *A. thaliana* MurE plants.

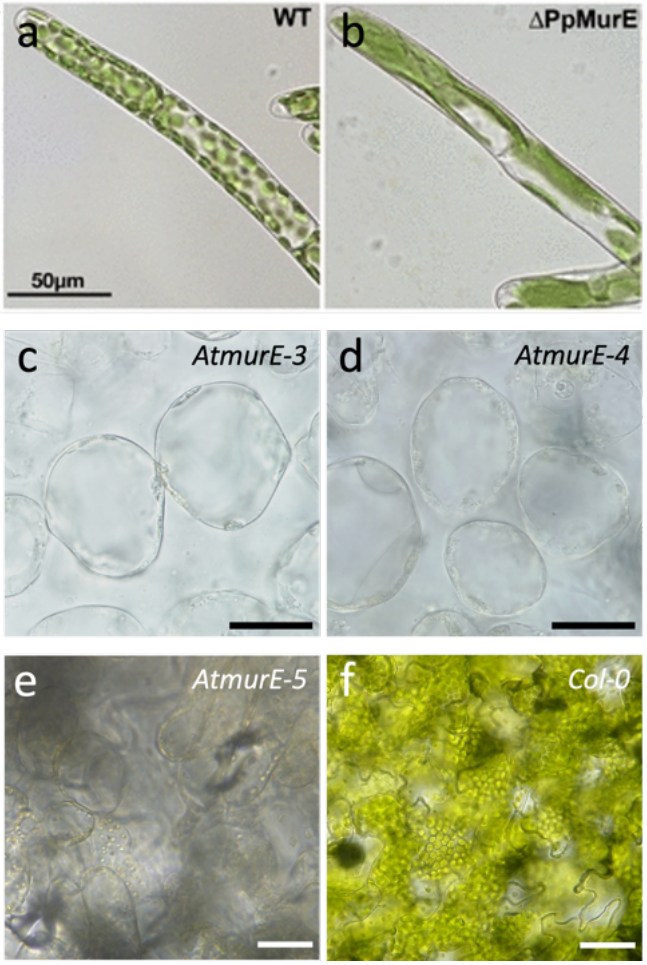

Figure 3.18: Microscopic bright field images of *P. patens* and *A. thaliana* MurE mutants. **(a, b)** *P. patens* protonema cells of the wild-type plants (WT) contained a normal number chloroplasts per cell, whereas the *PpmurE* KO lines (ΔPpMurE) contained macrochloroplasts. Adapted from Garcia et al. (2008). **(c - e)** *A. thaliana* mesophyll cells of *AtmurE*-3, *AtmurE*-4 and *AtmurE*-5 had no distinct chloroplast structure and little to no chlorophyll (scale bar 30 µm). **(f)** *A. thaliana* mesophyll cell of *Col-0* wild type contained spherical to oval shaped chloroplasts (scale bar 30 µm). Adapted from Tran et al. (2023).

In click chemistry experiments with *AtmurE*-5, canonical PGN amino acid derivatives did not accumulate around chloroplasts to form ring-like structures, indicating a disruption of the plastidic envelope in this mutant (Fig. 3.19) compared to the wild type (Fig. 3.6). The fluorescent signal is found in remaining plastid-like structures inside mesophyll cells. No autofluorescence was detectable due to a lack of chlorophyll in pale green seedlings; therefore, a plastid marker from Nelson et al. (2007) was used to visualize chloroplast remnants.

In addition to that, transient protein expression of *AtmurE*-3 mutants with peptidoglycan-recognizing enzymes *Hs*PGRP$_{\Delta SP}$-GFP, *Dm*PGRP$_{\Delta SP}$-GFP and *Ec*AMIN-GFP (see Sec. 3.4.1.1) also resulted in the loss of a characteristic accumulation around chloroplasts (Fig. A.12).

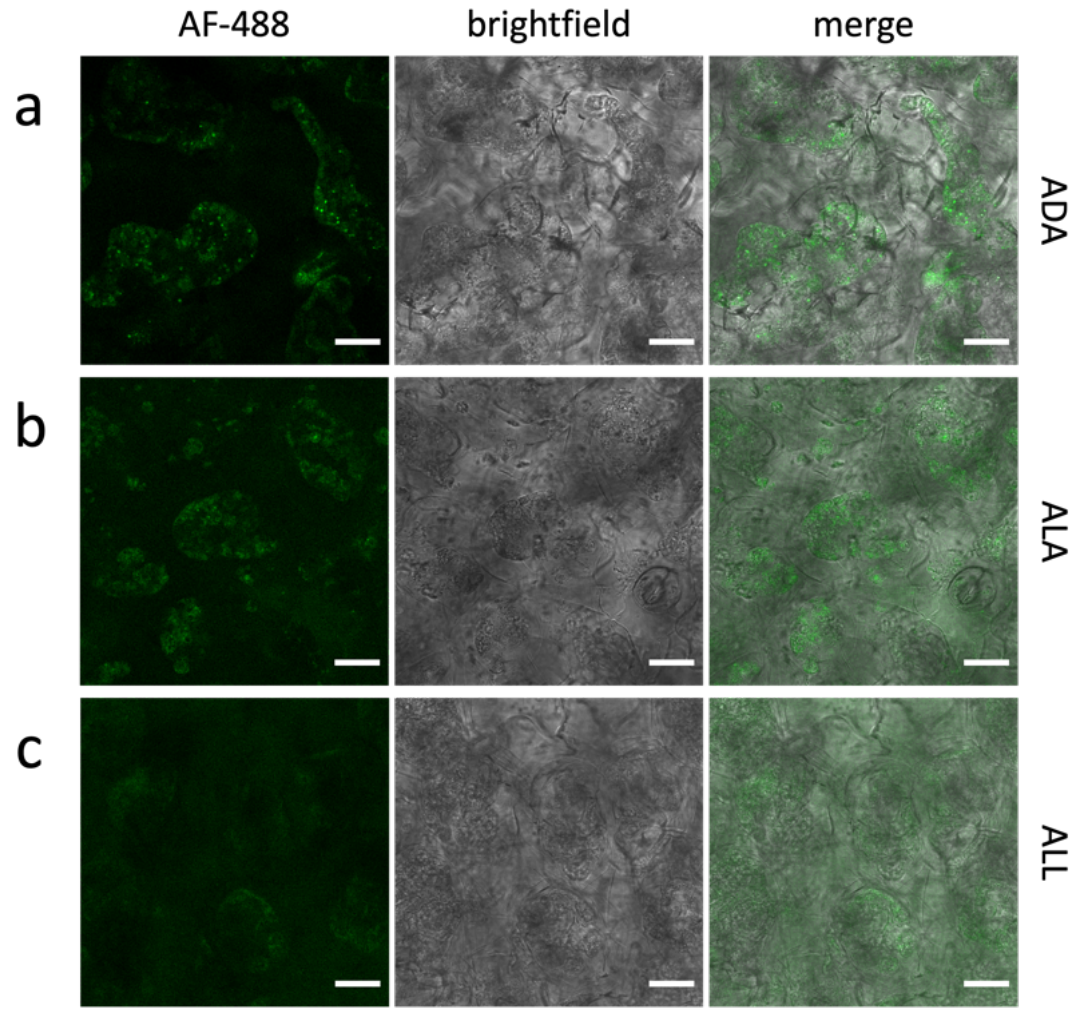

Figure 3.19: Fluorescent microscopic detection of azide amino acids in *AtmurE*-5 cells. *A. thaliana* chloroplasts of *AtmurE*-5 cells treated with **(a)** ADA, **(b)** ALA, **(c)** ALL and Atto-514-alkyne (scale bar 20 µm). Adapted from Tran et al. (2023).

4 Discussion

Nearly all bacteria share the distinctive feature of a unique peptidoglycan cell wall, a key evolutionary development that provided protection against mechanical lysis and osmotic pressure and helped dictate the cell's shape, growth, and proliferation (Errington, 2013). According to the endosymbiotic theory, eukaryotic energy-generating organelles, mitochondria and plastids originated billions of years ago through endosymbiosis between an ancient eukaryotic cell and bacteria (see Sec. 1). While it was initially thought that peptidoglycan was lost in these organelles during evolution, it was discovered around the 2000s that this crucial macromolecule has been retained in the plastids of streptophytes, glaucophytes, and bryophytes. Björn (2020) speculated that peptidoglycan in lycophytes might contribute to desiccation tolerance in some species. Dowson et al. (2022) suggested that the mature peptidoglycan in streptophytes must be modified to distinguish it from pathogens, as they evolved an immune system that includes proteins like LysM to recognize bacterial PGN-derived motifs (see Gust (2015) for more details). Around the same time, it was shown that several peptidoglycan biosynthesis genes are present in the genomes of both non-vascular and vascular plants, raising questions about their function in the plant kingdom (van Baren et al., 2016).

It remained unclear whether the bacterial peptidoglycan layer persisted in the plastid envelope throughout evolution up to today's vascular plants, including angiosperms, the youngest yet most abundant plant group. All agriculturally important plants, such as rice, maize, and wheat, belong to this group. This study provided several lines of evidence indicating that plastids of vascular plants are also surrounded by a peptidoglycan layer.

4.1 Peptidoglycan in Vascular Plants and Its Molecular Composition

4.1.1 Fluorescent Localization of Peptidoglycan Components in Plants

To investigate whether peptidoglycan is present in plants, a relatively new two-step labeling technique was employed to detect PGN components. This method involves the uptake and metabolism of a modified molecule by the organism *in vivo*. In the second step, the incorporated molecule is tagged with a fluorescent dye, which can be detected using fluorescence microscopy. This approach has been successfully applied to label peptidoglycan in bacteria and mosses. Liechti et al. (2013) utilized this technique to visualize the cell wall in *Chlamydia trachomatis*. Despite the availability of all PGN biosynthesis genes and the species' susceptibility to PGN-targeting antibiotics, classical attempts to detect and isolate peptidoglycan had been unsuccessful. This issue, known as the "chlamydial anomaly", was resolved using this new labeling method.

Higuchi et al. (2016) employed this method to visualize peptidoglycan in the Glaucophyte *Cyanophora paradoxa*, supporting the findings of Pfanzagl et al. (1996), who elucidated the primary structure of the cyanelle. Similarly, *P. patens* (a full PGN plant) possesses all ten genes necessary for PGN biosynthesis. It was previously believed that peptidoglycan, as an envelope component, was lost during the evolution of all green plants, including mosses and ferns. However, Hirano et al. (2016) utilized click chemistry to successfully localize and visualize a peptidoglycan component in *P. patens*. These results indicated that glaucophytes and mosses have retained a peptidoglycan wall around their chloroplasts, similar to their cyanobacterial ancestor.

Since the goal of this work had been to find different lines of evidence for peptidoglycan in the evolutionary younger vascular seed plants, the two-step metabolic labeling technique was used in this study to visualize peptidoglycan components in vascular plant species. To establish visualization of peptidoglycan in vascular plants using the same technique as Hirano et al. (2016), it was first tested if commercially available azide-modified amino acids can be used instead of EDA or EDA-DA, as the synthesis and purification of ethenyl derivatives can be complicated and time consuming. In a similar experimental setup, azido-D-alanine (ADA) was used as a D-alanine analogue instead of EDA-DA, and comparable results were obtained. In these proof-of-concept experiments, an accumulation of Atto-514-alkine signal around chloroplasts of *P. patens* protonema cells in a ring-like structure could be detected (Fig. 3.5). This suggests that azide-modified amino acids are taken up and metabolized in a similar way to ethenyl-modified amino acids and can be used in further click chemistry experiments to visualize peptidoglycan in plants.

The same approach was repeated in angiosperms to see if plant peptidoglycan may also be preserved in evolutionary younger plant species. Therefore, *A. thaliana* was tested using azide derivatives of canonical peptidoglycan amino acids (D-alanine, L-alanine, and L-lysine). These experiments were able to demonstrate that all three tested amino acid derivatives were accumulating around chloroplasts in a similar ring-like structure that was observed in *P. patens* protonema cells. In some cases, fluorescence signals could be detected, which resemble division planes in between two chloroplasts (Fig. 3.6). Control studies were conducted to rule out the possibility of azide-modified amino acids generally accumulating in this particular ring-like structure. Therefore azido-D-lysine was tested, which is commonly not found in any known peptidoglycan structure. It localized in the cytosol and was rather randomly distributed than found in distinct patterns. These results showed that chloroplasts of *A. thaliana* incorporate canonical peptidoglycan amino acids into their envelope similar to Glaucophytes and mosses, suggesting the presence of a structure similar to bacterial peptidoglycan.

N. benthamiana as another angiosperm was also tested to see if peptidoglycan is found in vascular plant species in general or if *A. thaliana* is an exception. Here, one can also find that D-alanine, L-alanine, and L-lysine azides were found in previously described distinct structures around chloroplasts. This means that canonical D- and L-amino acids could be found in two angiosperm species, suggesting that a peptide structure similar to bacterial peptidoglycan is conserved in the plastidic envelope of more than one angiosperm species.

Since amino acids typically found in bacterial peptidoglycan were shown to be incorporated into the chloroplast envelope of angiosperms, it suggested that not only the peptidoglycan oligopeptide chain remained largely unchanged, but also its sugar backbone. As detailed in Section 1.1, PGN consists of a backbone composed of two alternating sugars and an oligopeptide chain attached to Mur*N*Ac, which cross-links adjacent peptidoglycan chains to form a mesh-like structure around the cell. Given that three canonical amino acids of bacterial peptidoglycan are incorporated into plastid envelopes, we investigated whether the sugar backbone might also be similar in plant peptidoglycan. Consequently, Haag (2023) used the same click chemistry labeling technique described in Section 3.3.4 to test if plant peptidoglycan incorporates Mur*N*Ac into the plastid envelope. Similar to the tested canonical amino acids, Mur*N*Ac-azide was also observed agglomerating around the chloroplasts of *N. benthamiana* and *A. thaliana*, suggesting that the molecular composition of peptidoglycan in plants is comparable to that in bacteria.

4.1.2 Molecular and Structural Composition of Peptidoglycan in Plants

As described in Section 1.1, cyanobacteria are classified as Gram-negative, although their peptidoglycan layer is generally much thicker compared to other Gram-negative bacteria. Comparative phylogenetic analysis suggests that plastids most likely originated from heterocyst-forming filamentous cyanobacteria (Deusch et al., 2008).

Pfanzagl et al. (1996) analyzed the primary peptidoglycan structure of chloroplasts (cyanelles) of the Glaucophyte *Cyanophora paradoxa*. They isolated PGN monomers that are also found in *E. coli* (Mur*N*Ac-L-Ala-D-Glu-*m*-DAP, Mur*N*Ac-L-Ala-D-Glu-*m*-DAP-D-Ala). *O*-acetylation of glycans is usually part of the peptidoglycan maturation process. It is a modification that occurs after PGN synthesis and assembly (Sychantha et al., 2018). No *O*-acetylation was detected in cyanelle peptidoglycan. PGN chains are cross-linked between D-Ala and *m*-DAP. A significant modification was found in cyanelle peptidoglycan. Hereby, the 1-carboxyl group of glutamic acid is amidated with *N*-acetylputrescine (NAP), which has not been found in bacterial peptidoglycan yet. About 40 – 60 % of PGN subunits are modified with NAP. Cyanelle peptidoglycan is thinner compared to cyanobacterial peptidoglycan with less cross-linkage of PGN chains. Pfanzagl et al. (1996) proposed that the reduced thickness of this organelle helps to facilitate higher protein import from the cytoplasm. Glaucophytes were shown to have a peptidoglycan composition similar to Gram-negative bacteria but have modifications significantly different from any known bacterial PGN.

Since the concept of plant peptidoglycan is fairly new, the exact composition of PGN from different plant species is still elusive. Dowson et al. (2022) were one of the first groups to detect peptidoglycan precursors in *P. patens*. They used different antibiotics to facilitate the accumulation of PGN intermediates, which were then analyzed by mass spectrophotometric analysis of the trichloroacetic acid extracted metabolome. They were able to extract and detect UDP-Mur*N*Ac-L-Ala-D-Glu-*m*-DAP and UDP-Mur*N*Ac-L-Ala-D-Glu-*m*-DAP-

D-Ala-D-Ala among others. Since *m*-DAP is usually incorporated during peptidoglycan biosynthesis by Gram-negative bacteria, they concluded that *P. patens* uses the same precursors and its peptidoglycan is more similar to Gram-negative than -positive bacteria.

A first approach isolating peptidoglycan from vascular plants was conducted in this study. Therefore, the peptidoglycan isolation protocol by Bertsche and Gust (2017) was used to isolate and analyze peptidoglycan from *E. coli* as a control sample and from *A. thaliana* isolated chloroplasts to see if PGN fragments can be isolated and are detectable. Fragments from an UPLC/MS analysis of peptidoglycan isolated from *A. thaliana* chloroplasts and from *E. coli* were analyzed in Section 3.4.2. As expected, a few fragments were detected in the *E. coli* sample, that have the same mass as calculated PGN fragments from Gram-negative bacteria. A lot of *E. coli* specific masses, but also around 500 masses could be detected in both *E. coli* and *A. thaliana* chloroplasts. No Gram-negative specific fragments could be detected in the *A. thaliana* sample. It is important to notice that only the basic structure of peptidoglycan from Gram-negative bacteria and no modifications were considered for this preliminary analysis.

These results show that a PGN isolation protocol for bacteria was successfully applied to isolate yet unknown fragments from *A. thaliana* chloroplasts. Further data analysis is needed for this specific data set, where other PGN modifications, but also Gram-positive peptidoglycan fragments, should be included. Special attention should be paid to published peptidoglycan structures from cyanobacteria, since it is expected that peptidoglycan from chloroplasts might be more similar to cyanobacterial peptidoglycan as plastids originated from them according to the endosymbiotic theory.

Another argument for the comparison of plant peptidoglycan to PGN of Gram-positive bacteria is the incorporation of L-Lys into the plastidic envelope (see Section 3.6). L-lysine is usually found in Gram-positive bacteria in the third position of the pentapeptide chain of peptidoglycan. If we assume that *A. thaliana* incorporates L-Lys into their chloroplast envelope, *A. thaliana* may produce PGN fragments more similar to Gram-positive bacteria. This would in turn be an explanation as to why no Gram-negative PGN fragments could be identified in UPLC/MS experiments for *A. thaliana* samples so far. Repeating the PGN isolation with the right control sample (a Gram-positive bacterium) should result in the isolation of PGN fragments, which can be compared to the fragments isolated from *A. thaliana* chloroplasts.

Another approach to tackle this problem could be to isolate and test peptidoglycan from a vascular plant with a full PGN set (- PBP) like *N. benthamiana*. Therefore, the isolation of peptidoglycan from *Nicotiana* chloroplasts and subsequent UPLC/MS analysis can be conducted similar to PGN isolation from *A. thaliana*. A plant species with a nearly full PGN set may synthesize peptidoglycan fragments similar to mosses, which will be discussed later.

As an alternative to the molecular characterization of plant peptidoglycan, localization studies were carried out with transiently expressed GFP-tagged proteins, able to bind specific motifs of bacterial peptidoglycan. Due to their specific binding properties, these proteins were used as intrabodies to detect peptidoglycan *in planta*. Therefore, bacterial- and animal-

derived PGN-binding proteins with inherently different functions were chosen and transiently expressed in the two angiosperms, *A. thaliana* and *N. benthamiana*.

Different bacterial enzymes target the PGN macromolecule to cleave amide and glycosidic bonds to make space for new PGN monomers to be inserted. Rocaboy et al. (2013) solved the crystal structure of AmiC, which is a cell division Mur*N*Ac-L-Ala amidase and consists of two domains. The amidase N-terminal domain (AMIN) and the catalytic domain. "Because the AMIN domain is known to be sufficient for the localization of AmiC at the division site, it likely recognizes a specific characteristic of the septal peptidoglycan which remains, however, to be identified". They could show that the AMIN domain of AmiC from *E. coli* (*Ec*AMIN) directly interacts with peptidoglycan in pull-down assays. We used this characteristic in this study to test if *Ec*AMIN also recognizes a putative peptidoglycan structure in vascular plants. In Section 3.4.1.2, *Ec*AMIN was cloned into an expression vector with a GFP tag and transiently expressed in both tobacco leaves and *A. thaliana* seedlings. *Ec*AMIN accumulated in and around *Arabidopsis* and *Nicotiana* chloroplasts.

Although the oligopeptide chain in peptidoglycan with its alternating L- and D-amino acids gives it its unique feature, making it resistant to conventional peptidases, animals, including insects, adapted and started to produce proteins that recognize these features of bacterial peptidoglycan. In Section 3.4.1.1, peptidoglycan-recognizing proteins from human and fruit fly (*D. melanogaster*) were utilized to investigate the similarity between bacterial and plant peptidoglycan. PGRPs, integral to the innate immune systems of animals and insects, possess an active binding site that recognizes Mur*N*Ac and the first three amino acids of peptidoglycan (see Sec. 1.3.2 for further details). PGRPs from humans and fruit flies were tagged with a genetic GFP marker. These proteins were cloned without a secretory peptide and transiently transformed into *A. thaliana* and *N. benthamiana* to study their localization *in planta*. Both proteins accumulated in and around chloroplasts, suggesting the presence of a structure similar to bacterial peptidoglycan.

*Dm*PGRP (PGRP-SA) binds preferably Lys-type peptidoglycan (Swaminathan et al., 2006), whereas *Hs*PGRP (PGLYRP-1) can bind both Lys- and DAP-type PGN (Wang et al., 2007; Slonova et al., 2020). Having both PGRPs accumulating in and around *Arabidopsis* and *Nicotiana* chloroplasts may indicate the structure of peptidoglycan present in vascular plants. Including data obtained from click chemistry experiments in Section 3.3, one can assume that both plant species produce Lys-type peptidoglycan intermediates.

To detect plant peptidoglycan in a non-microscopic way, *Np*AmiC2cat was tested in an *in vitro* peptidoglycan binding assay described by Rocaboy et al. (2013), analogous to an immunoprecipitation. Peptidoglycan from *E. coli* and *A. thaliana* chloroplasts was isolated according to Bertsche and Gust (2017) and incubated with a *Np*AmiC2cat protein extract. As described in Section 3.4.1.3, *Np*AmiC2cat was able to bind isolated bacterial and plant PGN, indicating that a structure similar to bacterial PGN could be isolated from *A. thaliana* chloroplasts that can be recognized by a peptidoglycan-binding protein with cyanobacterial origin.

In Section 3.5.1, tests with lysozyme and mutanolysin were conducted and showed that these enzymes caused agglomeration of isolated *A. thaliana* chloroplasts. In further analysis,

the effect of lysozyme on chloroplast structure was tested and analyzed with FACS. Hereby, a gradual increase of granularity was observed, which led to the assumption that lysozyme makes the chloroplast envelope to become looser or less stable, which increases the area of its surface, leading to an increase in side scatter. At a certain concentration, chloroplasts agglomerated, creating an even bigger surface. This agglomeration is likely due to an accumulation of chloroplasts around bigger lysozyme crystals since it does not dissolve fully in the buffer or solvent (data not shown). Based on these results, we conclude that *A. thaliana* chloroplasts must have a structure, most likely peptidoglycan, that is detected by lysozyme.

In another experiment, Dr. Louis-Philippe Maier (ZMBP, University of Tübingen; data not shown) investigated the perception of chloroplast peptidoglycan in *Arabidopsis*. The extracellular alkalinization response was measured following PGN addition, but no changes were observed. One suggestion for this observation was that the PGN isolation protocol might not be suitable for this assay, as the enzymatic digestion could have resulted in the production of glycan fragments that are too short to be recognized by plants (Gust, 2015).

An alternative explanation could be that the structure of plant peptidoglycan has adapted together with the development of the plant immune system throughout evolution. Pfanzagl et al. (1996) discovered a unique modification in the peptidoglycan of early-diverging Glaucophytes that is absent in any bacterial species. It is plausible that additional modifications were acquired over the course of evolution, particularly with the development of an immune system, to prevent plants from recognizing their own peptidoglycan fragments and triggering an immune response. The lack of response in *Arabidopsis* could be due to the non-immunogenic nature of peptidoglycan isolated from its chloroplasts, which might not be recognized by LysM proteins in plants.

Given that plants detect long fragments of the bacterial peptidoglycan sugar backbone, glycan modifications of plant peptidoglycan are a reasonable assumption. This would protect plastidic PGN from being recognized by the plants' LysM proteins. Since Haag (2023) demonstrated the incorporation of Mur*N*Ac into the chloroplast envelope of angiosperms, these results suggests no alteration of the Mur*N*Ac molecule. This hypothesis is further supported by experiments with lysozyme (Sec. 3.5.1), a Mur*N*Ac hydrolase, that binds Mur*N*Ac. Peptidoglycan-binding proteins (see Sec. 3.4.1) also recognize Mur*N*Ac and the first two to three amino acids, but not Glc*N*Ac.

We propose that the fundamental peptidoglycan monomer in angiosperms is similar to bacterial peptidoglycan, with the potential for an altered Glc*N*Ac molecule. Since lysozyme hydrolyses β-(1,4)-glycosidic bond between Glc*N*Ac and Mur*N*Ac at the fourth carbon atom of Glc*N*Ac, it is not likely to have modifications at this position. The oligopeptide chain is made up of L-alanine, D-glutamic acid, L-lysine, and two D-alanine molecules. It remains uncertain whether D-Glu is also amidated with NAP as in cyanelle peptidoglycan, but it cannot be ruled out that other or additional modifications have been acquired throughout evolution. Fig. 4.1 shows lysosyme and mutanolysin cleavage sites (red), as well as, peptidoglycan-recognizing protein binding sites (blue). Glc*N*Ac, D-Glu, and the interpeptide bridge (green) are potentially chemically altered to avoid self-recognition of plant peptidoglycan by, e.g., LysM factors or similar PGN-binding proteins.

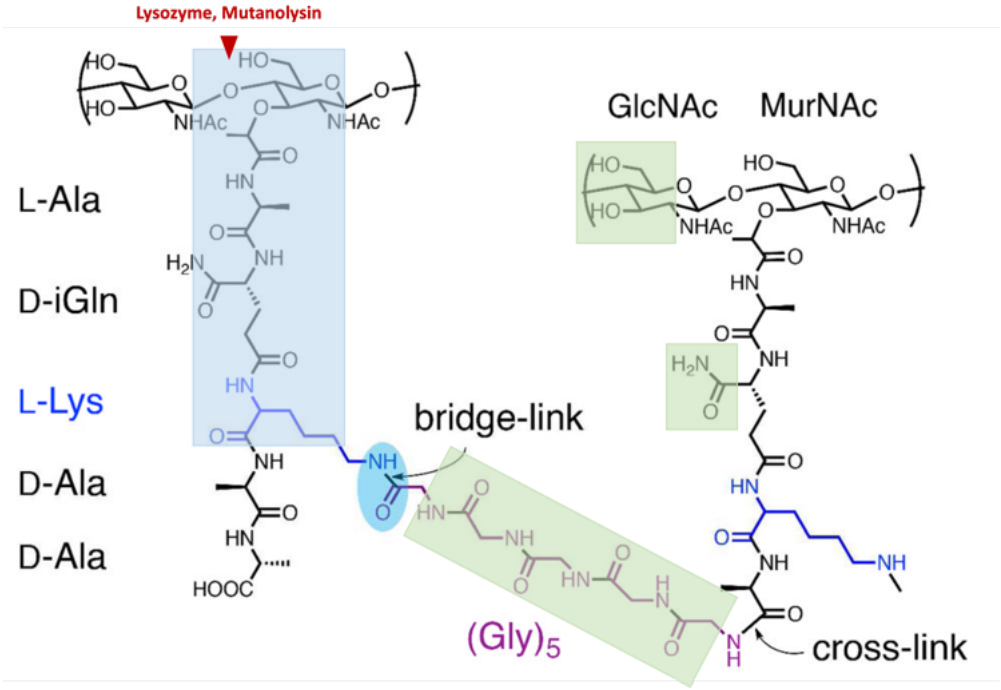

Figure 4.1: Proposed chemical structure of plant peptidoglycan, cross-linked through a five Glycine interpeptide bridge to connect L-Lys in the third position of one stem to D-Ala in the fourth position of an adjacent stem through the cleavage of the terminal D-Ala. Peptidoglycan recognizing protein binding sites are highlighted in blue. Possible modification sites are highlighted in green. Modified after Zhou and Cegelski (2012).

4.2 Characterization of Peptidoglycan Functions in Plants

4.2.1 Peptidoglycan-Targeting Antibiotics and Their Influence on Plants

As described in Section 1.2.3, a lot of antibiotics that target enzymes involved in bacterial peptidoglycan biosynthesis had an effect on plant morphology and plastid division. Kasten and Reski (1997) investigated the effects of β-lactam antibiotics on chloroplast division in the moss *P. patens* and tomato. They inhibited chloroplast formation in *P. patens*, leading to fewer but larger chloroplasts per cell (giant chloroplast phenotype). These findings could not be observed in tomato, leading to the conclusion that moss chloroplast division is more closely related to bacterial cell division, which involves peptidoglycan synthesis, than chloroplast division in vascular plants, including tomato. Tounou et al. (2002) studied the effect of β-lactam antibiotics on chloroplast division in the liverwort *M. polymorpha* and came to the same conclusion. The number of chloroplasts per cell in *M. polymorpha* cell cultures was reduced and resulted in enlarged macrochloroplasts, which was reversible after removal of antibiotics.

Katayama et al. (2003) tested various antibiotics that affect peptidoglycan biosynthesis in bacteria in *P. patens* and discovered that D-cycloserine disturbed chloroplast division in the same way that β-lactam antibiotics did. Matsumoto et al. (2012) investigated the effect

of PGN synthesis blocking antibiotics in the unicellular charophyte *Closterium*, which also resulted in an inhibition of chloroplast division. These studies show that the chloroplast division in algae and non-vascular plants is a conserved mechanism with bacterial origin that involves peptidoglycan and its corresponding genes. The division process can be disrupted by PGN-targeting antibiotics, and the effects are reversible upon removal, indicating the evolutionary connection between bacterial cell division and chloroplast division in early diverging plant species.

Later studies could also show that antibiotics had physiological effects on vascular plants (see 1.2.3 for more detail). Experiments described in Sections 3.2 and 3.3.2 show that DCS is also disturbing plastid division and root growth in *A. thaliana*. Although DCS did not result in the appearance of giant chloroplasts, like in algae and mosses, a disruption of the overall chloroplast structure and envelope integrity was observed. Altogether, these effects of PGN biosynthesis-blocking antibiotics on plants indicate that not only structure but also biosynthesis of plant peptidoglycan is similar to the bacterial PGN biosynthesis process.

4.2.2 Genetic Evaluation of Peptidoglycan Synthesis Genes in Plants

The biosynthesis of peptidoglycan in bacteria is very well conserved and involves ten key proteins. van Baren et al. (2016) used a comparative genetic analysis of bacterial peptidoglycan biosynthesis genes in the plant kingdom ranging from glaucophyte algae over early land plants including mosses/ferns to angiosperms to show that some, if not most of those genes required to synthesize PGN were retained up to a certain extent in all plant genomes. Taking a closer look into which plant species retained which genes (see Fig. 1.3), three things stood out:

1. Red algae are the only group that lost all genes for peptidoglycan synthesis.
2. There is a patchiness seen across the land plants, where some species contain the full pathway, while others do not.
3. Four genes were present in almost all species (MurE, MurG, DDL, and MraY).

One question arose from the composition of the *Arabidopsis* and tobacco genomes: The first one just harbors the mentioned four genes, whereas the other one contains an almost full set.

Sato and Takano (2017) analyzed the origins of enzymes involved in the biosynthesis of plastid peptidoglycan. They concluded that only two genes (*murA, mraY*) are closely related to cyanobacterial homologs. Other enzymes, including PBPs, have diverse evolutionary origins. Interestingly, MurB, MurD, and MurF were closely related to *Chlamydia* homologs. Some PBPs are derived from cyanobacteria, consistent with the endosymbiotic theory, while others may have originated from different bacterial lineages, indicating multiple horizontal gene transfer events.

Fig. 4.2 shows a phylogenetic tree summarizing the current knowledge (as of 2022) of plant peptidoglycan in the Archaeplastida, especially Viridiplantae. Plant PGN was verified

in some species (solid red lines) and is likely to be present in others (dotted red lines) with either a "full PGN" set of peptidoglycan biosynthesis genes or an impaired chloroplast division phenotype upon antibiotic treatment, which have been proven to block peptidoglycan biosynthesis in bacteria.

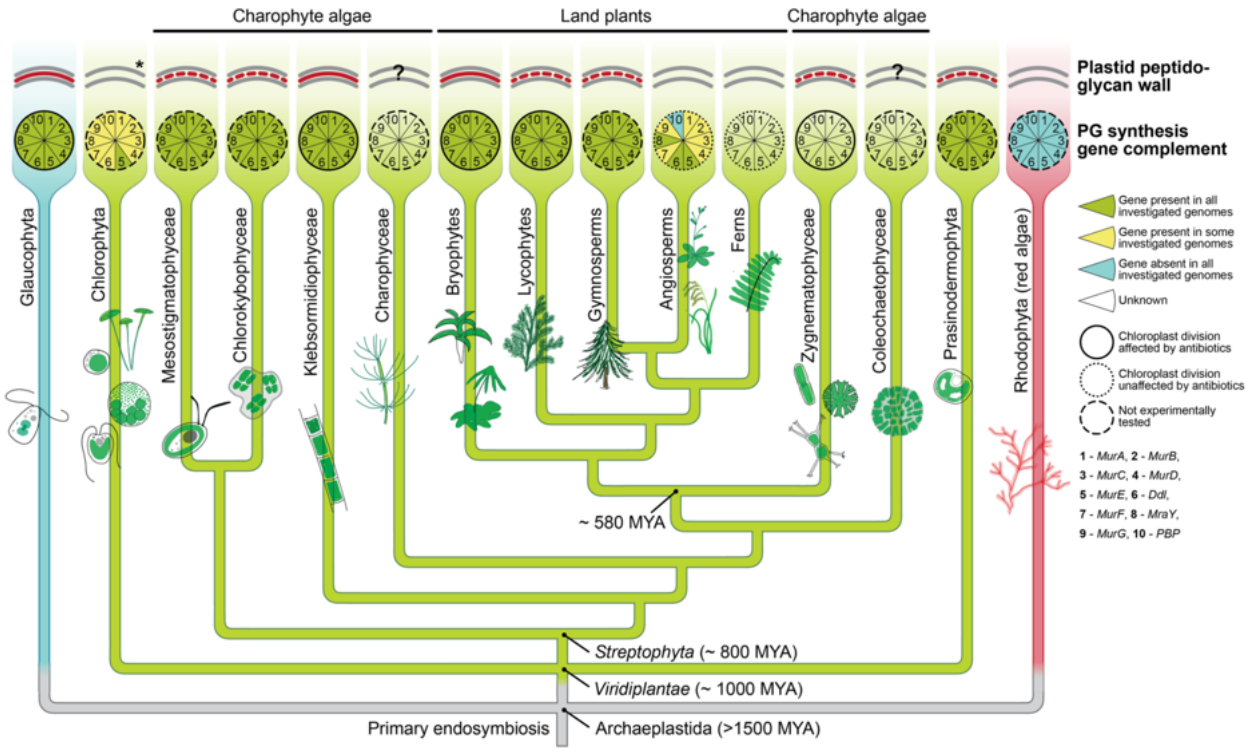

Figure 4.2: Phylogenetic tree and current knowledge of plant peptidoglycan of Archaeplastida with a focus on Charophyte alga and land plants. Solid red lines represent groups where the presence of plant peptidoglycan was experimentally determined. Dotted red lines represent "full PGN" plant species with all 10 genes needed for PGN biosynthesis (van Baren et al., 2016; Lin et al., 2017; Li et al., 2020) and/or inhibition of chloroplast division by PGN synthesis blocking antibiotics. Adapted from (Radin and Haswell, 2022)

MacLeod et al. (2024) used phylogenomic approaches to analyze the distribution of peptidoglycan biosynthesis genes in different plant and algal species and confirmed the presence of PBP orthologs in seed plants, which were previously thought to be absent in this clade (van Baren et al., 2016). PBPs are essential for the peptidoglycan maturation process and cross-link adjacent peptidoglycan strands. This indicates that bryophytes like *P. patens* with a "full PGN" set, as well as "full PGN - PBP" plants, including *N. benthamiana*, have all necessary genes to carry out peptidoglycan biosynthesis.

As previously discussed in Tran et al. (2023), we proposed that flowering plants may have evolved a novel pathway for peptidoglycan synthesis that involves only a subset of four peptidoglycan synthesis genes, which are found in nearly all species. In plants with a "full PGN" set, the traditional bacterial peptidoglycan biosynthesis pathway might have been preserved. It is uncertain whether plants with a complete PGN set can use the same novel synthesis pathway as those with the "4-PGN" set. The presence of these genes in some lineages but not in others indicates multiple independent gene loss events. Surprisingly, even within a single plant order, species with a "4-PGN" set coexist with those having a "full

PGN" set, indicating convergent gene loss. This supports the hypothesis of an alternative peptidoglycan synthesis pathway in plants. In "4-PGN" species, plant-derived enzymes may have replaced the function of missing key enzymes necessary for peptidoglycan synthesis, which enable PGN biosynthesis through a novel pathway.

4.2.3 Functional Characterization of Mur Genes in Plants

For characterization of peptidoglycan functions in vascular plants, mutants for two of these genes - DDL and MurE - were analyzed in *A. thaliana*. DDL is a D-alanyl-D-alanine ligase, catalyzing the formation of DA-DA, which is an essential precursor for bacterial peptidoglycan biosynthesis (Lugtenberg and Schijndel-van Dam, 1973). Plants and some algae have a duplicated DDL fusion protein. Both the C- and N-terminal halves are homologous to bacterial DDL proteins (Sato and Takano, 2017).

Katayama et al. (2003) and Hirano et al. (2016) investigated the role of DDL and the impact of its inhibitor DCS in the Bryophyte *P. patens*. Treatment of protonema cells with DCS resulted in a reduction in the number of chloroplasts per cell, a phenotype that was also observable in the DDL KO mutant. Both studies concluded that this bacterial-derived enzyme, typically involved in peptidoglycan biosynthesis, is linked to chloroplast division in Bryophytes.

Hirano et al. (2016) further examined *A. thaliana* DDL KO mutants, *Atddl*-1 and *Atddl*-2, and found them to be phenotypically unaffected with no observed changes in chloroplast morphology. This suggests that *At*DDL is not involved in plastid division in *A. thaliana* as it is in *P. patens*. They also concluded that DDL in angiosperms does not participate in peptidoglycan biosynthesis and might have developed a different function.

In Section 3.1, experiments were conducted to reevaluate the DDL mutants in *A. thaliana*. This gene encodes a fusion protein comprising two bacterial DDL proteins (Hirano et al., 2016). Both *A. thaliana* DDL mutants have a T-DNA insertion in the N-terminal region. Examination of the C-terminal *At*DDL gene revealed a translatable coding sequence with both a start and stop codon. RT-PCR experiments using primers specific to this second half of the fusion protein produced a transcript (Fig. 3.1b), suggesting that a functional C-terminal *At*DDL protein, $At\text{DDL}_{\Delta\text{N}}$, was transcribed.

In localization studies, this $At\text{DDL}_{\Delta\text{N}}$ was fused to GFP and transiently expressed in *N. benthamiana*. pH7FWG2-$At\text{DDL}_{\Delta\text{N}}$-GFP was translated and localized in the cytosol. Both of these experiments could show that the C-terminal *At*DDL region can be translated and may be functionally active as an enzyme, which needs to be proven in enzyme assays.

Hirano et al. (2016) did not observe defects in chloroplasts of *At*DDL mutants, which stands in contrast to microscopic observations made in Section 3.2. Fig. 3.4 shows mesophyll cells of *At*DDL mutants and wild-type plants. Chloroplasts of *Atddl*-1 and *Atddl*-2 look damaged, and the chlorophyll gathers in the cytosol. They do not have a giant chloroplast phenotype like moss DDL mutants but their phenotype also differs significantly from wild-type chloroplasts.

To analyze *Atddl* mutants in more detail, click chemistry experiments were carried out

in these mutants to see if there is some remaining activity of the truncated AtDDL$_{\Delta N}$ protein. Fig. 3.7 shows that ADA is accumulating around *Atddl*-1 chloroplasts similar to *A. thaliana* wild type. In another approach, ADA incubation was conducted simultaneously with DCS treatment, which was applied to inhibit all D-alanine-binding proteins. In some newly formed mesophyll cells, chlorophyll B autofluorescence is no longer found in single chloroplasts and ethenyl-Atto-514 could not accumulate in specific patterns due to the missing plastidic structure (Fig. 3.8). This is an indicator that the truncated AtDDL$_{\Delta N}$ protein may still be partly active. It is still able to bind and metabolize D-Ala up to a certain extent and its enzymatic activity can be inhibited by DCS, resulting in a deformed or destroyed chloroplast phenotype.

To see if AtDDL function differs from PpDDL, complementation assays should be carried out to see if AtDDL would be able to rescue the giant chloroplast phenotype in *Ppddl*. Another approach would be to produce an AtDDL mutant with CRISPR/Cas where both fusion proteins are knocked out and to observe their microscopic phenotype. It might be that this mutant has the same chloroplast morphology as *P. patens* DDL KO mutants.

MurE, the other candidate gene analyzed in this regard, is adding the third amino acid to the oligopeptide chain during peptidoglycan synthesis. Almost all plant species have a MurE homolog, and Machida et al. (2006) suggested that MurE from *P. patens* (PpMurE) is located in the stroma of *P. patens* chloroplasts. A disruption of this gene caused an appearance of macro- or giant chloroplasts in *P. patens* protonema and leave cells, which means that the number of plastids per cell was reduced. Complementation of *PpmurE* mutants with PpMurE in protonema cells could reverse the giant chloroplast phenotype. Electron micrographs of *PpmurE* mutants showed no significant difference in thylakoid shape and stacking compared to wild-type plants. They concluded that MurE was important for chloroplast morphology, especially chloroplast division in *P. patens*.

Garcia et al. (2008) were investigating MurE in *A. thaliana* in more detail. They isolated four *AtmurE* mutant lines *AtmurE*-1, -2, -3, and -4, which had a white seedling phenotype. For further experiments, *AtmurE*-1 was used. Electron micrographs of *AtmurE*-1 leaves did not have mature thylakoid membranes and an irregular plastid structure. Transgenic *A. thaliana* plants overexpressing an antisense AtMurE gene showed a pale green phenotype. A complementation assay with *PpmurE* mutants expressing either *Anabaena* MurE or AtMurE was used to compare the enzymatic function of cyanobacterial and *A. thaliana* MurE proteins. In this experiment, expression of bacterial MurE was able to rescue the giant chloroplast phenotype of *PpmurE* mutants similar to PpMurE, but expression of AtMurE in *PpmurE* was not. Since the *AtmurE* mutant's phenotype looked significantly different from *PpmurE* mutants, they suggested that AtMurE is functionally divergent from PpMurE and is involved in plastid development rather than in plastid division.

Lin et al. (2017) were working on MurE in gymnosperms. They isolated a MurE homolog from *Larix gmelinii* (larch), which also localizes in chloroplasts. Since *Larix gmelinii* has all genes necessary for peptidoglycan synthesis like *P. patens*, they suggested that all full-set PGN plants have a peptidoglycan layer. In complementation assays, MurE from *Larix gmelinii* was not able to carry out the function of PpMurE in *PpmurE* mutants to rescue the

giant chloroplast phenotype. In contrast to that, they could show that transient expression of *Lt*MurE rescued the albino phenotype of *AtmurE* mutants. "This result also suggests that the new function of MurE in chloroplast development arose during evolution of vascular plants."

Since albino seedlings of *AtmurE*-1 could not be obtained in this laboratory, *AtmurE*-3 and -4 published by Garcia et al. (2008), as well as *AtmurE*-5, was examined in this work. The latter was an uncharacterized mutant allele with an albino phenotype described by Meinke (2020). In RT-PCR experiments in *AtmurE*-5, no transcript for MurE was detected, suggesting that this gene is disrupted and cannot produce a functional protein. As described earlier in Section 3.5.2, all *AtmurE* mutants had pale green or white seedlings. In microscopic images of mesophyll cells, a distinct chloroplast structure was not observable, and in click chemistry experiments with azide-modified canonical amino acids, a characteristic ring-like structure was missing. In addition to that, peptidoglycan recognizing proteins did not have a distinct pattern in transient protein expression experiments in *A. thaliana* MurE mutants.

These results show that MurE is a key enzyme in peptidoglycan biosynthesis not only in bacteria but also in mosses. It is debatable if MurE adapted over the course of evolution and took on another function, since neither MurE from gymnosperms nor angiosperms could rescue the macrochloroplast phenotype in *PpmurE*. It might be that *AtmurE* mutants had a different phenotype compared to *PpmurE* because disturbing peptidoglycan biosynthesis in vascular plants is so severe that defective plants cannot even form macrochloroplasts.

Dowson et al. (2022) treated *P. patens* with different antibiotics to drive the accumulation of peptidoglycan intermediates and used mass spectrophotometry to analyze the extracted metabolome. They were able to find elevated levels of PGN precursors, including UDP-Mur*N*Ac-*m*-DAP-pentapeptide. They analyzed MurE from *P. patens* and *Anabaena sp.* (*Nostoc sp.* strain PCC 7120) proteins and could show that both preferred to incorporate *m*-DAP over L-Lys. With these findings, they concluded that plant peptidoglycan in *P. patens* is made up of Gram-negative peptidoglycan precursors. Given that *A. thaliana* incorporates L-Lys into the plastidic envelope (see Sec. 3.6), it is reasonable to assume that *P. patens* MurE and *A. thaliana* MurE have different substance specificity (*m*-DAP and L-Lys, respectively). This could explain why the giant chloroplast phenotype was not rescued in complementation assays with *P. patens* MurE mutants expressing either *A. thaliana* MurE or *Larix gmelinii* MurE. It might not be that MurE in vascular plants is functionally divergent but has a substrate preference for Lys-type rather than DAP-type peptidoglycan.

A way to test this could be to use complementation assays with *PpmurE* mutants expressing MurE from a Gram-positive bacterium to see if it has a similar enzymatic function and can rescue the giant chloroplast phenotype. Another approach could be to perform complementation assays with *AtmurE* mutants expressing MurE from a Gram-positive bacterium. If it has a similar function to *A. thaliana* MurE and *Larix gmelinii* MurE and reverses the albino phenotype, it would suggest that the phenotype is caused by an impairment of Lys-type peptidoglycan biosynthesis.

Homi et al. (2009) investigated the function of two other peptidoglycan biosynthesis genes in plants: MurA and MraY. MurA is a UDP-Glc*N*Ac enolpyruvyl transferase that catalyzes

the first step of bacterial PGN biosynthesis. MraY is a phosphor-Mur*N*Ac-pentapeptide translocase and catalyzes the first membrane step by creating the lipid intermediate I (Typas et al.). MurA and MraY homologs are found in *P. patens*, and a disruption of these genes resulted in a decrease of overall chloroplast number per cell. A giant chloroplast phenotype was observed, leading to the assumption that these genes are also crucial for proper chloroplast division. They concluded that the involvement of peptidoglycan biosynthesis genes in chloroplast division suggests an evolutionary link between bacterial cell division mechanisms and chloroplast division in plants.

4.2.4 The Role of Plant Peptidoglycan and Its Synthesis Genes During Plastid Division

Latest data from Chang et al. (2024) could show that PDV2 is recruiting PBP to the chloroplast division site in moss cells to facilitate peptidoglycan synthesis and membrane constriction. These are first evidences that peptidoglycan synthesis proteins interact with proteins involved in chloroplast division. It is still unclear which proteins interact with plant peptidoglycan. It is possible that peptidoglycan is also used as an anchor for the plastidic division machinery in plants.

4.2.5 Comparison of Bacterial and Plastid Divison

It is known that plastids undergo cell division through binary fission, similar to bacteria. Bacterial cell elongation and division is tightly regulated and dependent on peptidoglycan biosynthesis (Rohs and Bernhardt, 2021). Disturbing the process of PGN synthesis leads to a weakened cell wall, causing loss of shape or even cell lysis. If chloroplasts in plants also loose their predetermined shape when one or more genes associated with bacterial PGN biosynthesis are inactivated, it is reasonable to assume that plastid division is also dependent on peptidoglycan synthesis genes in some way. It is also possible that the peptidoglycan macromolecule is retained up to a certain degree in plastids and plays a role in division.

Peptidoglycan is essential to preserve the integrity of the bacterial cell wall. As an integral cell wall component, it forms a rigid, mesh-like layer around the cell, which helps to maintain its shape and to protect it against osmotic pressure and other outer stressors (Vollmer et al., 2008). The final step of bacterial cell division occurs when newly formed daughter cells are fully separated from each other. This process requires a precise temporal and spatial coordination of multiple enzyme complexes to ensure proper cell separation while maintaining the cell wall integrity.

The mechanism of bacterial cell separation begins with septum formation. The FtsZ protein forms a ring at the midcell, initiating the invagination of the cell membrane and the cell wall to form a septum. The divisome complex, recruited by the Z-ring, synthesizes new peptidoglycan to form the septum (Egan and Vollmer, 2013). penicillin-binding proteins (PBPs) are key enzymes in this process to perform transglycosylation (catalyzing the formation of the glycan chains) and transpeptidation (catalyzing the cross-linking between peptide sub-

units) (Boes et al., 2019). Following septum formation, peptidoglycan remodeling occurs. An accumulation of peptidoglycan binding protein FtsN triggers septal peptidoglycan biosynthesis and the initiation of cell constriction (Rowlett and Margolin, 2015). The divisome complex, which includes penicillin-binding proteins (PBPs), synthesizes new peptidoglycan at the division site to form the septum. These activities ensure the construction of a new cell wall at the division site (Boes et al., 2019; den Blaauwen and Luirink, 2019).

Autolysins, such as *N*-acetylmuramic acid-L-alanine amidase, glycosidases like lysozyme, and endopeptidases, break down the peptidoglycan in the septum, facilitating the final separation of the two daughter cells (Priyadarshini et al., 2006; Typas et al.). The activity of these enzymes is tightly regulated by proteins such as FtsEX and EnvC to ensure that peptidoglycan degradation occurs precisely at the right time and place, preventing premature cell lysis (Rohs and Bernhardt, 2021).

Chen et al. (2017) pursued an in-depth analysis of the components and mechanisms involved in chloroplast division. The Z-ring, made up of the tubulin-like protein FtsZ, forms a contracting ring at the division site. It plays a vital role in initiating the division process, similar to the bacterial cell division protein FtsZ. The Min system and proteins like ARC6 are important for Z-ring positioning and stabilization. The PDV1 and PDV2 proteins are located on the outer membrane and are essential for recruiting the cytosolic division machinery. These proteins interact with the ARC5 protein, a dynamin-related protein that forms a ring on the cytosolic side of the outer membrane. Other homologs of bacterial cell-division proteins operate as chloroplast-division proteins, but many bacterial-derived cell-division genes were lost during plastid evolution, which is why eukaryotic genes got recruited to facilitate plastid division (Osteryoung and Pyke, 2014).

The dynamics of membrane constriction differ between bacteria and plastids. In bacteria, FtsZ drives the constriction of the inner membrane, and other proteins, such as the divisome complex, facilitate septum formation, with outer membrane constriction involving the Tol-Pal complex (Typas et al.). In plastids, inner membrane constriction is also driven by the FtsZ ring, while outer membrane constriction involves ARC5 and the outer plastid-dividing ring (Chen et al., 2017).

Over time, most plastids are thought to have lost their peptidoglycan layer, especially in angiosperms. Some Glaucophyte algae and mosses retain a peptidoglycan layer, indicating an evolutionary remnant. In contrast to bacterial cell division, it is thought that peptidoglycan is not involved in plastid division, particularly in vascular plants (Takano and Takechi, 2010; Miyagishima, 2011).

In summary, peptidoglycan is essential for bacterial cell division, maintaining cell wall integrity, facilitating septum formation, and enabling daughter cell separation. The coordinated synthesis and remodeling of peptidoglycan ensures that new cell wall material is correctly integrated during cell division, maintaining the structural integrity of the resulting daughter cells. In contrast, plastid division in vascular plants does not involve peptidoglycan. Although plastids originated from cyanobacteria with peptidoglycan in their cell walls, most plastids have evolved different mechanisms for division that apparently do not require peptidoglycan. These mechanisms involve proteins and processes adapted to the eukaryotic

cellular environment, highlighting the evolutionary divergence from their bacterial ancestors.

As discussed previously, new evidence shows that peptidoglycan is still present in at least early-diverging plant species, if not all throughout the plant kingdom. This raises the question if peptidoglycan and its synthesis genes were retained in plants and kept the same function. Peptidoglycan was shown to be involved in plastid division in Glaucophytes (Miyagishima, 2011), and a recent study showed that PDV2 interacts with PBP to facilitate membrane constriction during plastid division in *P. patens* (Chang et al., 2024). These are evidences for the evolutionary connection between bacterial cell division and chloroplast division in early-diverging plants. Taking the antibiotic sensitivity of peptidoglycan biosynthesis genes in plants into account, these findings suggest a conserved propagation mechanism. It seems that not only cell division and PGN synthesis genes are preserved to a certain degree but also their respective functions.

5 Conclusion

This study suggests that peptidoglycan is still present in plastids of all Viridiplantae, indicating that it has been retained throughout plant evolution. The points discussed in this work indicate that angiosperms are likely to synthesize and incorporate peptidoglycan into the chloroplast envelope. Click chemistry experiments and expression of PGN-binding proteins in plants provide further evidence to support this theory. A treatment of *A. thaliana* seedlings with PGN biosynthesis blocking antibiotics, as well as analyses of mutants lacking specific PGN synthesis genes, showed a severe growth impairment and had an influence on chloroplast structure. This emphasizes the significance of peptidoglycan in chloroplast biogenesis and plant development. This challenges previous beliefs that β-lactam antibiotics have no effect on vascular plants, implying that their limited effectiveness is due to low uptake or biodegradation. We studied the roles of DDL and MurE genes in angiosperms and suggest that an alternative PGN biosynthesis pathway has evolved in plants over time. The elucidation of this postulated plant-specific PGN biosynthesis pathway will be a challenge that needs to be answered in future experiments. In this regard, identifying interactors of MurE, MurG, MraY, or DDL could be a good starting point. Another approach could be isolating additional (pale green) mutants with defects in plastidic PGN biosynthesis and visualising them with click chemistry.

According to Dowson et al. (2022), the sturdy mesh-like peptidoglycan molecule of free-living bacteria was reduced to a minimal structure in organelles like chloroplasts, which reflects an evolutionary trend. This reduction could be explained by a lower risk of severe osmotic changes or dehydration within the host cell, suggesting that endosymbiotically acquired organelles needed less structural support from the PGN layer in comparison to their free-living counterparts. It may be needed to assemble the plastid division machinery similar to bacterial cell division. We propose that peptidoglycan plays an important role in chloroplast division and structural stability, which is necessary for optimal chloroplast function and overall plant health. Peptidoglycan of Glaucophytes, Streptophytes, and Angiosperms is probably modified to avoid detection by the plants' immune systems, but it maintains its function within the host cell. These modifications are possibly results of multiple horizontal gene transfer events from various bacterial species (Sato and Takano, 2017). Nevertheless, the molecular structure and function of plant PGN, as well as the question about differences of plastidic PGN between "4-PGN" and "full PGN" plants, can only be answered after successful isolation of peptidoglycan from plants like *Arabidopsis* and tobacco.

Chang et al. (2024) could show that PBP is essential for chloroplast division in *P. patens*. It interacts with PDV2, an outer chloroplast envelope membrane protein that is part of the plastid division machinery and required for binary fission of chloroplasts during plant cell division. This shows the importance of peptidoglycan in chloroplast division, as well as the role of bacterial-derived components in today's plant cell mechanisms. Future analyses will determine whether plastidic peptidoglycan is only required for chloroplast division or also plays a role in stability and osmoregulation.

6 Material and Methods

Unless stated otherwise, all chemicals were purchased in analytical grade from Duchefa Biochemie, Merck, Carl Roth, and Serva. Laboratory consumables have been obtained from Eppendorf, Greiner, Carl Roth, and Sarstedt. All used equipment (bench centrifuges, pipettes, etc.) met molecular-biological laboratory standards. Used enzymes and kits were obtained from Thermo Fisher Scientific, New England Biolabs, Qiagen, Jena Bioscience, and Atto-TEC.

6.1 Working with Plants

6.1.1 Seed Surface Sterilization

About 50 mg of *A. thaliana* seeds were surface sterilized in a 1.5 mL reaction tube either by chlorine gas or with ethanol.

Chlorine Gas Sterilization

The seeds containing reaction tubes were opened and placed in a micro tube rack, which was placed in a desiccator inside the fume hood. A beaker was filled with 50 mL of 12 % sodium hypochloride solution and placed next to the seed rack in the desiccator. 3 mL of 37 % hypocloric acid were added carefully into the beaker, and the desiccator lid was closed. The seeds were surface sterilized for about 4 – 6 h with the resulting chlorine gas. The desiccator was opened under the fume hood afterwards, allowing the gas to evaporate over night. The reaction tubes were closed tightly and stored in a dry and dark place.

Ethanol Sterilization

Ethanol solution	Ethanol	70 % (v/v)
	Triton X-100	0.01 % (v/v)

For ethanol sterilization, 1 mL of ethanol solution was added to each reaction tube containing *A. thaliana* seeds and shaken overhead for 15 – 20 min. The ethanol solution was replaced by 100 % EtOH and shaken overhead for 5 – 10 min. The seeds were pipetted onto sterile filter paper under a laminar flow hood. After EtOH has evaporated, sterilized seeds were transferred to a 1.5 mL reaction tube and stored in a dry and dark place upon further usage.

6.1.2 Plant Growth

1/2 MS medium	Murashige & Skoog basal salt mixture	2,151 g/L
	Sucrose	10 g/L
	adjust pH to 5.7 with KOH and HCl	
	Phytoagar (Duchefa)	8 g/L

A. thaliana plant material obtained from the greenhouse was grown under long-day conditions (16 h light, 8 h dark, 22 °C) in *Arabidopsis* soil for about four weeks.

To cultivate plants without soil, surface sterilized seeds were sown on rectangular petri dishes containing 1/2 MS medium with phytoagar. Plates were closed with breathable medical tape and stored in darkness at 4 °C for 2 days for cold stratification. Seeds were germinated in a plant growth chamber (Percival/CLF Plant Climatics) with long-day conditions (16 h light, 8 h dark, 22 °C, 30 % humidity, 70 % light intensity) and grown for 6 – 21 days.

N. benthamiana plants were cultivated in the greenhouse in GS90 soil at 23 °C (day)/20 °C (night) and 14 h/10 h light/dark condition with 60 % humidity for 4 weeks.

6.1.3 Mesophyll Cell Fixation

A modified protocol of Pyke and Leech (1991) was used to analyze mesophyll cells. Therefore, *A. thaliana* leaves were fixated under a fume hood in 3.5 % glutaraldehyde for 2 h. Glutaraldehyde was removed carefully and replaced with Na_2EDTA solution (1 M), so that the whole tissue was covered. The sample was shaken for 1.5 h at 65 °C to soften the leaf tissue. The fixated leaves were then placed onto a microscopy slide and taped gently with a forceps' blunt end to break up the tissue and release the mesophyll cells. A glass cover slip was placed on top, and samples were observed with an epifluorescence microscope (Keyence BZ-8000K, 60x 1.4 NA oil immersion objective) for brightfield imaging.

6.2 Extraction of Nucleic Acids

6.2.1 Extraction of Plasmid DNA from *E. coli*

MINI I	Tris/HCl pH 8	25 mM
	EDTA pH 8	10 mM
	Glucose	50 mM
MINI II	NaOH	0.2 M
	SDS	1 %
MINI III	KAc	3 M
	HAc	11.5 % (v/v)
TE + RNAse	Tris/HCl pH 8	10 mM
	EDTA pH 8	1 mM
	RNAse	50 mg/mL

The preparation of plasmid DNA was carried out using either a modified protocol for an alkaline lysis described by Birnboim and Doly (1979) or the QIAprep Spin Miniprep Kit from Qiagen.

For the extraction of plasmid DNA after Birnboim and Doly (1979), a single colony of *E. coli* was inoculated in 4 mL LB medium with appropriate selection antibiotics and incubated for 16 h at 37 °C shaking vigorously. Bacterial cells were harvested by centrifugation for 3 min at 6000 rpm. 200 µL of MINI I was added to resuspended the cells by vortexing. 400 µL of MINI II was added to induce cell lysis. For neutralization, 300 µL of MINI III were added, and the suspension was vortexed for 10 s. Cell residues were pelleted for 10 min at 14 000 rpm. The supernatant was transferred to a new reaction tube, and the DNA was precipitated by the addition of isopropanol (1:1) and centrifugation for at least 20 min at 4 °C and 14 000 rpm. The resulting pellet was washed once by adding 500 µL 70 % EtOH and 10 min of centrifugation at 4 °C and 14 000 rpm. The pellet was dried overhead for 1 h and resuspended in 50 µL TE + RNAse and stored at -20 °C until further usage.

Plasmid DNA extraction with the QIAprep Spin Miniprep Kit was carried out as described in the manufacturer's manual (p. 29 – 31).

6.2.2 Extraction of Genomic DNA from *A. thaliana*

Edwards buffer	Tris/HCl pH 7.5	200 mM
	NaCl	250 mM
	EDTA	25 mM
	SDS	0.5 %
	adjust pH to 7.5 with NaOH and HCl	

Genomic DNA from *A. thaliana* was extracted according to Edwards et al. (1991). Therefore, 3 – 5 seedlings or one leaf of a four-week-old *A. thaliana* plant was harvested, immediately

frozen in liquid nitrogen, and stored at -80 °C. For the extraction of genomic DNA, frozen samples were ground up under the addition of 100 µL of Edwards buffer. The homogenate was incubated at 65 °C for 10 min. 100 µL of chloroform-isoamyl alcohol (27:1) were added to the reaction tubes, vortexed for 10 s and centrifuged for 5 min at 13 000 rpm. For the precipitation of isolated genomic DNA, the upper aqueous phase was transferred into a new reaction tube, and isopropanol (1:1) was added. The tubes were inverted 10 times and centrifuged for 20 min at 13 000 rpm, 4 °C. The DNA pellet was washed by adding 500 µL of 70 % EtOH and centrifugation for 10 min at 14 000 rpm. The pellet was dried overhead for about 1 h. The DNA was resuspended in 20 – 80 µL TE + RNAse and stored at 4 °C over night. On the next day, the DNA was incubated at 65 °C for 10 min to inactivate DNAses. The genomic DNA was stored at -20 °C until usage.

6.2.3 Extraction of RNA from *A. thaliana*

The RNeasy® Plant Mini Kit (Qiagen) was used for the extraction of RNA from two-week-old *A. thaliana* plants.

6.3 Analysis of Nucleic Acids

6.3.1 Restriction of Plasmid DNA

The isolated plasmid DNA was analyzed by digestion with suitable restriction enzymes; the resulting fragment sizes were analyzed via agarose gel electrophoresis (Sec. 6.3.5). The fragment sizes were compared to an *in silico* digestion in ApE. Thermo Fisher Scientific's "DoubleDigest Calculator" was used for double digestions to find suitable buffer and reaction conditions.

6.3.2 Generation of cDNA via Reverse Transcription (RT)

RT master mix	RT buffer	4 µL
	dNTPs 10 mM	2 µL
	Ribonuclease inhibitor	0.5 µL

About 1.5 µg of RNA were diluted in nuclease-free DEPC water to 12.5 µL; 1 µL of oligodT primer was added and incubated for 5 min at 70 °C. After cooling on ice for 2 min, 6.5 µL of RT master mix were added to the mixture. The samples were mixed and incubated at 37 °C for 5 min. 1 µL of reverse transcriptase (Thermo Fisher Scientific) was added; the samples were incubated at 42 °C for 60 min and at 70 °C for 10 min. The synthesized copy DNA (cDNA) was stored at -20 °C upon further usage.

6.3.3 Polymer Chain Reaction (PCR)

DNA fragments of interest were either amplified from plasmids or genomic DNA from *E. coli* or *A. thaliana*, respectively. *Taq* DNA Polymerase was used for analytical PCRs. Phusion®

High-Fidelity DNA Polymerase was used to amplify DNA fragments for cloning purposes. Reaction components and PCR programs according to the manufacturer's manuals were used.

DNA fragments can also be amplified using a colony PCR protocol. Therefore, a single colony is resuspended in 25 µL ddH_2O. 5 µL were added to the PCR master mix instead of a template DNA. Bacterial cell-lysis occurs during the initial denaturation step.

6.3.4 Genotyping

T-DNA insertion lines of *A. thaliana* were analyzed by genotyping to check zygosity. This was done via PCR (Sec. 6.3.3) with suitable T-DNA-binding primers, listed in Table A.2.

6.3.5 Agarose Gel Electrophoresis

1X TAE buffer	Tris base	40 mM
	HAc	20 mM
	EDTA	1 mM
Loading dye	Glycerol	60 % (v/v)
	Tris/HCl	10 mM
	EDTA	60 mM
	Orange G	0.15 % (w/v)

DNA fragments were analyzed by size separation using an agarose gel electrophoresis. Therefore a 1 – 1.5 % (w/v) agarose gel (depending on fragment size) was prepared by dissolving an appropriate amount of agarose in 1X TAE buffer and boiling in a microwave. After cooling to about 50 °C, 10 µL of Midori Green (final concentration 50 µg/ mL) per 50 mL agarose gel solution was added as an intercalating DNA stain. The DNA stain was mixed in, the gel was poured into the casting mold, and a comb was added. 1X TAE buffer was used as a running buffer. Prior to loading onto the gel, DNA samples and λ/*Pst*I marker were mixed with loading dye 1:4 (v/v) for easier loading and visibility. Gels were running at 70 – 120 V (5 V/cm), and the DNA fragment sizes were analyzed in an UV chamber.

6.3.6 Sanger DNA Sequencing

Sanger DNA Sequencing was done by GENEWIZ (Azenta Life Sciences; USA/Germany).

6.4 Gateway® Cloning

pENTR™ Directional TOPO® cloning was carried out as described in the cloning kits user guide. BP- and LR-reactions were carried out as described in the Gateway® Technology user guide with 1/4th of the designated volumes.

6.5 Transformation of Competent Cells

LB medium (Luria/Miller)	NaCl	10 g/L
	Tryptone	10 g/L
	Yeast extract	5 g/L
LB agar (Luria/Miller)	NaCl	10 g/L
	Tryptone	10 g/L
	Yeast extract	5 g/L
	Agar-Agar	15 g/L
S.O.C. medium	NaCl	10 mM
	KCl	2.5 mM
	$MgCl_2$	10 mM
	$MgSO_4$	10 mM
	Glucose	20 mM
	Tryptone	2 %
	Yeast extract	0.5 %

6.5.1 Transformation of Chemically Competent *E. coli* Cells

An aliquot of chemically competent One Shot® TOP10 cells was thawed on ice for 60 min. 1 µL (0.1 – 1 µg) of plasmid DNA, 1 µL BP-/LR-reaction, or 2 µL of TOPO® cloning reaction were added to the cells, mixed gently, and incubated for 30 min on ice. The cells were heat-shocked at 42 °C for 30 s and cooled on ice for 5 min. 800 µL LB or S.O.C. medium (RT) were added to the samples, and cells were incubated for 45 – 60 min at 37 °C while shaking. The cells were centrifuged at 1000 g for 3 min; 800 µL of the supernatant were discarded; the pellet was resuspended and plated on prewarmed LB agar plates containing appropriate selection antibiotics and incubated over night at 37 °C.

6.5.2 Transformation of Chemically Competent *A. thumefaciens* Cells

An aliquot of chemically competent *Agrobacterium thumefaciens* (*A. thumefaciens*) cells (GV3101 or AGL1) was thawed on ice for 1 h. 5 µL (0.1 – 1 µg) of plasmid DNA were added to the cells, mixed gently, and incubated on ice for 5 min, followed by 5 min incubation in liquid nitrogen. The cells were heat-shocked at 37 °C for 5 min and cooled on ice for 5 min. 800 µL LB or S.O.C. medium (RT) were added to the samples, and cells were incubated for 2 – 4 h at 28 °C while shaking. The cells were centrifuged at 5000 g for 2 min; 800 µL of the supernatant were discarded; the pellet was resuspended and plated on prewarmed LB agar plates containing appropriate selection antibiotics and incubated at 28 °C for two days.

6.6 Protein Expression in *E. coli*

Washing buffer	Tris/HCl pH 8	10 mM
	NaCl	100 mM
	EDTA	1 mM

BL21 cells were transformed as described in Section 6.5.1 with desired expression plasmids generated according to Section 6.4. For the preculture, a single colony was resuspended in LB medium containing appropriate selection antibiotics and incubated at 37 °C for 16 h. The preculture was inoculated in LB medium without antibiotics (1:50 dilution) and incubated at 37 °C shaking until an OD_{600} of 0.4 – 0.8 was reached. pET28aHis8::*Np*AmiC2cat was induced with 1 mM IPTG for 2 h at 30 °C; pGEX-2TM-GW::*At*DAT1 was induced with 0.1 mM IPTG for 6 h at 37 °C. The cells were harvested in a Sorvall RC 6+ centrifuge (F12S-6x600 LEX rotor, Thermo Scientific) for 20 min at 4000 rpm and 4 °C. The pellet was washed once with 50 mL washing buffer. The cells can be stored at -20 °C.

6.7 Transient Protein Expression in Plants

6.7.1 Transient Protein Expression in *N. benthamiana*

AS medium	$MgCl_2$ 1 M	150 µL
	MES-KOH buffer 1 M, pH 5.6	150 µL
	Acetosyringone 150 mM in DMSO	15 µL
	H_2O	fill up to 15 mL

For the preculture a single colony or 50 µL of transformed *A. thumefaciens* containing the desired vector was inoculated in 3 mL LB media with appropriate selection antibiotics and incubated for about 16 h at 28 °C rotating. 3 mL of fresh LB media with antibiotics were inoculated with 0.5 mL of preculture and incubated for 4 – 6 h at 28 °C shaking. The cells were centrifuged at 3200 g for 2 min and the supernatant was discarded. The pellet was resuspended in AS medium (2x the original volume) and mixed in a 1:1(:1) ratio with p19 and optionally other construct(s) for co-infiltration. About 1 mL per leaf was infiltrated into four-week-old *N. benthamiana* plants using a 1 mL syringe without the needle. Protein expression in *N. benthamiana* was analyzed by confocal microscopy.

6.7.2 Transient Protein Expression in *A. thaliana*

1/2 MS + 0.5 % Suc medium	Murashige & Skoog basal salt mixture	2.151 g/L
	Sucrose	5 g/L
	adjust pH to 5.7 with KOH and HCl	
Phosphate buffer pH 5.5	KH_2PO_4 (13.61 g/L)	96.4 mL
	Na_2HPO_4 (35.81 g/L)	3.6 mL
Co-cultivation medium	Phosphate buffer pH 5.5	25 mL
	1/2 MS + 0.5 % Suc medium	25 mL
	MES-KOH buffer 1 M, pH 5.6	1.25 mL
	Acetosyringone 150 mM in DMSO	50 µL

For the transient transformation for protein expression in *A. thaliana* a modified version of the AGROBEST method was used (Wu et al., 2014; Winkler, 2022). About 15 – 20 *A. thaliana* seeds were placed in one well of a six well plate, containing 3 mL 1/2 MS + 0.5 % Suc medium and stratified in darkness at 4 °C for 2 – 3 d. The seedlings were grown for 4 – 7 d (12 h light, 12 h dark, 14 – 17 °C, 85 % humidity). Meanwhile a preculture of transformed *A. thumefaciens* containing the desired vector was prepared according to Section 6.5.2. 0.5 mL of preculture was added to 3 mL of fresh LB medium and incubated for 4 – 6 h at 28 °C shaking for the mainculture. 1 mL of mainculture was centrifuged at 5000 rpm for 3 min, the supernatant was discarded and the pellet was resuspended in 2 mL co-cultivation medium. The culture was diluted to an $OD_{600} = 0.2$ and incubated for 16 h at 28 °C rotating. The 1/2 MS + 0.5 % Suc medium in the 6-well plates was replaced by the *A. thumefaciens* culture in co-cultivation medium diluted to an $OD_{600} = 0.02$ and incubated for 2 – 5 d. Different cultures were mixed in a 1:1(:1) ratio with p19 and optionally other construct(s) for co-cultivation. The *A. thumefaciens* containing co-cultivation medium was replaced by 1/2 MS + 0.5 % Suc medium one day before examination with confocal microscopy.

6.8 Analysis of Proteins

6.8.1 Protein Extraction from *E. coli*

DPI buffer	HEPES pH 7.5	4 mM
	KCl	100 mM
	PMSF	100 nM
	Glycerol	8 %
	Protease Inhibitor Cocktail (1 tablet per 10 mL)	

To extract proteins from *E. coli*, prepared cells from Section 6.6 were resuspended in 4 mL DPI buffer and sonicated 6 times on ice for 15 s with 15 s breaks in between cycles. The crude lysate was centrifuged for 20 min at 4000 rpm, 4 °C. To separate the soluble and unsoluble proteins, the crude extract (supernatant) was centrifuged in an Eppendorf® 5810

R centrifuge for 15 min at 10.000 rpm. Unsoluble proteins are found in the resulting pellet. To precipitate soluble proteins, ice cold acetone was added to the supernatant (1:5 v/v). The mixture was incubated at -20 °C for 30 min and centrifuged for 15 min at 10.000 rpm to precipitate the soluble proteins. Both fractions are resuspended in DPI buffer for further analysis.

6.8.2 Protein Purification from *E. coli*

To purify polyhistidine-tagged proteins, Protino® Ni-NTA Agarose and Columns (Macherey-Nagel) were used. Protein expression and extraction was carried out as described in Sections 6.6 and 6.8.1. Equilibration of Protino® Ni-NTA Agarose and batch binding of proteins was done according to the manufacurer's "Batch purification of polyhistidine-tagged proteins under native conditions" protocol. Afterwards, the suspension was loaded onto a column and the remaining washing and elution steps were carried out according to the "Gravity flow purification of polyhistidine-tagged proteins under native conditions" protocol.

6.8.3 Protein Extraction from Plant Material

Tris/HCl buffer	Tris/HCl	100 mM
	adjust pH to 8 with NaOH and HCl	

To extract proteins from plant material, 4 – 5 *A. thaliana* seedlings or about 1 cm^2 of infiltrated tobacco leafs were collected and frozen in liquid nitrogen. Samples were homogenized in 200 µL TRIS/HCl buffer, incubated on ice for 1 h and centrifuged at 14.000 rpm, 4 °C for 5 min. The supernatant was further analyzed as described in the following Sections 6.8.4 – 6.8.7.

6.8.4 Sodium Dodecylsulfate Polyacrylamide Gel Electrophoresis (SDS-PAGE)

Bottom buffer	Tris/HCl pH 8.8	1 M
	SDS	0.27 % (w/v)
	sterile filtrate solution	
Top buffer	Tris/HCl pH 6.8	250 mM
	SDS	0.2 % (w/v)
	sterile filtrate solution	
10x SDS buffer	Tris base	30.2 g/L
	Glycine	144 g/L
	SDS	15 g/L
	adjust pH to 8.3 with KOH and HCl	
2x SDS loading dye	Tris/HCl pH 6.8	120 mM
	Glycerol	20 % (v/v)
	SDS	4 % (w/v)
	Bromphenol blue	0.05 % (w/v)
	β-mercaptoethanol	10 % (v/v)

To size separate proteins, SDS-PAGE was used. Therefore, a 10 – 12.5 % running gel (depending on size of protein of interest) and a 4.5 % stacking gel was cast. Extracted or purified proteins were mixed with 2 x SDS loading dye before loading onto the gel. The TriColor-Broad Protein Ladder (company) was used as a marker. The SDS-PAGE was performed in Mini-PROTEAN Tetra Cell from Bio-Rad Laboratories, Inc. (USA) using 1 x SDS as running buffer. A current of 20 mA per gel was applied. For further analysis, gels can be used in Western Blots (Sec. 6.8.5), or for Coomassie Staining (Sec. 6.8.7).

6.8.5 Western Blot Analysis

Transfer buffer	Tris base	3.9 g/L
	Glycine	14.3 g/L
	EtOH	20 % (v/v)

For a Western Blot analysis, size separated proteins (see Sec. 6.8.4) were transferred onto an immobilizing PVDF membrane using the Wet/Tank Blotting System from Bio-Rad Laboratories. Therefore, the following setup was used: anode, sponge, whatman paper, activated PVDF membrane, SDS gel, whatman paper, sponge and cathode. PVDF membrane was shortly activated in 100 % MeOH before. The whole set up was submerged in transfer buffer and the transfer was carried out at 4 °C with a current of 30 mA over night or with 300 mA for 1.5 h at room temperature.

6.8.6 Immunodetection

10x TBS buffer	Tris/HCl	0.5 M
	NaCl	1.5 M
	adjust pH to 7.5 with NaOH and HCl	
TBS-T	10x TBS buffer	100 mL/L
	Tween-20	0.1 % (v/v)
Blocking solution	Skim milk powder	5 % in 1x TBS
AP buffer	Tris/HCl	12.144 g/L
	NaCl	5.844 g/L
	$MgCl_2$	1.0165 g/L
	adjust pH to 9.5 with NaOH and HCl	
AP staining solution	AP buffer	5 mL
	NBT	44 µL
	BCIP	33 µL

To detect immobilized proteins, the PVDF membrane was incubated in blocking solution at 4 °C for 3 h or over night to block non-specific binding sites. The blots were washed three times in TBS-T for 5 – 10 min each. The primary tag-recognizing antibody was incubated for 1.5 h at room temperature or over night at 4 °C. The membrane was washed three times to wash away excess antibodies. The secondary anti-species specific antibody, fused to the reporter enzyme horseradish peroxidase (HRP), was incubated for 1 h at room temperature and excess antibodies were washed away three times. Amersham ECL Prime Western Blotting Detection Reagent was used in a 1:1 ratio to detect chemiluminescence with the Amersham ImageQuant™ 800 western blot imaging system.

For His-tagged proteins, either a monoclonal α-His-tag antibody conjugated to alkaline phosphatase (AP), or a combination of anti-His (mouse) and anti-mouse-AP antibodies were used. One blot was incubated in AP staining solution in darkness and washed with distilled water to stop the enzyme-substrate reaction. Blots were scanned for documentation.

6.8.7 Coomassie Staining

Coomassie staining solution	Isopropanol	25 % (v/v)
	Acetic acid	10 % (v/v)
	Coomassie R-250	0.05 % (w/v)
Destainer solution	Acetic acid	10 % (v/v)

The SDS gel was incubated shaking in coomassie staining solution for 20 min and washed

with destainer solution several times (3 – 4x) until protein bands were visible. Stained gels were scanned for documentation.

6.9 Chloroplast Isolation

Isolation medium	HEPES pH 8	20 mM
	EDTA	5 mM
	EGTA	5 mM
	$MgCl_2$	5 mM
	$NaHCO_3$	10 mM
	Sorbitol	300 mM
Sorbitol gradient	30 % (w/w) Sorbitol	3 mL
	42 % (w/w) Sorbitol	3.5 mL
	60 % (w/w) Sorbitol	3.5 mL
HEPES-Sorbitol medium	HEPES pH 8	0.3 M
	Sorbitol	0.3 M

Chloroplast isolation was carried out as described in Krieger (2020) with minor modifications. Keskin (2020) tested the isolation using either a Percoll or sorbitol gradient. It was shown that both gradients are suitable, although more "intact" chloroplasts could be observed using a Percoll gradient. Every step during chloroplast isolation was carried out on ice. To prevent chloroplast damage due to centripetal forces, a swing-out rotor in an Eppendorf® 5810 R centrifuge was used, the brake velocity was lowered to 2 and all centrifuging steps were carried out at 4 °C. *A. thaliana* leafs of four week old plants were harvested in a 50 mL Falcon tube, covered with isolation medium and homogenized for 2 x 1 s using an Ultra-Turrax (Janke & Kunkel Homogenizer Type TP 18/10). The suspension was filtered through four layer of gauze and subsequently centrifuged at 360 g for 6 min. The supernatant was discarded and the pellet was resuspended very carefully in fresh isolation medium. Suspended chloroplasts were loaded onto a freshly prepared sorbitol gradient and separated at 1660 g for 12 min. The upper green band was collected and chloroplasts were carefully washed two times with isolation medium. Isolated chloroplasts were finally resuspended in about 1 mL HEPES-sorbitiol media, depending on the amount of starting material.

6.10 Peptidoglycan Isolation

Solution A	NaCl	1 M
Solution B	Tris/HCl pH 6.8	0.1 M
	$CaCl_2$	200 µM
	$MgCl_2$	33 µM
	DNase	15 µg/mL
	RNase	60 µg/mL
Solution C	Trypsin	50 µg/mL
Solution D	HCl	1 M
Digestion buffer	NaH_2PO_4 pH 5.5	12.5 mM

Peptidoglycan isolation was done according to Bertsche and Gust (2017) with minor modifications. An over night culture of *E. coli* (chemically competent TOP10 cells) was prepared in 4 mL LB medium. 2 x 2 mL of over night culture and the same amount of isolated chloroplasts from Section 6.9 was spun down for 5 min at 10,000 g. The supernatant was discarded and the pellets were resuspended in 1 mL of solution A, a hole was poked into the reaction tubes lid before boiling in a Thermomix (heating block) for 30 min at 100 °C. Afterwards the suspension was spun down for 5 min at 10,000 g and washed two times with 1 mL ddH_2O and finally resuspended in 1 mL ddH_2O. The sample was sonified for 30 min at 4 °C. 500 µL of solution B was added and incubated for 1 h at 37 °C in a Thermomix. 500 µL of solution C was added and incubated for 1 h at 37 °C to digest enzymes and residual proteins. The samples were boiled for 3 min at 100 °C to heat inactivate the enzymes. The suspension was spun down for 5 min at 10,000 g and the pellet was washed once with 1 mL ddH_2O. 500 µL of solution D was added and incubated for 4 – 6 h at 37 °C. The samples were spun down for 5 min at 10,000 g and washed 3 – 4 times with ddH_2O until a pH of 5 – 6 was reached. The supernatant was discarded after the last washing step and the pellet was resuspended in 50 µL digestion buffer (+ 25 µL of 1000 U mutanolysin, 15 µL of 50 mg/mL lysozyme) and incubated over night for 16 h at 37 °C shaking. Enzymes were heat inactivated for 3 min at 100 °C; the samples were spun down for 5 min at 10,000 g and the supernatant was used for further analysis (Sec. 6.11, 6.12).

6.11 Peptidoglycan Binding Assay

Bindiing buffer	Tris/HCl pH 6.8	30 mM
	NaCl	50 mM
	$MgCl_2$	10 mM
HEPES buffer	HEPES pH 7.5	100 mM

The peptidoglycan binding assay was carried out as described in Rocaboy et al. (2013) with several modifications. For the analysis of *Dm*PGRP and *At*DAT1 about 20 – 40 µg of crude extract (Sec. 6.8.1) or 10 µg purified protein (Sec. 6.8.2), 3 µL of PGN supernatant (Sec. 6.10) were mixed and binding buffer was added to a final volume of 50 µL. The samples were mixed and incubated at 4 °C for 2 or 24 h. The mixture was centrifuged for 15 min at 14,000 g. The supernatant was collected in a new reaction tube and the pellets were washed two times with 40 µL of HEPES buffer. The final pellets were resuspended in 40 µL HEPES buffer. The supernatant, the resuspended pellets and the supernatant from both washing steps were mixed with 2x SDS loading dye and analyzed using SDS-PAGE (Sec. 6.8.4) and Western blot (Sec. 6.8.5). A α-His-tag antibody was used as a primary antibody for HRP immunodetection (Sec. 6.8.6).

6.12 Ultra Performance Liquid Chromatography Mass Spectrometry (UPLC-MS)

Ultra Performance Liquid Chromatography Mass Spectrometry (UPLC-MS) was carried out by Dr. Mark Stahl according to Kühner et al. (2014) using the digested supernatant from Section 6.10.

6.13 Enzymatic Digestion of Chloroplasts with Lysozyme and Mutanolysin

This experiment was carried out and analyzed by Erva Keskin (2020). Therefore, isolated chloroplasts from Section 6.9 were mixed with lysozyme (1 – 2 mg/L) and/or mutanolysin (1000 U/L), and incubated for 17 h at 37 °C and subsequently analyzed using the Keyence BZ-8000K epifluorescence microscope. For experiments with inactivated enzymes, they were heat-inactivated at 99 °C for 2 h. Since lysozyme is quite stable, it was heat-inactivated at a pH of 13 – 14. The pH was lowered to 10 with HCl before adding to chloroplast samples.

For FACS analyses, chloroplasts were incubated with different lysozyme concentrations (10 µg/mL, 30 µg/mL, 35 µg/mL, 50 µg/mL, 70 µg/mL, and 100 µg/mL) over night at 37 °C. This experiment was carried out and analyzed by Paul Winkler (2022).

6.14 Click Chemistry *in planta*

The Click-iT® Cell Reaction Buffer Kit (Thermo Fisher Scientific) was used for *in planta* fluorescent labeling. Azide-modified amino acids were used to study the incorporation of canonical peptidoglycan amino acids. Fluorescent alkyne-modified dyes were used to label azide-modified molecules after incorporation. The click chemistry reaction for *P. patens* and *A. thaliana* was performed as described in Tran et al. (2023).

P. patens protonema cells were incubated in BCD medium containing ADA (0.25 mM) for 22 h in order to visualize peptidoglycan. After washing the cells once in BCD medium, they were incubated for 2 h in a mixture of BCD medium and a Click-iT cell reaction cocktail (1:1) that contained Atto-514-alkyne (1 – 5 µM). BCD medium was used to wash the cells once before they were imaged using a fluorescent confocal microscope (Zeiss LSM 880, or Leica TCS SP8).

For click chemistry in adult *A. thaliana* and *N. benthamiana* plants, leaves were infiltrated with 1/2 MS medium with 0.25 mM azide-modified D-amino acids (D-Ala, D-Lys) or 0.125 mM azide-modified L-amino acids (L-Ala, L-Lys), and incubated for 24 – 48 h at room temperature. Samples of treated leaves were cut out and incubated with 1/2 MS medium containing Click-iT cell reaction cocktail (1:1) and Atto-514- or AF488-alkyne dye for 1.5 – 2 h. The leaves were washed and in shortly incubated in 1/2 MS medium before imaging. For *A. thaliana* seedings, the whole plant was used in all steps.

6.15 Confocal Fluorescence Microscopy

Imaging of fluorescent dyes was carried out as described in Tran et al. (2023). Fluorescent confocal microscopes (Zeiss LSM 880, or Leica TCS SP8) were used with a 63x NA 1.2 water immersion objective. Fluorescent dyes were excited (ex) with an appropriate laser and emission (em) was detected in sequential line scanning mode for Zeiss LSM 880, or with HyD detectors for Leica TCS SP8: GFP and AF488 (ex/em, 488 nm/490 – 535 nm), Chlorophyll B (ex/em, 488 nm/690 – 760 nm), Atto-514 (ex/em, 514 nm/520 – 560 nm) and RFP (ex/em, 561 nm/590 – 645 nm). The pinholes were adjusted to 1 AU per wavelength.

List of References

A. Aliashkevich, L. Alvarez, and F. Cava. New insights into the mechanisms and biological roles of d-amino acids in complex eco-systems. *Front. Microbiol.*, 9, April 2018.

E. Angert. Alternatives to binary fission in bacteria. *Nature Reviews Microbiology*, 3:214–224, 2005. doi: https://doi.org/10.1038/nrmicro1096.

Z. M. Bar-On, Phillips R., and Milo R. The biomass distribution on earth. *Proceedings of the National Academy of Sciences*, 115(25):6506–6511, 2018. doi: 10.1073/pnas.1711842115. URL `https://www.pnas.org/doi/abs/10.1073/pnas.1711842115`.

U. Bertsche and A. A. Gust. *Peptidoglycan Isolation and Binding Studies with LysM-Type Pattern Recognition Receptors*, pages 1–12. Springer New York, New York, NY, 2017. ISBN 978-1-4939-6859-6. doi: 10.1007/978-1-4939-6859-6_1. URL `https://doi.org/10.1007/978-1-4939-6859-6_1`.

H. C. Birnboim and J. Doly. A rapid alkaline extraction procedure for screening recombinant plasmid DNA. *Nucleic Acids Res*, 7(6):1513–1523, Nov. 1979.

L. O. Björn. Peptidoglycan in eukaryotes: Unanswered questions. *Phytochemistry*, 175: 112370, 2020. ISSN 0031-9422. doi: https://doi.org/10.1016/j.phytochem.2020.112370. URL `https://www.sciencedirect.com/science/article/pii/S0031942219309586`.

A. Boes, S. Olatunji, E. Breukink, and M. Terrak. Regulation of the peptidoglycan polymerase activity of PBP1b by antagonist actions of the core divisome proteins FtsBLQ and FtsN. *mBio*, 10(1), January 2019.

E. Bok. *The amidase AmiC2 and its peptidoglycan substrate in filamentous cyanobacteria*. PhD thesis, Eberhard Karls Universität Tübingen, 2022. URL `http://dx.doi.org/10.15496/publikation-52360`.

W. A. Bonner. Chirality and life. *Origins of Life and Evolution of the Biosphere*, 25(1): 175–190, Jun 1995. ISSN 1573-0875. doi: 10.1007/BF01581581. URL `https://doi.org/10.1007/BF01581581`.

J. B. Bruning, A. C. Murillo, O. Chacon, R. G. Barletta, and J. C. Sacchettini. Structure of the *Mycobacterium tuberculosis* D-Alanine:D-Alanine Ligase, a Target of the Antituberculosis Drug D-Cycloserine. *Antimicrobial Agents and Chemotherapy*, 55(1):291–301, 2011. doi: 10.1128/AAC.00558-10. URL `https://journals.asm.org/doi/abs/10.1128/AAC.00558-10`.

N. A. Campbell and J. B. Reece. *Biologie 6. aktualisierte Auflage*. Pearson Studium, 2006.

M. D. Cantine and G. P. Fournier. Environmental Adaptation from the Origin of Life to the Last Universal Common Ancestor. *Origins of Life and Evolution of Biospheres*, 48:35–54, 2015. doi: 10.1007/s11084-017-9542-5. URL https://doi.org/10.1007/s11084-017-9542-5.

C.-I. Chang, K. Ihara, Y. Chelliah, D. Mengin-Lecreulx, S. Wakatsuki, and J. Deisenhofer. Structure of the ectodomain of *Drosophila* peptidoglycan-recognition protein LCa suggests a molecular mechanism for pattern recognition. *Proceedings of the National Academy of Sciences*, 102(29):10279–10284, 2005. doi: 10.1073/pnas.0504547102. URL https://www.pnas.org/doi/abs/10.1073/pnas.0504547102.

Z. Chang, N. Tang, and M. Zhang. The peptidoglycan synthase pbp interacts with plastid division2 to promote chloroplast division in physcomitrium patens. *New Phytologist*, 241(3):1115–1129, 2024. doi: https://doi.org/10.1111/nph.19268. URL https://nph.onlinelibrary.wiley.com/doi/abs/10.1111/nph.19268.

C. Chen, J. S. MacCready, D. C. Ducat, and K. W. Osteryoung. The Molecular Machinery of Chloroplast Division. *Plant Physiology*, 176(1):138–151, 11 2017. ISSN 0032-0889. doi: 10.1104/pp.17.01272. URL https://doi.org/10.1104/pp.17.01272.

P. J. Delves and I. M. Roitt. The Immune System. *New England Journal of Medicine*, 343 (1):37–49, 2000. doi: 10.1056/NEJM200007063430107. URL https://doi.org/10.1056/NEJM200007063430107. PMID: 10882768.

T. den Blaauwen and J. Luirink. Checks and balances in bacterial cell division. *mBio*, 10(1): e00149–19, 2019. doi: 10.1128/mBio.00149-19. URL https://journals.asm.org/doi/abs/10.1128/mBio.00149-19.

O. Deusch, G. Landan, M. Roettger, N. Gruenheit, K. V. Kowallik, J. F. Allen, W. Martin, and T. Dagan. Genes of Cyanobacterial Origin in Plant Nuclear Genomes Point to a Heterocyst-Forming Plastid Ancestor. *Molecular Biology and Evolution*, 25(4):748–761, 01 2008. ISSN 0737-4038. doi: 10.1093/molbev/msn022. URL https://doi.org/10.1093/molbev/msn022.

N. K. Devaraj and M. G. Finn. Introduction: Click Chemistry. *Chemical Reviews*, 121(12): 6697–6698, 2021. doi: 10.1021/acs.chemrev.1c00469. URL https://doi.org/10.1021/acs.chemrev.1c00469. PMID: 34157843.

W. D. Donachie. Co-ordinate regulation of the *Escherichia coli* cell cycle or The cloud of unknowing. *Molecular Microbiology*, 40(4):779–785, 2001. doi: https://doi.org/10.1046/j.1365-2958.2001.02439.x. URL https://onlinelibrary.wiley.com/doi/abs/10.1046/j.1365-2958.2001.02439.x.

A. J. Dowson, A. J. Lloyd, A. C. Cuming, D. I. Roper, L. Frigerio, and C. G. Dowson. Plant peptidoglycan precursor biosynthesis: Conservation between moss chloroplasts and

Gram-negative bacteria. *Plant Physiology*, 190(1):165–179, 04 2022. ISSN 0032-0889. doi: 10.1093/plphys/kiac176. URL https://doi.org/10.1093/plphys/kiac176.

R. Dziarski. Peptidoglycan recognition proteins (PGRPs). *Molecular Immunology*, 40(12): 877–886, 2004. ISSN 0161-5890. doi: https://doi.org/10.1016/j.molimm.2003.10.011. URL https://www.sciencedirect.com/science/article/pii/S0161589003003195. Innate Immunity.

R. Dziarski and D. Gupta. The peptidoglycan recognition proteins (PGRPs). *Genome Biology*, 7(8):232, 2006. doi: https://doi.org/10.1186/gb-2006-7-8-232. URL https://genomebiology.biomedcentral.com/articles/10.1186/gb-2006-7-8-232.

K. Edwards, C. Johnstone, and C. Thompson. A simple and rapid method for the preparation of plant genomic DNA for PCR analysis. *Nucleic Acids Res*, 19(6):1349, Mar 1991.

A. J. F. Egan and W. Vollmer. The Physiology of Bacterial Cell Division. *Annals of the New York Academy of Sciences*, 1277(1):8–28, 2013. doi: 10.1111/j.1749-6632.2012.06818.x. URL https://nyaspubs.onlinelibrary.wiley.com/doi/abs/10.1111/j.1749-6632.2012.06818.x.

J. Errington. L-form bacteria, cell walls and the origins of life. *Open Biology*, 3(1):120143, 2013. doi: 10.1098/rsob.120143. URL https://royalsocietypublishing.org/doi/abs/10.1098/rsob.120143.

M. Garcia, F. Myouga, H. Takechi, K.and Sato, K. Nabeshima, N. Nagata, S. Takio, K. Shinozaki, and H. Takano. An *Arabidopsis* Homolog of the Bacterial Peptidoglycan Synthesis Enzyme MurE Has an Essential Role in Chloroplast Development. *The Plant Journal*, 53(6):924–934, 2008. doi: 10.1111/j.1365-313X.2007.03379.x. URL https://onlinelibrary.wiley.com/doi/abs/10.1111/j.1365-313X.2007.03379.x.

H. R. Gelderblom and D. H. Krüger. 1 - helmut ruska (1908–1973): His role in the evolution of electron microscopy in the life sciences, and especially virology. volume 182 of *Advances in Imaging and Electron Physics*, pages 1–94. Elsevier, 2014. doi: https://doi.org/10.1016/B978-0-12-800146-2.00001-1. URL https://www.sciencedirect.com/science/article/pii/B9780128001462000011.

G. Genchi. An overview on D-amino acids. *Amino Acids*, 49(9):1521–1533, 2017. doi: 10.1007/s00726-017-2459-5.

R. Guan, A. Roychowdhury, B. Ember, S. Kumar, G.-J Boons, and R. A. Mariuzza. Structural basis for peptidoglycan binding by peptidoglycan recognition proteins. *Proceedings of the National Academy of Sciences*, 101(49):17168–17173, 2004. doi: 10.1073/pnas.0407856101. URL https://www.pnas.org/doi/abs/10.1073/pnas.0407856101.

R. Guan, Q. Wang, E. J. Sundberg, and R. A. Mariuzza. Crystal Structure of *Human* Peptidoglycan Recognition Protein S (PGRP-S) at 1.70Å Resolution. *Journal*

of Molecular Biology, 347(4):683–691, 2005. ISSN 0022-2836. doi: https://doi.org/10.1016/j.jmb.2005.01.070. URL https://www.sciencedirect.com/science/article/pii/S0022283605001282.

M. E. Gudiño, N. Blanco-Touriñán, V. Arbona, A. Gómez-Cadenas, M. A Blázquez, and F. Navarro-García. β-Lactam Antibiotics Modify Root Architecture and Indole Glucosinolate Metabolism in Arabidopsis thaliana. *Plant and Cell Physiology*, 59(10):2086–2098, 07 2018. ISSN 0032-0781. doi: 10.1093/pcp/pcy128. URL https://doi.org/10.1093/pcp/pcy128.

A. A. Gust. Peptidoglycan perception in plants. *PLoS Pathog.*, 11(12):e1005275, December 2015.

M. Haag. *Studies on Peptidoglycans in the Envelopes of Plant Chloroplasts and Mitochondria*. Master's thesis, University of Tübingen, 2023.

R. Hatzenpichler, V. Krukenberg, R. L. Spietz, and Z. J. Jay. Next-generation physiology approaches to study microbiome function at single cell level. *Nature Reviews Microbiology*, 256(18):241–256, 2020. doi: 10.1038/s41579-020-0323-1. URL https://doi.org/10.1038/s41579-020-0323-1.

C. Heidrich, M. F. Templin, A. Ursinus, M. Merdanovic, J. Berger, H. Schwarz, M. A. de Pedro, and J.-V. Höltje. Involvement of *N*-acetylmuramyl-l-alanine amidases in cell separation and antibiotic-induced autolysis of *Escherichia coli*. *Molecular Microbiology*, 41 (1):167–178, 2001. doi: https://doi.org/10.1046/j.1365-2958.2001.02499.x. URL https://onlinelibrary.wiley.com/doi/abs/10.1046/j.1365-2958.2001.02499.x.

C. D. Hein, X. M. Liu, and D. Wang. Click chemistry, a powerful tool for pharmaceutical sciences. *Pharmaceutical Research*, 25(10):2216–30, 2008. doi: 10.1007/s11095-008-9616-1. URL https://doi.org/10.1007/s11095-008-9616-1.

J. Heslop-Harrison. Structure and Morphogenesis of lamellar systems in grana-containing chloroplasts. *Planta*, 60:243–260, 1963. doi: 10.1007/BF01937960. URL https://doi.org/10.1007/BF01937960.

H. Higuchi, K. Takechi, and H. Takano. Visualization of cyanelle peptidoglycan in cyanophora paradoxa using a metabolic labeling method with click chemistry. *CYTOLOGIA*, 81(4):357–358, 2016. doi: 10.1508/cytologia.81.357.

D. G. Hillis, J. Fletcher, K. R. Solomon, and P. K. Sibley. Effects of ten antibiotics on seed germination and root elongation in three plant species. *Archives of Environmental Contamination and Toxicology*, 60(2):220–232, 2011. doi: https://doi.org/10.1007/s00244-010-9624-0. URL https://doi.org/10.1007/s00244-010-9624-0.

T. Hirano, K. Tanidokoro, Y. Shimizu, Y. Kawarabayasi, T. Ohshima, M. Sato, S. Tadano, H. Ishikawa, S. Takio, K. Takechi, and H. Takano. Moss chloroplasts are surrounded by

a peptidoglycan wall containing D-amino acids. *The Plant Cell*, 28(7):1521–1532, 2016. ISSN 1040-4651. doi: 10.1105/tpc.16.00104. URL http://www.plantcell.org/content/28/7/1521.

E. Hoiczyk and A. Hansel. Cyanobacterial cell walls: News from an unusual prokaryotic envelope. *Journal of Bacteriology*, 182(5):1191–1199, 2000. doi: 10.1128/JB.182.5.1191-1199.2000. URL https://journals.asm.org/doi/abs/10.1128/JB.182.5.1191-1199.2000.

H.-D. Höltje. Molekulare Wirkungsmechanismen einiger Antibiotika. *Pharmazie in unserer Zeit*, 5(6):161–169, 1976. doi: 10.1002/pauz.19760050601. URL https://onlinelibrary.wiley.com/doi/abs/10.1002/pauz.19760050601.

S. Homi, K. Takechi, K. Tanidokoro, H. Sato, S. Takio, and H. Takano. The Peptidoglycan Biosynthesis Genes MurA and MraY are Related to Chloroplast Division in the Moss Physcomitrella patens. *Plant and Cell Physiology*, 50(12):2047–2056, 09 2009. ISSN 0032-0781. doi: 10.1093/pcp/pcp158. URL https://doi.org/10.1093/pcp/pcp158.

M. C. Horner-Devine, K. M. Carney, and B. J. M. Bohannan. An ecological perspective on bacterial biodiversity. *Proc. Biol. Sci.*, 271(1535):113–122, January 2004.

A. Julg. *Origin of the L-Homochirality of Amino-Acids in the Proteins of Living Organisms*, pages 33–52. Springer Netherlands, Dordrecht, 1989. ISBN 978-94-009-1173-4. doi: 10.1007/978-94-009-1173-4_3. URL https://doi.org/10.1007/978-94-009-1173-4_3.

K. G. Karol, K. Arumuganathan, J. L. Boore, A. M. Duffy, K. D. E. Everett, J. D. Hall, S. K. Hansen, J. V. Kuehl, D. F. Mandoli, B. D. Mishler, R. G. Olmstead, K. S. Renzaglia, and P. G. Wolf. Complete plastome sequences of *Equisetum arvense* and *Isoetes flaccida*: implications for phylogeny and plastid genome evolution of early land plant lineages. *BMC Evolutionary Biology*, 10:321, 2012. doi: 10.1186/1471-2148-10-321. URL https://doi.org/10.1186/1471-2148-10-321.

B. Kasten and R. Reski. β-Lactam Antibiotics Inhibit Chloroplast Division in a Moss (*Physcomitrella patens*) but not in Tomato (*Lycopersicon esculentum*). *Journal of Plant Physiology*, 150(1):137–140, 1997. ISSN 0176-1617. doi: https://doi.org/10.1016/S0176-1617(97)80193-9. URL http://www.sciencedirect.com/science/article/pii/S0176161797801939.

N. Katayama, H. Takano, M. Sugiyama, S. Takio, A. Sakai, K. Tanaka, H. Kuroiwa, and K. Ono. Effects of Antibiotics that Inhibit the Bacterial Peptidoglycan Synthesis Pathway on Moss Chloroplast Division. *Plant and Cell Physiology*, 44(7):776–781, 07 2003. ISSN 0032-0781. doi: 10.1093/pcp/pcg096. URL https://doi.org/10.1093/pcp/pcg096.

Kenry and B. Liu. Bio-orthogonal Click Chemistry for *In Vivo* Bioimaging. *Trends in Chemistry*, 1(8):763–778, 2019. ISSN 2589-5974. doi: https://doi.org/10.1016/j.trechm.2019.08.003. URL https://www.sciencedirect.com/science/article/pii/S2589597419302011.

E. Keskin. *Studies on the Existence of a Putative Peptidoglycan Layer in the Chloroplast Envelope of Higher Plants*. Bachelor's thesis, University of Tübingen, 2020.

M. S. Kim, M. Byun, and B. H. Oh. Crystal structure of peptidoglycan recognition protein LB from *Drosophila melanogaster*. *Nature Immunology*, 4:787–793, 2005. ISSN 1529-2916. doi: https://doi.org/10.1038/ni952. URL https://www.nature.com/articles/ni952.

H. C. Kolb, M. G. Finn, and K. B. Sharpless. Click Chemistry: Diverse Chemical Function from a Few Good Reactions. *Angewandte Chemie International Edition*, 40 (11):2004–2021, 2001. doi: https://doi.org/10.1002/1521-3773(20010601)40:11<2004::AID-ANIE2004>3.0.CO;2-5. URL https://doi.org/10.1002/1521-3773(20010601)40:11<2004::AID-ANIE2004>3.0.CO;2-5.

N. Krieger. *Expression, localization, and interaction studies of the plastidic PII protein from textArabidopsis thaliana*. PhD thesis, Eberhard Karls Universität Tübingen, 2020. URL http://dx.doi.org/10.15496/publikation-42641.

C. Ku, S. Nelson-Sathi, M. Roettger, F. L. Sousa, P. J. Lockhart, D. Bryant, E. Hazkani-Covo, J. O. McInerney, G. Landan, and W. F. Martin. Endosymbiotic origin and differential loss of eukaryotic genes. *Nature*, 524:427–432, 2015. doi: 10.1038/nature14963. URL https://doi.org/10.1038/nature14963.

H. Kumar, T. Kawai, and S. Akira. Pathogen Recognition by the Innate Immune System. *International Reviews of Immunology*, 30(1):16–34, 2011. doi: 10.3109/08830185.2010.529976. URL https://doi.org/10.3109/08830185.2010.529976. PMID: 21235323.

S. Kumar, A. Roychowdhury, B. Ember, Q. Wang, R. Guan, R. A. Mariuzza, and G.-J. Boons. Selective Recognition of Synthetic Lysine and *meso*-Diaminopimelic Acid-type Peptidoglycan Fragments by *Human* Peptidoglycan Recognition Proteins Iα and S*. *Journal of Biological Chemistry*, 280(44):37005–37012, 2005. ISSN 0021-9258. doi: https://doi.org/10.1074/jbc.M506385200. URL https://www.sciencedirect.com/science/article/pii/S0021925820593393.

U. Kutschera and K. J. Niklas. Endosymbiosis, cell evolution, and speciation. *Theory in Biosciences*, 124(4):1–24, 2005. doi: https://doi.org/10.1016/j.thbio.2005.04.001.

D. Kühner, M. Stahl, D. D. Demircioglu, and U. Bertsche. From cells to muropeptide structures in 24h: Peptidoglycan mapping by UPLC-MS. *Scientific Reports*, 4(1):7494, Dec 2014. ISSN 2045-2322. doi: 10.1038/srep07494. URL https://doi.org/10.1038/srep07494.

H. Leyon and D. von Wettstein. Der Chromatophoren-Feinbau bei den Phaeophyceen. *Zeitschrift für Naturforschung*, 9b:471—475, 1954. URL https://zfn.mpdl.mpg.de/data/Reihe_B/9/ZNB-1954-9b-0471.pdf.

L. Li, S. Wang, H. Wang, S. K. Sahu, B. Marin, H. Li, Y. Xu, H. Liang, Z. Li, S. Cheng, T. Reder, Z. Çebi, S. Wittek, M. Petersen, B. Melkonian, H. Du, H. Yang, J. Wang, G. K.-S. Wong, X. Xu, X. Liu, Y. Van de Peer, M. Melkonian, and H. Liu. The genome of prasinoderma coloniale unveils the existence of a third phylum within green plants. *Nature Ecology & Evolution*, 4(9):1220–1231, 2020. doi: 10.1038/s41559-020-1221-7. URL https://doi.org/10.1038/s41559-020-1221-7.

G. W. Liechti, E. Kuru, E. Hall, A. Kalinda, Y. V. Brun, M. Van Nieuwenhze, and A. T. Maurelli. A New Metabolic Cell-Wall Labelling Method Reveals Peptidoglycan in Chlamydia trachomatis. *Nature*, 506:507 EP –, 12 2013. URL https://doi.org/10.1038/nature12892.

J.-H. Lim, M.-S. Kim, H.-E. Kim, T. Yano, Y. Oshima, K. Aggarwal, W. E. Goldman, N. Silverman, S. Kurata, and B.-H. Oh. Structural Basis for Preferential Recognition of Diaminopimelic Acid-type Peptidoglycan by a Subset of Peptidoglycan Recognition Proteins. *Journal of Biological Chemistry*, 281(12):8286–8295, 2006. ISSN 0021-9258. doi: https://doi.org/10.1074/jbc.M513030200. URL https://www.sciencedirect.com/science/article/pii/S0021925819766472.

X. Lin, N. Li, H. Kudo, Z. Zhang, J. Li, W. Wang, L.and Zhang, K. Takechi, and H. Takano. Genes Sufficient for Synthesizing Peptidoglycan are Retained in Gymnosperm Genomes, and MurE from Larix gmelinii can Rescue the Albino Phenotype of Arabidopsis MurE Mutation. *Plant and Cell Physiology*, 58(3):587–597, 01 2017. ISSN 0032-0781. doi: 10.1093/pcp/pcx005. URL https://doi.org/10.1093/pcp/pcx005.

H. Lorenz, A. Perlberg, D. Sapoundjiev, M. P. Elsner, and A. Seidel-Morgenstern. Crystallization of enantiomers. *Chemical Engineering and Processing: Process Intensification*, 45 (10):863–873, 2006. ISSN 0255-2701. doi: https://doi.org/10.1016/j.cep.2005.11.013. URL https://www.sciencedirect.com/science/article/pii/S025527010600095X. Particulate Processes A Special Issue of Chemical Engineering and Processing.

E. J. J. Lugtenberg and A. v. Schijndel-van Dam. Temperature-Sensitive Mutant of *Escherichia coli* K-12 with an Impaired D-Alanine:D-Alanine Ligase. *Journal of Bacteriology*, 113(1):96–104, 1973. doi: 10.1128/jb.113.1.96-104.1973. URL https://journals.asm.org/doi/abs/10.1128/jb.113.1.96-104.1973.

M. Machida, K. Takechi, H. Sato, S. Jin Chung, H. Kuroiwa, S. Takio, M. Seki, K. Shinozaki, T. Fujita, M. Hasebe, and H. Takano. Genes for the Peptidoglycan Synthesis Pathway Are Essential for Chloroplast Division in Moss. *Proceedings of the National Academy of Sciences*, 103(17):6753–6758, 2006. doi: 10.1073/pnas.0510693103. URL https://www.pnas.org/content/103/17/6753.

A. I. MacLeod, M. R. Knopp, and S. B. Gould. A mysterious cloak: the peptidoglycan layer of algal and plant plastids. *Protoplasma*, 261(1):173–178, Jan 2024. ISSN 1615-6102. doi: 10.1007/s00709-023-01886-y. URL https://doi.org/10.1007/s00709-023-01886-y.

E. L. Madsen. Microorganisms and their roles in fundamental biogeochemical cycles. *Current Opinion in Biotechnology*, 22(3):456–464, 2011. ISSN 0958-1669. doi: https://doi.org/10.1016/j.copbio.2011.01.008. URL https://www.sciencedirect.com/science/article/pii/S095816691100022X. Energy biotechnology – Environmental biotechnology.

E. Maréchal. *Primary Endosymbiosis: Emergence of the Primary Chloroplast and the Chromatophore, Two Independent Events*, pages 3–16. Springer US, New York, NY, 2018. ISBN 978-1-4939-8654-5. doi: 10.1007/978-1-4939-8654-5_1. URL https://doi.org/10.1007/978-1-4939-8654-5_1.

W. Margolin. Themes and variations in prokaryotic cell division. *FEMS Microbiology Reviews*, 24(4):531–548, 2000. doi: https://doi.org/10.1111/j.1574-6976.2000.tb00554.x. URL https://onlinelibrary.wiley.com/doi/abs/10.1111/j.1574-6976.2000.tb00554.x.

W. F. Martin, S. Garg, and V. Zimorski. Endosymbiotic theories for eukaryote origin. *Philosophical Transactions of the Royal Society B: Biological Sciences*, 370(1678):20140330, 2015. doi: 10.1098/rstb.2014.0330. URL https://royalsocietypublishing.org/doi/abs/10.1098/rstb.2014.0330.

H. Matsumoto, K. Takechi, H. Sato, S. Takio, and H. Takano. Treatment with Antibiotics that Interfere with Peptidoglycan Biosynthesis Inhibits Chloroplast Division in the Desmid Closterium. *PLOS ONE*, 7(7):1–6, 07 2012. doi: 10.1371/journal.pone.0040734. URL https://doi.org/10.1371/journal.pone.0040734.

C. S. McKay and M. G. Finn. Click Chemistry in Complex Mixtures: Bioorthogonal Bioconjugation. *Chemistry & Biology*, 21(9):1075–1101, 2014. ISSN 1074-5521. doi: https://doi.org/10.1016/j.chembiol.2014.09.002. URL https://www.sciencedirect.com/science/article/pii/S1074552114002920.

D. W. Meinke. Genome-wide identification of embryo-defective (emb) genes required for growth and development in arabidopsis. *New Phytologist*, 226(2):306–325, 2020. doi: https://doi.org/10.1111/nph.16071. URL https://nph.onlinelibrary.wiley.com/doi/abs/10.1111/nph.16071.

P. Mellroth, J. Karlsson, and H. Steiner. A Scavenger Function for a *Drosophila* Peptidoglycan Recognition Protein. *Journal of Biological Chemistry*, 278(9):7059–7064, 2003. ISSN 0021-9258. doi: https://doi.org/10.1074/jbc.M208900200. URL https://www.sciencedirect.com/science/article/pii/S0021925819326353.

C. Mereschkowsky. *Über Natur und Ursprung der Chromatophoren im Pflanzenreiche*. Biolog. Centralblatt. Rosenthal, J., 1905. URL https://ia600700.us.archive.org/28/items/cbarchive_51353_bernaturundursprungderchromato1881/bernaturundursprungderchromato1881.pdf.

V. Minden, A. Deloy, A. M. Volkert, S. D. Leonhardt, and G. Pufal. Antibiotics impact plant traits, even at small concentrations. *AoB Plants*, 9(2), 2017. doi: https://doi.org/10.1093/aobpla/plx010. URL https://www.sciencedirect.com/science/article/pii/0022519367900793.

S. Miyagishima. Mechanism of Plastid Division: From a Bacterium to an Organelle. *Plant Physiology*, 155(4):1533–1544, 02 2011. ISSN 0032-0889. doi: 10.1104/pp.110.170688. URL https://doi.org/10.1104/pp.110.170688.

K. Mühlethaler and A. Frey-Wyssling. Entwicklung und Struktur der Proplastiden. *The Journal of Biophysical and Biochemical Cytology*, 6(3):507–512, 12 1959. ISSN 0095-9901. doi: 10.1083/jcb.6.3.507. URL https://doi.org/10.1083/jcb.6.3.507.

B. K. Nelson, X. Cai, and A. Nebenführ. A multicolored set of invivo organelle markers for co-localization studies in arabidopsis and other plants. *The Plant Journal*, 51(6): 1126–1136, 2007. doi: https://doi.org/10.1111/j.1365-313X.2007.03212.x. URL https://onlinelibrary.wiley.com/doi/abs/10.1111/j.1365-313X.2007.03212.x.

O. Opriş, F. Copaciu, M. Loredana Soran, D. Ristoiu, Ü. Niinemets, and L. Copolovici. Influence of nine antibiotics on key secondary metabolites and physiological characteristics in triticum aestivum: Leaf volatiles as a promising new tool to assess toxicity. *Ecotoxicology and Environmental Safety*, 87:70–79, 2013. ISSN 0147-6513. doi: https://doi.org/10.1016/j.ecoenv.2012.09.019. URL https://www.sciencedirect.com/science/article/pii/S0147651312003387.

K. W. Osteryoung and K. A. Pyke. Division and dynamic morphology of plastids. *Annual Review of Plant Biology*, 65(Volume 65, 2014):443–472, 2014. ISSN 1545-2123. doi: https://doi.org/10.1146/annurev-arplant-050213-035748. URL https://www.annualreviews.org/content/journals/10.1146/annurev-arplant-050213-035748.

N. R. Pace. A molecular view of microbial diversity and the biosphere. *Science*, 276(5313): 734–740, 1997. doi: 10.1126/science.276.5313.734. URL https://www.science.org/doi/abs/10.1126/science.276.5313.734.

G. A. Pankey and L. D. Sabath. Clinical Relevance of Bacteriostatic versus Bactericidal Mechanisms of Action in the Treatment of Gram-Positive Bacterial Infections. *Clinical Infectious Diseases*, 38(6):864–870, 03 2004. ISSN 1058-4838. doi: 10.1086/381972. URL https://doi.org/10.1086/381972.

M. Petitjean. Chirality in metric spaces. *Optimization Letters*, 14(2):329–338, Mar 2020. ISSN 1862-4480. doi: 10.1007/s11590-017-1189-7. URL https://doi.org/10.1007/s11590-017-1189-7.

B. Pfanzagl, A. Zenker, E. Pittenauer, G. Allmaier, J. Martinez-Torrecuadrada, E. R. Schmid, M. A. de Pedro, and W. Löffelhardt. Primary structure of cyanelle peptidoglycan of cyanophora paradoxa: a prokaryotic cell wall as part of an organelle envelope.

Journal of Bacteriology, 178(2):332–339, 1996. doi: 10.1128/jb.178.2.332-339.1996. URL https://journals.asm.org/doi/abs/10.1128/jb.178.2.332-339.1996.

E. V. Pikuta, R. B. Hoover, B. Klyce, P. C. W. Davies, and P. Davies. Bacterial utilization of L-sugars and D-amino acids. In Richard B. Hoover, Gilbert V. Levin, and Alexei Y. Rozanov, editors, *Instruments, Methods, and Missions for Astrobiology IX*, volume 6309, page 63090A. International Society for Optics and Photonics, SPIE, 2006. doi: 10.1117/12.690434. URL https://doi.org/10.1117/12.690434.

M. Pollan. *The Omnivore's Dilemma: A Natural History of Four Meals*. Penguin Publishing Group, 2006. ISBN 9781594200823. URL https://books.google.de/books?id=Qh7dkdVsbDkC.

T. V. Potapova and O. A. Koksharova. Filamentous Cyanobacteria as a Prototype of Multicellular Organisms. *Russian Journal of Plant Physiology*, 67:17–30, 2020. doi: 10.1134/S102144372001015X. URL https://doi.org/10.1134/S102144372001015X.

R. Priyadarshini, D. L. Popham, and K. D. Young. Daughter cell separation by penicillin-binding proteins and peptidoglycan amidases in escherichia coli. *Journal of Bacteriology*, 188(15):5345–5355, 2006. doi: 10.1128/jb.00476-06. URL https://journals.asm.org/doi/abs/10.1128/jb.00476-06.

K. A. Pyke and R. M. Leech. Rapid image analysis screening procedure for identifying chloroplast number mutants in mesophyll cells of arabidopsis thaliana (l.) heynh. *Plant Physiol*, 96(4):1193–1195, August 1991.

I. Radin and E. S. Haswell. Looking at mechanobiology through an evolutionary lens. *Current Opinion in Plant Biology*, 65:102112, 2022. ISSN 1369-5266. doi: https://doi.org/10.1016/j.pbi.2021.102112. URL https://www.sciencedirect.com/science/article/pii/S1369526621001126.

S. A. Ragland and A. K. Criss. From bacterial killing to immune modulation: Recent insights into the functions of lysozyme. *PLOS Pathogens*, 13(9):1–22, 09 2017. doi: 10.1371/journal.ppat.1006512. URL https://doi.org/10.1371/journal.ppat.1006512.

O. Ramström. The nobel prize in chemistry 2022, 2022. URL https://www.nobelprize.org/prizes/chemistry/2022/ceremony-speech/.

M. Rocaboy, R. Herman, E. Sauvage, H. Remaut, K. Moonens, M. Terrak, P. Charlier, and F. Kerff. The crystal structure of the cell division amidase AmiC reveals the fold of the AMIN domain, a new peptidoglycan binding domain. *Molecular Microbiology*, 90(2):267–277, 2013. doi: https://doi.org/10.1111/mmi.12361. URL https://onlinelibrary.wiley.com/doi/abs/10.1111/mmi.12361.

P. D. A. Rohs and T. G. Bernhardt. Growth and division of the peptidoglycan matrix. *Annual Review of Microbiology*, 75(Volume 75, 2021):315–336, 2021. ISSN 1545-3251. doi: https://doi.org/10.1146/annurev-micro-020518-120056. URL https://www.annualreviews.org/content/journals/10.1146/annurev-micro-020518-120056.

V. W. Rowlett and W. Margolin. The bacterial divisome: ready for its close-up. *Philosophical Transactions of the Royal Society B: Biological Sciences*, 370(1679):20150028, 2015. doi: 10.1098/rstb.2015.0028. URL https://royalsocietypublishing.org/doi/abs/10.1098/rstb.2015.0028.

L. Sagan. On the origin of mitosing cells. *Journal of Theoretical Biology*, 14(3):225–IN6, 1967. ISSN 0022-5193. doi: https://doi.org/10.1016/0022-5193(67)90079-3. URL https://www.sciencedirect.com/science/article/pii/0022519367900793.

J. Sasabe and M. Suzuki. Distinctive roles of D-amino acids in the homochiral world: chirality of amino acids modulates mammalian physiology and athology. *The Keio Journal of Medicine*, 68(1):1–16, 2018. doi: 10.2302/kjm.2018-0001-IR.

N. Sato and H. Takano. Diverse origins of enzymes involved in the biosynthesis of chloroplast peptidoglycan. *Journal of Plant Research*, 130(4):635–645, 2017. doi: 10.1007/s10265-017-0935-3. URL https://doi.org/10.1007/s10265-017-0935-3.

D. Schenten and R. Medzhitov. The control of adaptive immune responses by the innate immune system. *Adv Immunol*, 109:87–124, 2011.

A. F. W. Schimper. *Über die Entwicklung der Chlorophyllkörner und Farbkörper nachtrag.* éditeur non identifié, 1883. URL https://books.google.de/books?id=7TXIuQEACAAJ.

K. H. Schleifer and O. Kandler. Peptidoglycan types of bacterial cell walls and their taxonomic implications. *Bacteriol Rev.*, 36(4):407–77, 1972. doi: 10.1128/br.36.4.407-477.1972. URL https://doi.org/10.1128/br.36.4.407-477.1972.

T. Schneider and H.-G. Sahl. An oldie but a goodie – cell wall biosynthesis as antibiotic target pathway. *International Journal of Medical Microbiology*, 300(2):161–169, 2010. ISSN 1438-4221. doi: https://doi.org/10.1016/j.ijmm.2009.10.005. URL https://www.sciencedirect.com/science/article/pii/S1438422109001234. Pathophysiology of staphylococci in the post-genomic era.

F. Schötz and L. Diers. Über die Bildung von Stromasubstanz und Thylakoiden im Raum zwischen dem äusseren und inneren Teil der Plastiden-Doppelmembran. *Planta*, 69:258–287, 1966. doi: 10.1007/BF00384878. URL https://doi.org/10.1007/BF00384878.

A. C. Shaw, S. Joshi, H. Greenwood, A. Panda, and J. M. Lord. Aging of the innate immune system. *Current Opinion in Immunology*, 22(4):507–513, 2010. ISSN 0952-7915. doi: https://doi.org/10.1016/j.coi.2010.05.003. URL https://www.sciencedirect.com/science/article/pii/S0952791510000889.

D. Slonova, A. Posvyatenko, A. Kibardin, E. Sysolyatina, E. Lyssuk, S. Ermolaeva, S. Obydennyi, N. Gnuchev, G. Georgiev, K. Severinov, and S. Larin. Human short peptidoglycan recognition protein PGLYRP1/Tag-7/PGRP-S inhibits listeria monocytogenes intracellular survival in macrophages. *Front Cell Infect Microbiol*, 10:582803, December 2020.

A. C. Smith and M. A. Hussey. *Gram Stain Protocols*. American Society for Microbiology, 2016.

N. W. Sokol, E. Slessarev, G. L. Marschmann, A. Nicolas, S. J. Blazewicz, E. L. Brodie, M. K. Firestone, M. M. Foley, R. Hestrin, B. A. Hungate, B. J. Koch, B. W. Stone, M. B. Sullivan, O. Zablocki, G. Trubl, K. McFarlane, R. Stuart, E. Nuccio, P. Weber, Y. Jiao, M. Zavarin, J. Kimbrel, K. Morrison, D. Adhikari, A. Bhattacharaya, P. Nico, J. Tang, N. Didonato, L. Paša-Tolić, A. Greenlon, E. T. Sieradzki, P. Dijkstra, E. Schwartz, R. Sachdeva, J. Banfield, J. Pett-Ridge, and LLNL Soil Microbiome Consortium. Life and death in the soil microbiome: how ecological processes influence biogeochemistry. *Nature Reviews Microbiology*, 20(7):415–430, 2022.

J. Suarez, C. Hener, V.-A. Lehnhardt, S. Hummel, M. Stahl, and Ü. Kolukisaoglu. *Frontiers in Plant Science*, 10, 2019. ISSN 1664-462X. doi: 10.3389/fpls.2019.01609. URL `https://www.frontiersin.org/articles/10.3389/fpls.2019.01609`.

C. P. Swaminathan, P. H. Brown, A. Roychowdhury, Q. Wang, R. Guan, N. Silverman, W. E. Goldman, G.-J. Boons, and R. A. Mariuzza. Dual strategies for peptidoglycan discrimination by peptidoglycan recognition proteins (PGRPs). *Proceedings of the National Academy of Sciences*, 103(3):684–689, 2006. doi: 10.1073/pnas.0507656103. URL `https://www.pnas.org/doi/abs/10.1073/pnas.0507656103`.

D. Sychantha, A. S. Brott, C. S. Jones, and A. J. Clarke. Mechanistic pathways for peptidoglycan O-Acetylation and De-O-Acetylation. *Front Microbiol*, 9:2332, October 2018.

B. Söderström and D. O. Daley. The bacterial divisome: more than a ring? *Current Genetics*, 63:161–164, 2017. doi: 10.1007/s00294-016-0630-2. URL `https://doi.org/10.1007/s00294-016-0630-2`.

H. Takano and K. Takechi. Plastid peptidoglycan. *Biochimica et Biophysica Acta (BBA) - General Subjects*, 1800(2):144–151, 2010. ISSN 0304-4165. doi: https://doi.org/10.1016/j.bbagen.2009.07.020. URL `https://www.sciencedirect.com/science/article/pii/S0304416509002116`. Special Issue: Nucleocytoplasmic Glycosylation.

S. Temnyk. *And Only Four Remain: Functionally Characterizing the Peptidoglycan-Related Genes in Flowering Plants*. Master's thesis, Arizona State University, 2024.

J. Thimmapuram, H. Duan, L. Liu, and M. A. Schuler. Bicistronic and fused monocistronic transcripts are derived from adjacent loci in the *Arabidopsis* genome. *RNA*, 11(2):128–138, 2005. doi: 10.1261/rna.7114505. URL `http://rnajournal.cshlp.org/content/11/2/128.abstract`.

D. J. Tipper. Mode of action of β-lactam antibiotics. *Pharmacology Therapeutics*, 27(1): 1–35, 1985. ISSN 0163-7258. doi: https://doi.org/10.1016/0163-7258(85)90062-2. URL https://www.sciencedirect.com/science/article/pii/0163725885900622.

E. Tounou, S. Takio, A. Sakai, K. Ono, and H. Takano. Ampicillin Inhibits Chloroplast Division in Cultured Cells of the Liverwort *Marchantia polymorpha*. *CYTOLOGIA*, 67 (4):429–434, 2002. doi: 10.1508/cytologia.67.429.

X. Tran, E. Keskin, P. Winkler, M. Braun, and Ü. Kolukisaoglu. The chloroplast envelope of angiosperms contains a peptidoglycan layer. *Cells*, 12(4), 2023. ISSN 2073-4409. doi: 10.3390/cells12040563. URL https://www.mdpi.com/2073-4409/12/4/563.

A. Typas, M. Banzhaf, C. A. Gross, and W. Vollmer. *Nature reviews. Microbiology*, (2): 123–136, 12 . doi: 10.1038/nrmicro2677.

M. J. van Baren, C. Bachy, E. N. Reistetter, S. O. Purvine, J. Grimwood, S. Sudek, H. Yu, C. Poirier, T. J. Deerinck, A. Kuo, I. V. Grigoriev, C.-H. Wong, R. D. Smith, S. J. Callister, C.-L. Wei, J. Schmutz, and A. Z. Worden. Evidence-based green algal genomics reveals marine diversity and ancestral characteristics of land plants. *BMC Genomics*, 17(1):267, 2016. doi: 10.1186/s12864-016-2585-6. URL https://doi.org/10.1186/s12864-016-2585-6.

W. Vollmer, D. Blanot, and M. A. de Pedro. Peptidoglycan Structure and Architecture. *FEMS Microbiology Reviews*, 32(2):149–167, 8/23/2019 2008. doi: 10.1111/j.1574-6976.2007.00094.x. URL https://doi.org/10.1111/j.1574-6976.2007.00094.x.

M. Wang, L.-H. Liu, S. Wang, X. Li, X. Lu, D. Gupta, and R. Dziarski. Human Peptidoglycan Recognition Proteins Require Zinc to Kill Both Gram-Positive and Gram-Negative Bacteria and Are Synergistic with Antibacterial Peptides1. *The Journal of Immunology*, 178(5):3116–3125, 03 2007. ISSN 0022-1767. doi: 10.4049/jimmunol.178.5.3116. URL https://doi.org/10.4049/jimmunol.178.5.3116.

X. Wang, D. Ryu, R. H. Houtkooper, and J. Auwerx. Antibiotic Use and Abuse: A Threat to Mitochondria and Chloroplasts with Impact on Research, Health and Environment. *BioEssays*, 37(10):1045–1053, 2015. doi: 10.1002/bies.201500071. URL https://onlinelibrary.wiley.com/doi/abs/10.1002/bies.201500071.

Z.-M. Wang, X. Li, R. R. Cocklin, M. Wang, M. Wang, K. Fukase, S. Inamura, S. Kusumoto, D. Gupta, and R. Dziarski. *Human* Peptidoglycan Recognition Protein-L Is an *N*-Acetylmuramoyl-L-alanine Amidase. *Journal of Biological Chemistry*, 278(49):49044–49052, 2003. ISSN 0021-9258. doi: https://doi.org/10.1074/jbc.M307758200. URL https://www.sciencedirect.com/science/article/pii/S0021925820756759.

D. J. Waxman and J. L. Strominger. Penicillin-binding proteins and the mechanism of action of beta-lactam antibiotics. *Annual Review of Biochemistry*, 52(Volume 52, 1983):825–869, 1983. ISSN 1545-4509. doi: https://doi.org/10.1146/annurev.bi.52.070183.004141.

URL https://www.annualreviews.org/content/journals/10.1146/annurev.bi.52.070183.004141.

P. Winkler. *Zytometrische und fluoreszenz-mikroskopische Untersuchungen in A. thaliana und N. benthamiana zum Nachweis von plastidärem Peptidoglycan*. Bachelor's thesis, University of Tübingen, 2022.

B. T. Worrell, J. A. Malik, and V. V. Fokin. Direct Evidence of a Dinuclear Copper Intermediate in Cu(I)-Catalyzed Azide-Alkyne Cycloadditions. *Science*, 340(6131):457–460, 2013. ISSN 0036-8075.

H.-Y. Wu, K.-H. Liu, Y.-C. Wang, J.-F. Wu, W.-L. Chiu, C.-Y. Chen, S.-H. Wu, J. Sheen, and E.-M. Lai. Agrobest: an efficient agrobacterium-mediated transient expression method for versatile gene function analyses in arabidopsis seedlings. *Plant Methods*, 10(1):19, Jun 2014. ISSN 1746-4811. doi: 10.1186/1746-4811-10-19. URL https://doi.org/10.1186/1746-4811-10-19.

A. Zapun, C. Contreras-Martel, and T. Vernet. Penicillin-binding proteins and β-lactam resistance. *FEMS Microbiology Reviews*, 32(2):361–385, 02 2008. ISSN 0168-6445. doi: 10.1111/j.1574-6976.2007.00095.x. URL https://doi.org/10.1111/j.1574-6976.2007.00095.x.

Y. Zhang, S. Luo, Y. Tang, L. Yu, K.-Y. Hou, J.-P. Cheng, X. Zeng, and P. G. Wang. Carbohydrate–Protein Interactions by "Clicked" Carbohydrate Self-Assembled Monolayers. *Analytical Chemistry*, 78(6):2001–2008, 2006. doi: 10.1021/ac051919+. URL https://doi.org/10.1021/ac051919+. PMID: 16536439.

X. Zhou and L. Cegelski. Nutrient-dependent structural changes in s. aureus peptidoglycan revealed by solid-state NMR spectroscopy. *Biochemistry*, 51(41):8143–8153, October 2012.

V. Zimorski, C. Ku, W. F. Martin, and S. B. Gould. Endosymbiotic theory for organelle origins. *Current Opinion in Microbiology*, 22:38–48, 2014. ISSN 1369-5274. doi: https://doi.org/10.1016/j.mib.2014.09.008. URL https://www.sciencedirect.com/science/article/pii/S1369527414001283.

List of Figures

List of Tables

Appendix

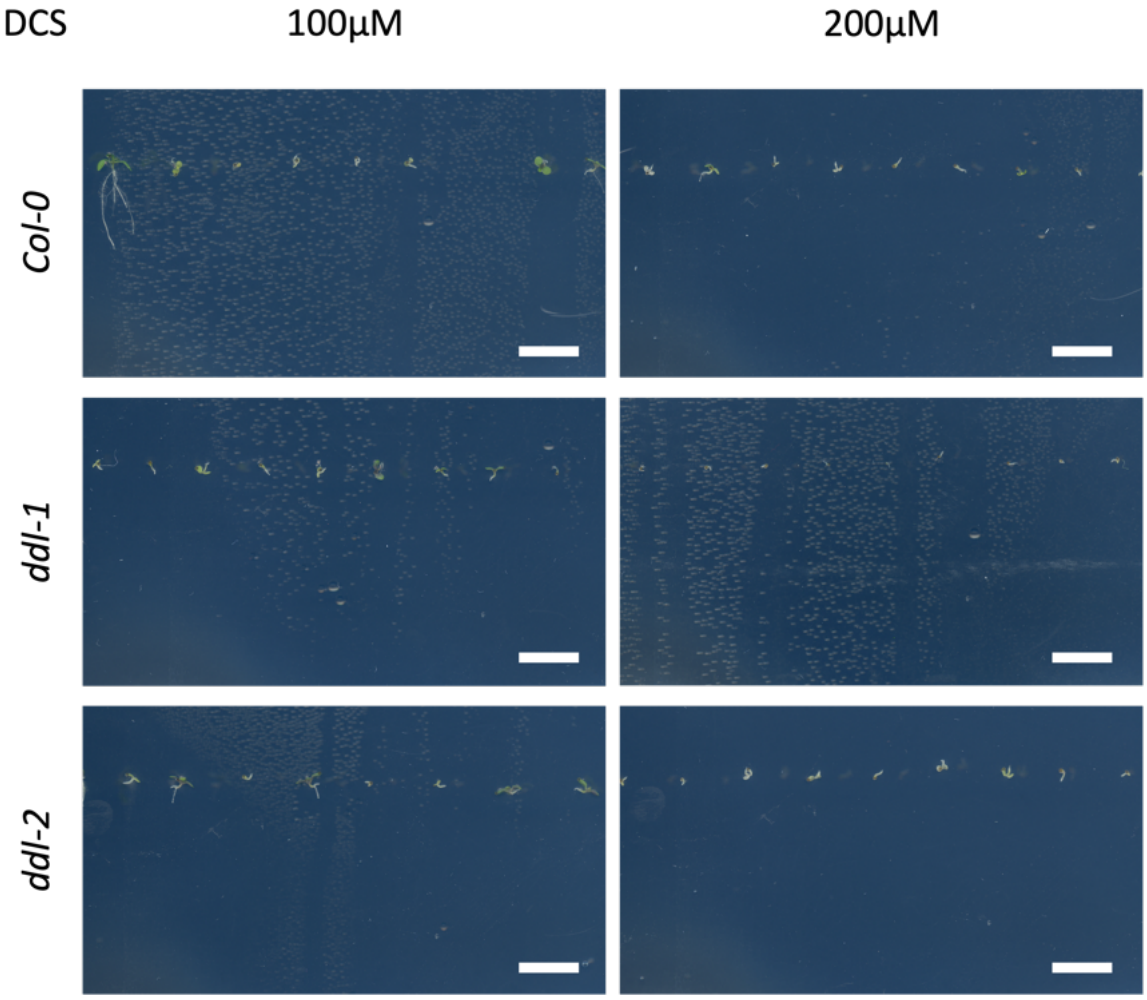

Figure A.1: *A. thaliana* seedling germination and root growth is inhibited by DCS. *Arabidopsis* seeds (*Col-0*) were germinated for 12 days under long-day conditions on growth media, containing 100, and 200 µM D-cycloserine. Scale bar: 10 mm

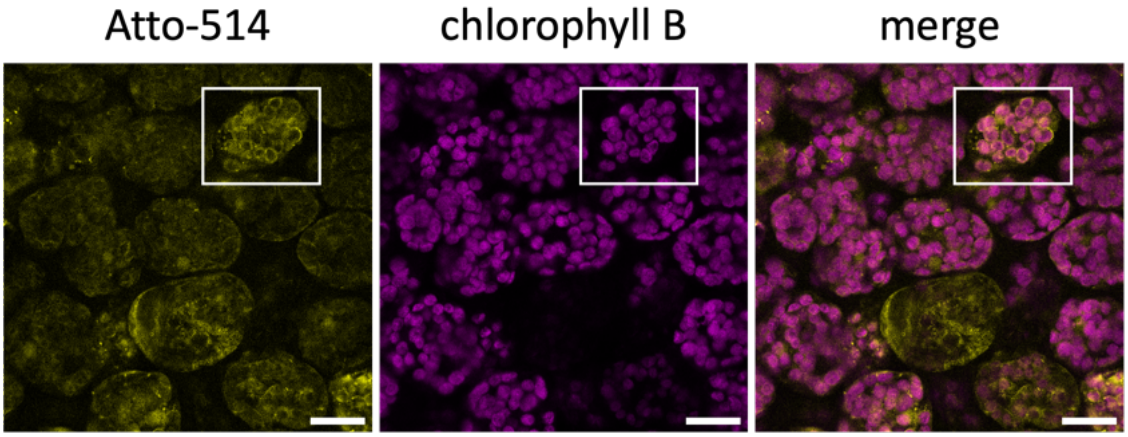

Figure A.2: Fluorescent microscopic detection of ADA around plastids in *A. thaliana* cells. *A. thaliana* chloroplasts of wild-type *Col-0* cells treated with **(a)** ADA and Atto-514-alkyne. The white box shows a mesophyll cell that incorporated ADA into the chloroplast's envelope. Scale bar: 20 µm.

Table A.1: Calculated peptidoglycan fragments for Gram-negative and Gram-positive bacteria.

	Peptides	**Glycans**	**Mass (M+H)+**	**Mass (M+2H)2+**
Monomer	**Gram negative**			
	L-Ala-D-Glu-*m*-DAP	-	391.1775	196.09265
	L-Ala-D-Glu-*m*-DAP	G-M	869.3491	435.17845
	L-Ala-D-Glu-*m*-DAP-D-Ala	-	462.2236	231.6157
	L-Ala-D-Glu-*m*-DAP-D-Ala	G-M	940.3952	470.7015
	L-Ala-D-Glu-*m*-DAP-D-Ala-D-Ala	-	533.2697	267.13875
	L-Ala-D-Glu-*m*-DAP-D-Ala-D-Ala	G-M	1011.4413	506.22455
Dimer	**Gram negative**			
	L-Ala-D-Glu-*m*-DAP + L-Ala-D-Glu-*m*-DAP-D-Ala	-	834.3697	417.68875
	L-Ala-D-Glu-*m*-DAPD-Ala + L-Ala-D-Glu-*m*-DAP-D-Ala	-	905.4248	453.2163
	L-Ala-D-Glu-*m*-DAPD-Ala + L-Ala-D-Glu-*m*-DAP-D-Ala-D-Ala	-	976.4709	488.73935
	L-Ala-D-Glu-*m*-DAP + L-Ala-D-Glu-*m*-DAP-D-Ala	G-M	1312.5429	656.77535
	L-Ala-D-Glu-*m*-DAPD-Ala + L-Ala-D-Glu-*m*-DAP-D-Ala	G-M	1383.5964	692.3021
	L-Ala-D-Glu-*m*-DAPD-Ala + L-Ala-D-Glu-*m*-DAP-D-Ala-D-Ala	G-M	1454.6425	727.82515
	L-Ala-D-Glu-*m*-DAP + L-Ala-D-Glu-*m*-DAP-D-Ala	G-M + G-M	1790.7161	895.86195
	L-Ala-D-Glu-*m*-DAPD-Ala + L-Ala-D-Glu-*m*-DAP-D-Ala	G-M + G-M	1861.768	931.3879
	L-Ala-D-Glu-*m*-DAPD-Ala + L-Ala-D-Glu-*m*-DAP-D-Ala-D-Ala	G-M + G-M	1932.8141	966.91095

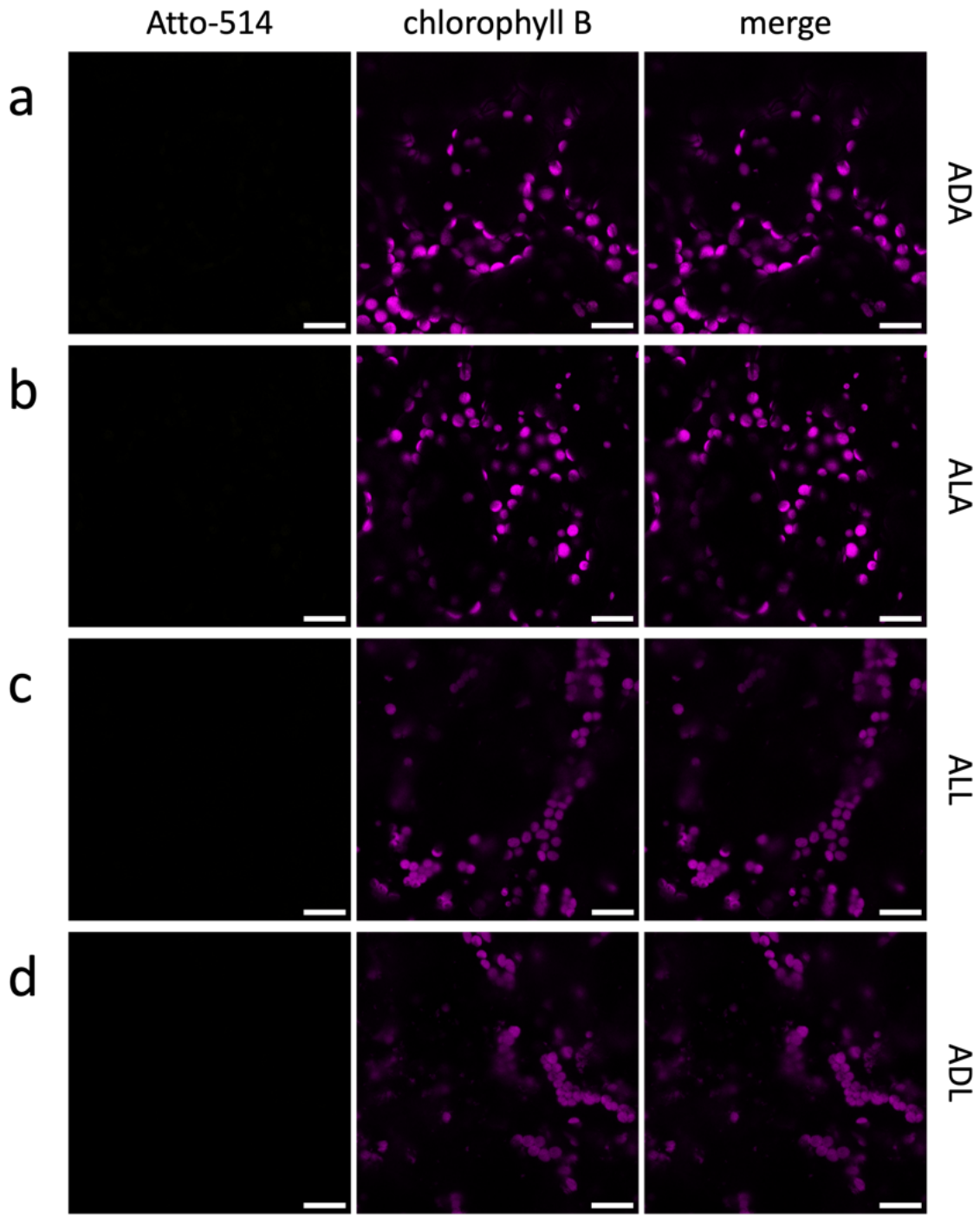

Figure A.3: Click chemistry control experiments with azide amino acids in *A. thaliana* cells, but without Atto-514-alkyne. Fluorescent microscopic observation of *A. thaliana* chloroplasts of wild-type *Col-0* cells treated with **(a)** ADA, **(b)** ALA, **(c)** ALL, **(d)** ADL. Scale bar: 20 µm.

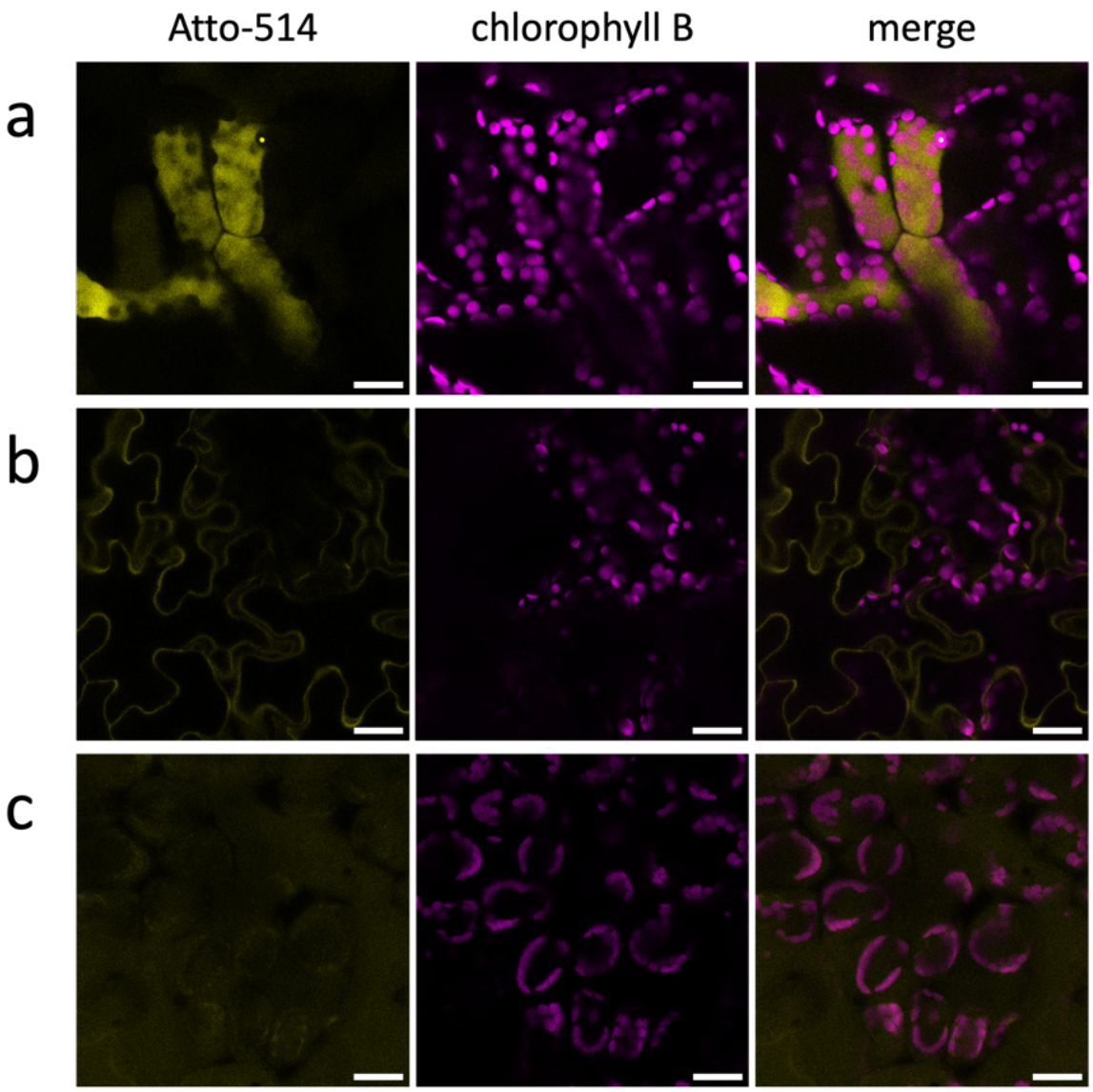

Figure A.4: Click chemistry control experiments with Atto-514-alkyne in *A. thaliana* cells, but without azide amino acids. Fluorescent microscopic observation of *A. thaliana* chloroplasts of wild-type *Col-0* cells treated with Atto-514-alkyne. Fluorescent dye shows **(a)** vaculolar localization, **(b, c)** cytosolic localization. Scale bar: 20 µm.

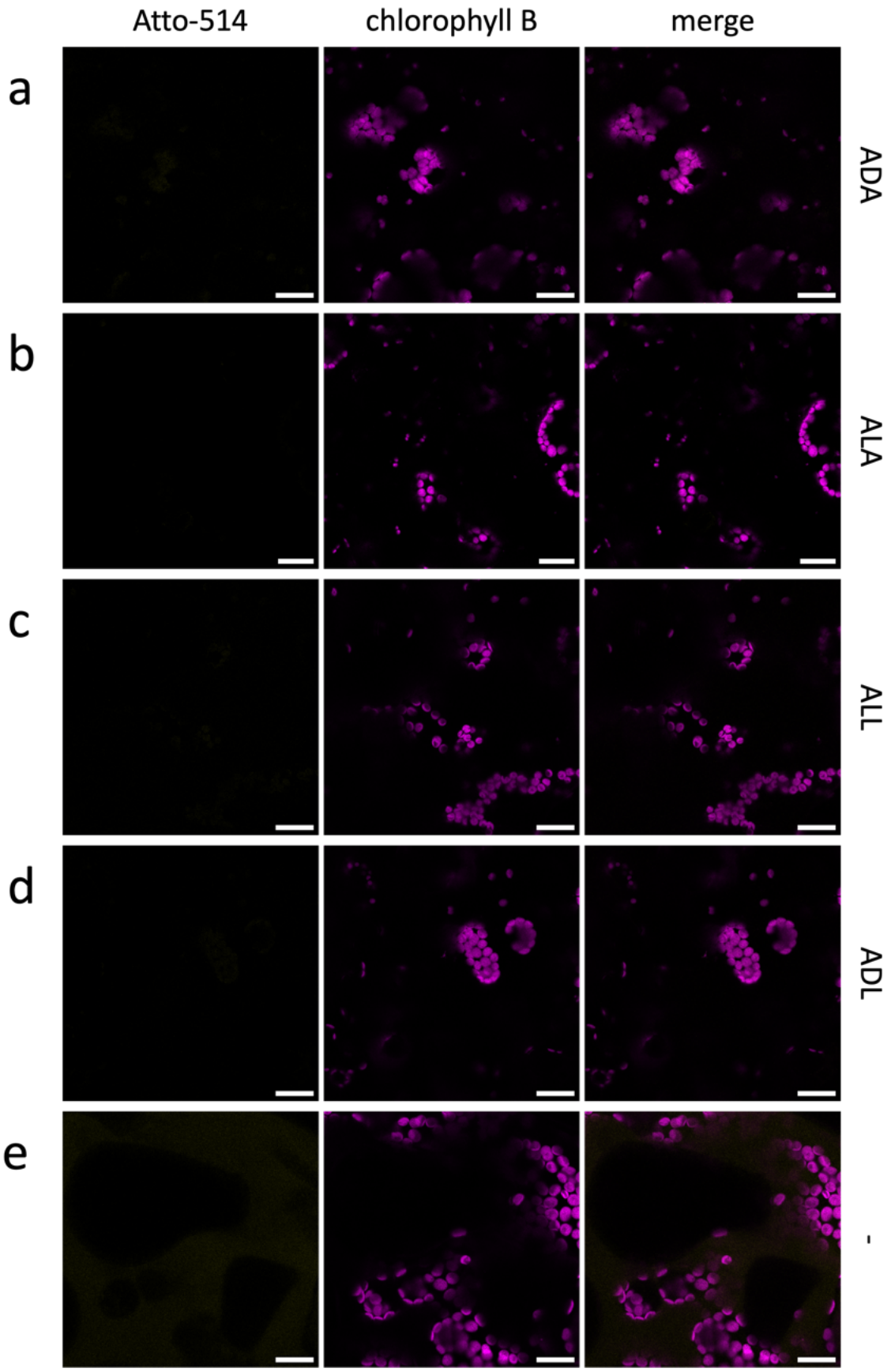

Figure A.5: Click chemistry control experiments with azide amino acids in *A. thaliana* cells, but without Atto-514-alkyne. Fluorescent microscopic observation of *N. benthamiana* cells treated with **(a)** ADA, **(b)** ALA, **(c)** ALL, **(d)** ADL. **(a – d)** are not treated with Atto-514-alkyne. **(e)** shows a sample treated with Atto-514-alkyne, but without azide amino acids. Scale bar: 20 µm.

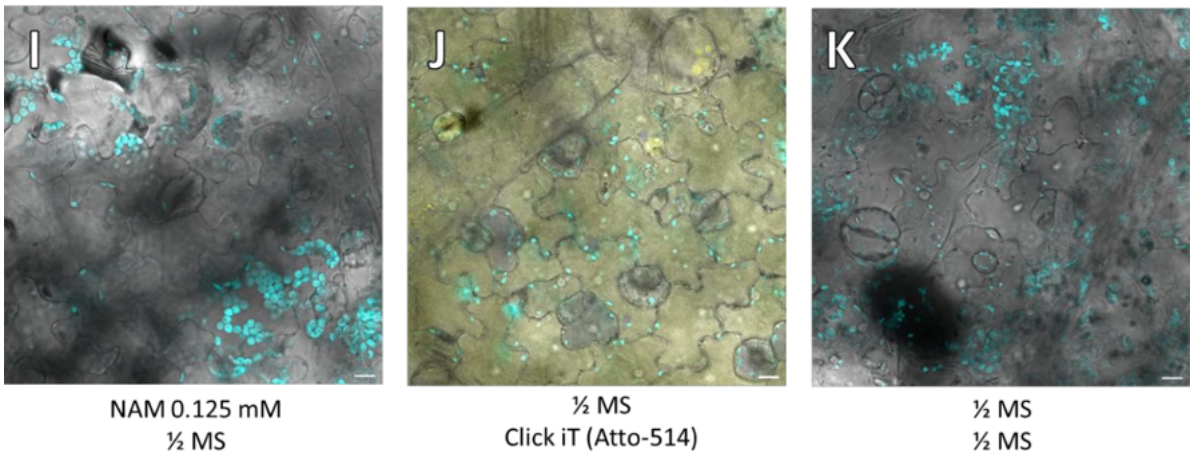

Figure A.6: Haag (2023): Click chemistry with NAM-azide for visualization of PGN in adult *N. benthamiana* plants. Fluorescent emission was detected exciting at 514 nm. **I-K**: Negative controls. Merged images of the Atto-514 emission, the chlorophyll autofluorescence and the brightfield channel. Nicotiana leaves infiltrated with 0.125 mM NAM-azide in 1/2 MS (**I**) or 1/2 MS (**J, K**) and cut-outs later incubated in 1/2 MS (**I, K**) or Click-iT cell reaction cocktail containing Atto-514 (**J**). The scale bar is 10 µm.

Table A.2: List of primers used in this study.

name	**sequence**
ddl1-S1	5´-CAGTTTCATGGCATTGGTGATC-3´
ddl1.3 End	5´-ACTTACATCTACATATCTTTGC-3´
ddl1.3 Start	5´-CACCATGGCGTCCATGGCGAC-3´
ddlA1	5´-CAAGTAGTTTGGTACTGTCATG-3´
SAIL-LB2	5´-GCTTCCTATTATATCTTCCCAAATTACCAATACA-3´
SALK-LB1	5´-AATCAGCTGTTGCCCGTCTCACTGGTGAA-3´
murES1	5´- CACTGCTTGCTTTCTCAGTCTC-3´
murE-S2 (murE5)	5´- CATGGAAAACACCAAAGCCGATG- 3´
murE-A2	5´- CAACAGCACAACGTACAGCTAC -3´
Wisc-LB4	5´- TGATCCATGTAGATTTCCCGGACATGAAG-3´
murE-S3	5´- GGAAGGTAACACTAGGATCAAC-3´
murE-A3	5´- CGCATTGTCGAAATCCACTTC-3´
Wisc-LT6	5´- AATAGCCTTTACTTGAGTTGGCGTAAAAG-3´
PGRP-S2 (DmPGRP)	5´- CACCATGGGAAAGTCTAGACAAAGATCTC-3´
PGRP-End (DmPGRP)	5´- AGGATTAGAAAGCCAATGAGG-3´
PGLYRP-S2 (HsPGRP)	5´- CACCATGCAAGAAACTGAAGATCCTGCTTG-3´
PGLYRP-End (HsPGRP)	5´- AGGAGATCTATAATGAGGCCA-3´
AmiC1-End	5´- TCGTTTGAGGTACTGAAGAATACCGCGAG-3´
AmiC2-Start	5´- CACCATGGGGAAATTACTAGTTGTGATTGAC-3´
AmiC2-End	5´- ACGCTGTAAGTATTTTAGGATG-3´
AmiC1-Start	5´- CACCATGTCAGTATTCATCGACCCCGGACAC-3´
EcAmiC-AMIN-Start	5´- CACCATGCAGGTCGTGGCGGTGCGC-3´
EcAmiC-AMIN-End	5´- GGCCGGATAGAGGTCCATCACC-3´

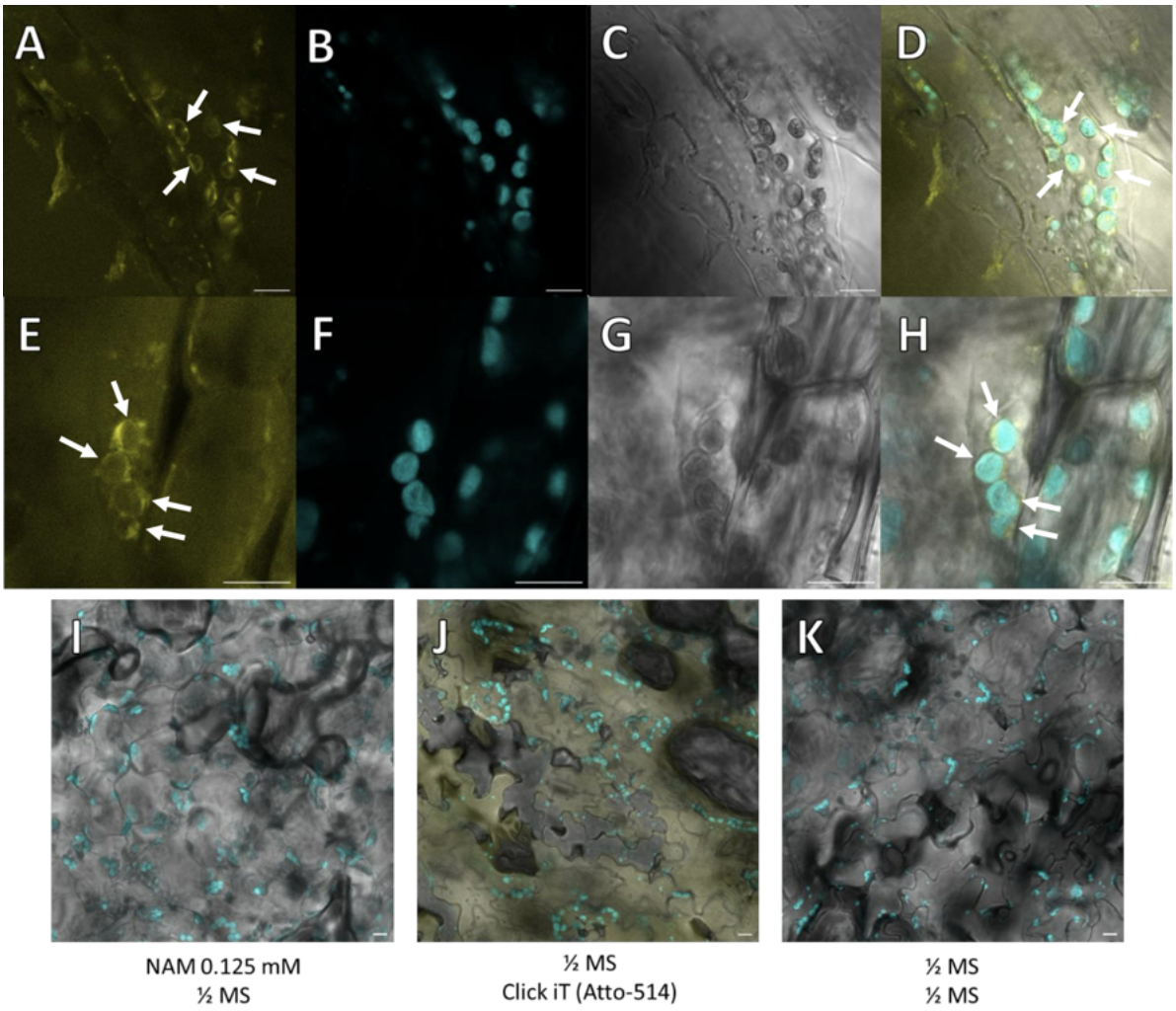

Figure A.7: Haag (2023): Click chemistry with Mur*N*Ac-azide for visualization of PGN in adult *A. thaliana* plants. Fluorescent emission was detected exciting at 514 nm. **A-H**: Arabidopsis leaves infiltrated with 0.125 mM NAM-azide and incubated in Click-iT cell reaction cocktail containing Atto-514- alkyne. **A, E** Atto-514 emission. **B, F** autofluorescence of chlorophyll. **C, G** brightfield channel. **D, H** merged image of A/E, B/F and C/G. White arrows indicate chloroplasts surrounded by fluorescent ring-like structures. The scale bar is 5 µm. **I-K**: Negative controls. Merged images of the Atto-514 emission, the chlorophyll autofluorescence and the brightfield channel. *A. thaliana* leaves infiltrated with 0.125 mM NAM-azide in 1/2 MS (**I**) or 1/2 MS (**J, K**) and cut-outs later incubated in 1/2 MS (**I, K**) or Click-iT cell reaction cocktail containing Atto-514 (**J**). The scale bar is 10 µm.

DmPGRP$_{\Delta SP}$

```
  1 ATGGGAAAGTCTAGACAAAGATCTCCTGCTAATTGTCCTACTATTAAGCTTAAGAGACAATGGGGAGGAAAGCCTTCTCTTGGACTTCAT  90
    M  G  K  S  R  Q  R  S  P  A  N  C  P  T  I  K  L  K  R  Q  W  G  G  K  P  S  L  G  L  H

 91 TATCAAGTTAGACCTATTAGATATGTTGTTATTCATCATACTGTTACTGGAGAATGTTCTGGACTTCTTAAGTGTGCTGAAATTCTTCAA 180
    Y  Q  V  R  P  I  R  Y  V  V  I  H  H  T  V  T  G  E  C  S  G  L  L  K  C  A  E  I  L  Q

181 AATATGCAAGCTTATCATCAAAATGAACTTGATTTTAATGATATTTCTTATAATTTTCTTATTGGAAATGATGGAATTGTTTATGAAGGA 270
    N  M  Q  A  Y  H  Q  N  E  L  D  F  N  D  I  S  Y  N  F  L  I  G  N  D  G  I  V  Y  E  G

271 ACTGGATGGGGACTTAGAGGAGCTCATACTTATGGATATAATGCTATTGGAACTGGAATTGCTTTTATTGGAAATTTTGTTGATAAGCTT 360
    T  G  W  G  L  R  G  A  H  T  Y  G  Y  N  A  I  G  T  G  I  A  F  I  G  N  F  V  D  K  L

361 CCTTCTGATGCTGCTCTTCAAGCTGCTAAGGATCTTCTTGCTTGTGGAGTTCAACAAGGAGAACTTTCTGAAGATTATGCTCTTATTGCT 450
    P  S  D  A  A  L  Q  A  A  K  D  L  L  A  C  G  V  Q  Q  G  E  L  S  E  D  Y  A  L  I  A

451 GGATCTCAAGTTATTTCTACTCAATCTCCTGGACTTACTCTTTATAATGAAATTCAAGAATGGCCTCATTGGCTTTCTAATCCT 534
    G  S  Q  V  I  S  T  Q  S  P  G  L  T  L  Y  N  E  I  Q  E  W  P  H  W  L  S  N  P
```

HsPGRP$_{\Delta SP}$

```
  1 ATGCAAGAAACTGAAGATCCTGCTTGTTGTTCTCCTATTGTTCCTAGAAATGAATGGAAGGCTCTTGCTTCTGAATGTGCTCAACATCTT  90
    M  Q  E  T  E  D  P  A  C  C  S  P  I  V  P  R  N  E  W  K  A  L  A  S  E  C  A  Q  H  L

 91 TCTCTTCCTCTTAGATATGTTGTTGTTTCTCATACTGCTGGATCTTCTTGTAATACTCCTGCTTCTTGTCAACAACAAGCTAGAAATGTT 180
    S  L  P  L  R  Y  V  V  V  S  H  T  A  G  S  S  C  N  T  P  A  S  C  Q  Q  Q  A  R  N  V

181 CAACATTATCATATGAAGACTCTTGGATGGTGTGATGTTGGATATAATTTTCTTATTGGAGAAGATGGACTTGTTTATGAAGGAAGAGGA 270
    Q  H  Y  H  M  K  T  L  G  W  C  D  V  G  Y  N  F  L  I  G  E  D  G  L  V  Y  E  G  R  G

271 TGGAATTTTACTGGAGCTCATTCTGGACATCTTTGGAATCCTATGTCTATTGGAATTTCTTTTATGGGAAATTATATGGATAGAGTTCCT 360
    W  N  F  T  G  A  H  S  G  H  L  W  N  P  M  S  I  G  I  S  F  M  G  N  Y  M  D  R  V  P

361 ACTCCTCAAGCTATTAGAGCTGCTCAAGGACTTCTTGCTTGTGGAGTTGCTCAAGGAGCTCTTAGATCTAATTATGTTCTTAAGGGACAT 450
    T  P  Q  A  I  R  A  A  Q  G  L  L  A  C  G  V  A  Q  G  A  L  R  S  N  Y  V  L  K  G  H

451 AGAGATGTTCAAAGAACTCTTTCTCCTGGAAATCAACTTTATCATCTTATTCAAAATTGGCCTCATTATAGATCTCCT 528
    R  D  V  Q  R  T  L  S  P  G  N  Q  L  Y  H  L  I  Q  N  W  P  H  Y  R  S  P
```

Figure A.8: Coding sequences and amino acid sequences of *Dm*PGRP$_{\Delta SP}$ and *Hs*PGRP$_{\Delta SP}$. Adapted from Tran et al. (2023).

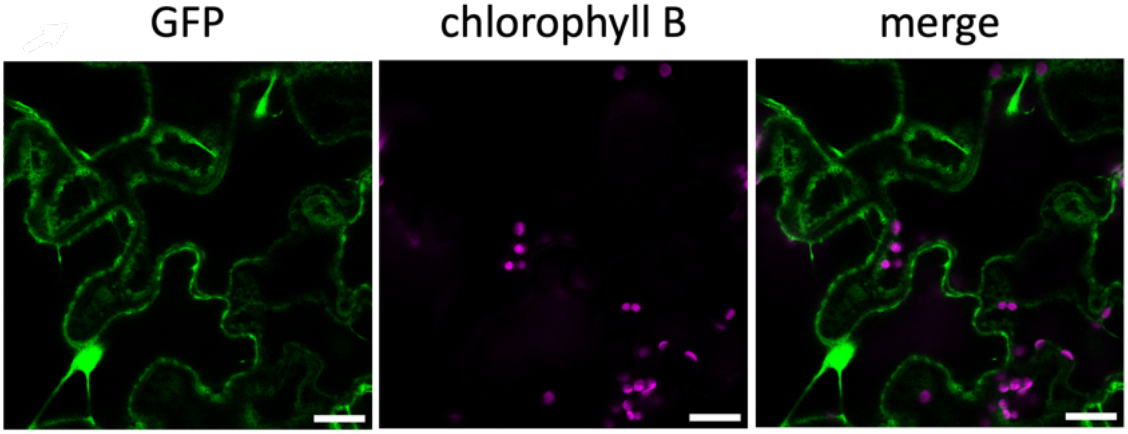

Figure A.9: Transient protein expression of GFP in *N. benthamiana*. Scale bar: 20 µm.

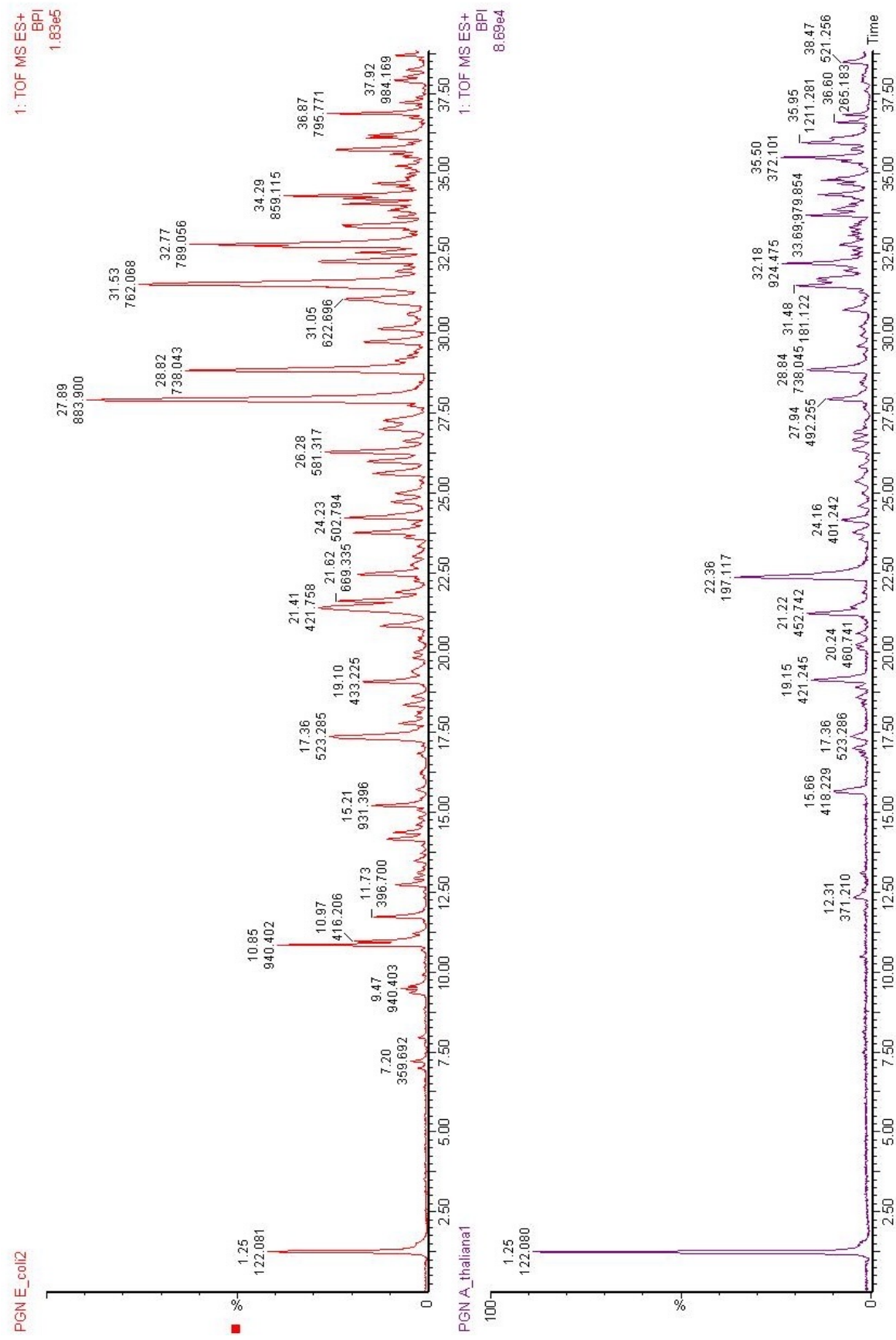

Figure A.10: Mass chromatogram of *E. coli* and *A. thaliana* peptidoglycan after UPLC/MS analysis.

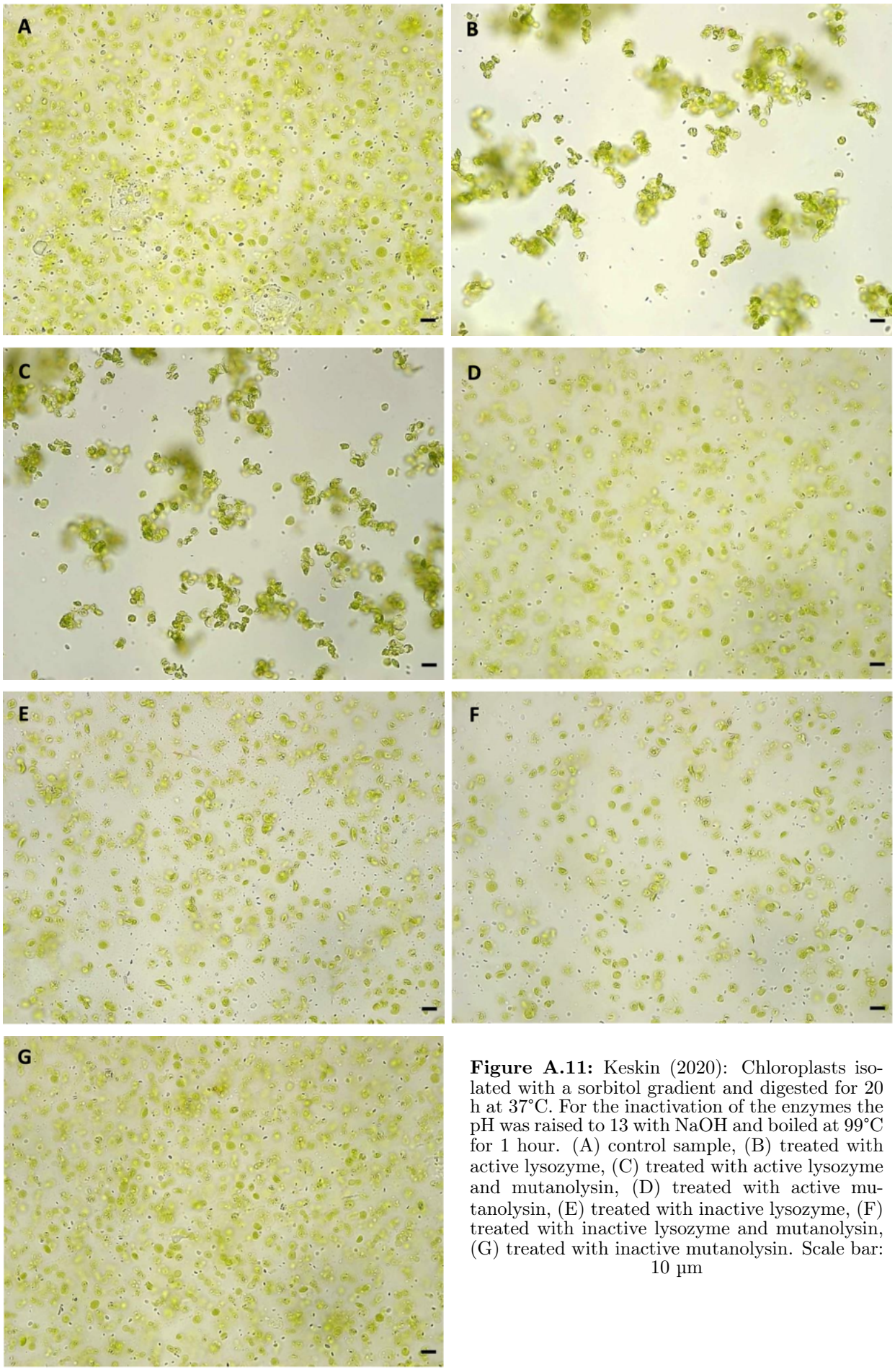

Figure A.11: Keskin (2020): Chloroplasts isolated with a sorbitol gradient and digested for 20 h at 37°C. For the inactivation of the enzymes the pH was raised to 13 with NaOH and boiled at 99°C for 1 hour. (A) control sample, (B) treated with active lysozyme, (C) treated with active lysozyme and mutanolysin, (D) treated with active mutanolysin, (E) treated with inactive lysozyme, (F) treated with inactive lysozyme and mutanolysin, (G) treated with inactive mutanolysin. Scale bar: 10 µm

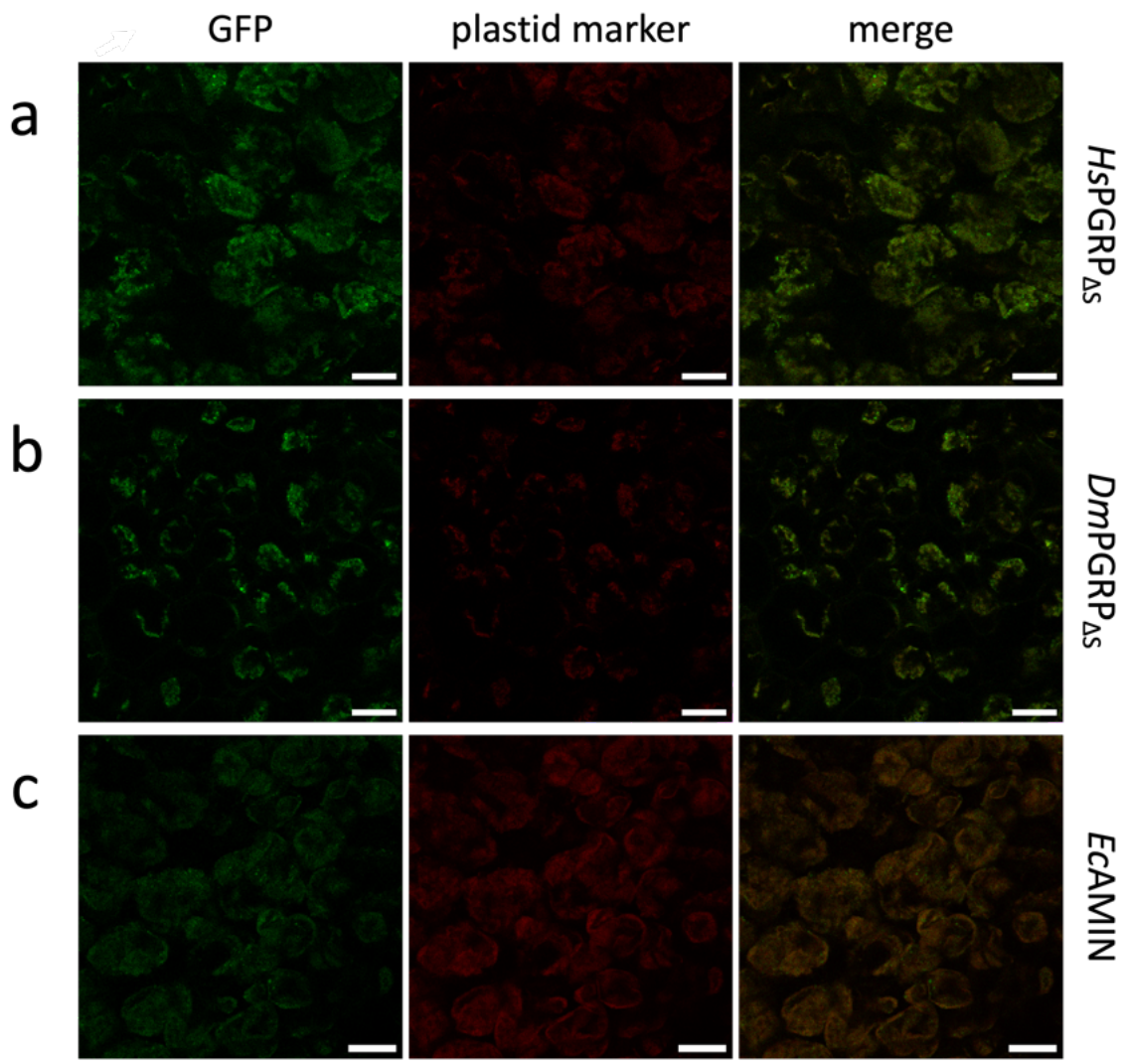

Figure A.12: Fluorescent detection of transiently expressed PGRPs and *Ec*AMIN in *A. thaliana AtmurE*-3 cells. All three proteins localize in chloroplast remnants of *AtmurE*-3 mutants. **(a)** *Hs*PGRP$_{\Delta SP}$-GFP, **(b)** *Dm*PGRP$_{\Delta SP}$-GFP, **(c)** *Ec*AMIN. Scale bar: 20 µm. Adapted from Tran et al. (2023).

Acknowledgment

And last but definitely not least, I'd like to take this opportunity to thank everyone involved in this project for their support. I wouldn't have achieved this goal without you.

First and foremost, I want to express my sincere gratitude to my doctoral thesis supervisor, Klaus Harter, for the opportunity to be a part of his amazing group at the ZMBP and for his support for my scholarship applications. I'd also like to thank my second reviewer, Karl Forchhammer, who took over this position on short notice.

I am very grateful for my PI, Üner Kolukisaoglu. With your continuous support, you inspired me to push my limits and achieve goals I've never dreamed of. With all of our late afternoon discussions, conversations, and critical remarks, you've not only helped me become a better scientist, but also helped me grow personally. Thank you for believing in me. I will do my best to give 100 % in everything I do (not just 95 %).

I'd also like to thank Sensei Jumpei Sasabe for hosting me in his lab for six months. Working in an animal lab was something new for me, and I learned a lot. Our evening conversations, your thirst for knowledge and interest in subjects other than your own research reignited my enthusiasm for science again.

Furthermore, I want to thank my students for working with me on this project; for repeating experiments again and again, to ensure that everything is alright, or simply for making it work. It would not have been possible without you Erva, Marvin, Paul, and Jonas. I'm also very grateful for Sabine Hummel's contribution to this project. I'm sorry you won't be able to see the final result of our work together.

Thank you, Mark Stahl, for running and analyzing the UPLC/MS experiments. Thanks to Kenneth Berendzen for assisting Paul with his FACS experiments and reanalyzing his data.

Many thanks to the RG Harter members, especially Marvin, Luise, Nata, Leander, Amelie, and Thomas. You made the daunting lab days more enjoyable and turned ordinary days into great ones with interesting discussions, experimental advice, good coffee breaks, motivational pep talks, a great working atmosphere, and funny outings and retreats.

Thank you Tom, Chris, and Robby, for proofreading my thesis, and Johannes, for your support over the years.

Joshua, thank you for encouraging and motivating me to finish this thesis. I can't wait for what comes next.

Lastly, I'd like to thank my mom and my brother for their unconditional love and support; you've always had my back and believed in me, and I'm more than grateful to have you as my family. I want to dedicate this work to my dad. I know you'd be proud of me, but I wish you were here to celebrate with us.